12-15-2007

Luminescent Quantum dots for Cellular Analysis

Lifang Shi
University of New Orleans

Luminescent Quantum dots for Cellular Analysis

A Dissertation

Submitted to the Graduate faculty of the
University of New Orleans
in partial fulfillment of the
requirements for the Degree of

Doctor of Philosophy
In
The Department of Chemistry

By

Lifang Shi

Bachelor of Science (1999), Xiamen University
Master of Science (2002), Xiamen University

December, 2007

In the memory of my grandmother

Wuhong Wu

ACKNOWLEDGMENTS

First I would like to express my gratitude to my research advisor, Professor Zeev Rosenzweig, for his invaluable guidance, support, and encouragement throughout my graduate research.

I am also very grateful to my advisory committee members Professor Matthew A. Tarr, Professor Richard Cole, and Professor Guijun Wang for their advices and suggestions during my research work.

I also sincerely thank Professor Nitsa Rosenzweig for her imperative role in guiding me through hurdles presented by the complex biological systems that were the subject of my studies.

I would like give a special thank the support of Laurie Locascio and Michael Gaitan's research group of NIST and the NIST administration for enabling the completion of the research project at NIST at the aftermath of Hurricane Katrina.

I would like to thank all past and present group members in Rosenzweig group for your friendship and kindness. The time I spent with you will be remembered.

I would like to thank my close friends, Ming Zhang, Ying Long, Xiaobo Gu, Yan Wu, Yun Cai, Jinghong Zheng, Yingli Xu, Meijun Li for their friendships which have accompanied me through years

Last, but not the least, I would like to thank my beloved family for the love and support all the time, father Wuhuan, mother Jinsuo, sisters Liyin, Licai, Likun and their kids Weihuai, Weiqu, Chujun.

TABLE OF CONTENTS

LIST OF FIGURES

LIST OF SCHEMES

ABSTRACT

Luminescent quantum dots have attracted great interest in recent years among biological researchers since they provide solutions to problems associated with use of organic fluorophores in cellular studies. Quantum dots show high photostability, high emission quantum yield, narrow and symmetric emission peaks and size-dependent wavelength tunability. The objective of my PhD studies was to develop CdSe/ZnS quantum dot-based probes and utilize them in cellular assays.

The first phase of the work was to develop luminescent quantum dot fluorescence resonance energy transfer (FRET) based probes for protease activity. The probes were based on FRET interactions between quantum dots that serve as donors and rhodamine molecular acceptors that were immobilized to the surface of the quantum dots through peptide linkers, which contained selective enzymatic cleavage sites. Upon enzymatic cleavage of the peptide linkers, the rhodamine molecules no longer provided an efficient energy transfer channel to the quantum dots, which brightened the previously quenched quantum dots. The probes were applied to detect enzyme activity, screen enzyme inhibitors, and discriminate between normal and cancerous cells primarily because of the difference in the proteolytic activity in extracellular matrices.

The second phase of my work was to take advantage of FRET and quantum dots to develop pH sensor. First quantum dots were modified with metallothionein (MT) to be water-soluble and biocompatible. The MT-coated quantum dots were labeled with Rhodamine through the formation of amide bonds with ε-amine group of lysine in MT peptide to form the probes. FRET efficiency between quantum dots (donor) and rhodamine (acceptor) was pH dependent.

The final phase of my studies focused on the first preparation of reversible quantum dot-based cellular probes for labile iron. The MT coated quantum dots was modified with EDTA to form probes. When captured by the EDTA molecules, iron ions quenched the emission of quantum dots. Removal of iron from the quantum dot surface by free EDTA or other iron chelators with higher binding affinity resulted in a rise in the luminescence of quantum dots. The analytical properties of the probes including sensitivity, selectivity, and reversibility were characterized. Intracellular assays in iron-enriched astrocytes will be carried out.

Keywords: Quantum dots; FRET; Protease sensor; pH sensor; Iron sensor; Cellular analysis

CHAPTER 1 INTRODUCTION

1.1 Objectives and aims

The main objective of my work was to develop luminescent quantum dots based bioanalytical probes for cellular analysis, which enable simultaneous analysis of a large number of cells and optical response to cellular signaling events in real time. Because of the discrete electronic state of each particle, the photophysical properties of quantum dots are sensitive to the presence and characteristics of ligands or molecules on their surface. The newly developed quantum dots respond to changes in the cellular environment by changing their luminescence intensity. The specific aims of my study were: i) to develop quantum dots FRET based protease sensor for real time monitoring of Matrix Metalloproteinases (MMPs) in cell cultures, ii) to develop quantum dots FRET based pH sensor, and iii) to develop reversible quantum dots based sensors for labile iron in iron rich cells.

1.2 Significance

The detection of biomolecules at the molecular level using state-of-the-art imaging techniques has been one of the most important tasks in life sciences (1), especially the development of high sensitivity and high specificity sensors for cancer research, including basic tumor biology, *in vivo* imaging and early detection. Fluorescence methods are the most common method of detecting biomolecules in cells. Many of the organic dye and protein-based fluorophores suffer from serious chemical and photophysical limitations, such as broad emission spectra, low photobleaching thresholds, and poor

chemical stability. They are also limited in long term imaging and multicolor detection. Further progress in the field has been realized through the development of agents that have small size and high photostability. Luminescent quantum dots have attracted the attention of biological researchers due to the unique electronic and optical properties. Since water-soluble and biocompatible quantum dots were first reported in 1998(2, 3), luminescent quantum dots have been a new promising approach to fluorescent chemical sensing and cancer detection (4). An important goal in quantum dots research is to develop nanoscale assemblies to continuously monitor targets in cell. My PhD project focused on the development of quantum dots based probes for cellular analysis.

1.3 Fluorescence principle (5-6)

Luminescence is the emission of light from any substance and occurs from electronically excited states. Based on the nature of the excited state, luminescence is divided into fluorescence, phosphorescence and chemiluminescence. Fluorescence and phosphorescence are similar because the excitation is formed by absorption of photos. Fluorescence occurs when a molecule in an excited singlet state returns to the electronic ground state by emission of a photon. Phosphorescence is the emission of light from the triple state to the ground state. Fluorescence and phosphorescence are different because fluorescence does not involve the change in electron spin. Chemiluminescence occurs when the excitation is bought by a chemical reaction and excited species returns to the ground state by light emission.

1.3.1 Jablonski diagram

The process on light absorption and emission are usually illustrated by Jablonski diagrams (figure 1.1). S_0, S_1 and S_2 represent the singlet ground state, first and second excited states respectively. T_1 is the first triplet state. Usually the energy of the first excited triplet state is lower than the energy of the corresponding singlet states. Numerous vibration energy levels exist in each of these electronic energy levels. The light absorbed by a molecule excites an electron from the singlet ground state, S_0, to excited states S_1 or S_2 according to the magnitude of the absorbed energy. This transitions process happens in $10^{-14} \sim 10^{-15}$ s. The routes for the excited molecules return to its ground state can be divided into two categories: radiative and nonradiative deactivation process.

Fluorescence and phosphorescence are two different radiative transitions. If the photon emission occurs from singlet excited states to ground state (S_1 to S_0), it is termed fluorescence. These emission rates of fluorescence are typically10^8 s^{-1}. If the photo emission occurs from triplet excited states to ground state (T_1 to S_0), it is termed phosphorescence. Transitions from triplet excited state to the ground state are forbidden and the emission rates are slow (10^3-100 s^{-1}), so phosphorescence lifetimes are typically milliseconds to seconds. Phosphorescence is usually not seen in fluid solutions at room temperature.

There are four significant nonradiative deactivation processes: vibrational relaxation (VR), internal conversion (IC), intersystem crossing (IsC) and external conversion (EC). The transition from higher vibrational energy level to lower vibrational energy level is called vibrational relaxation. Internal conversion is the radiationless transition between

energy states of the same spin state (e.g. S_2 to S_1). This process takes place 10^{-12} s or less. Intersystem crossing is a radiationless transition between different spin states (e.g. S_1 to T_1). The deactivation of an excited electronic state involves interaction and energy transfer between the excited molecule and the solvent or other solutes is called external conversion.

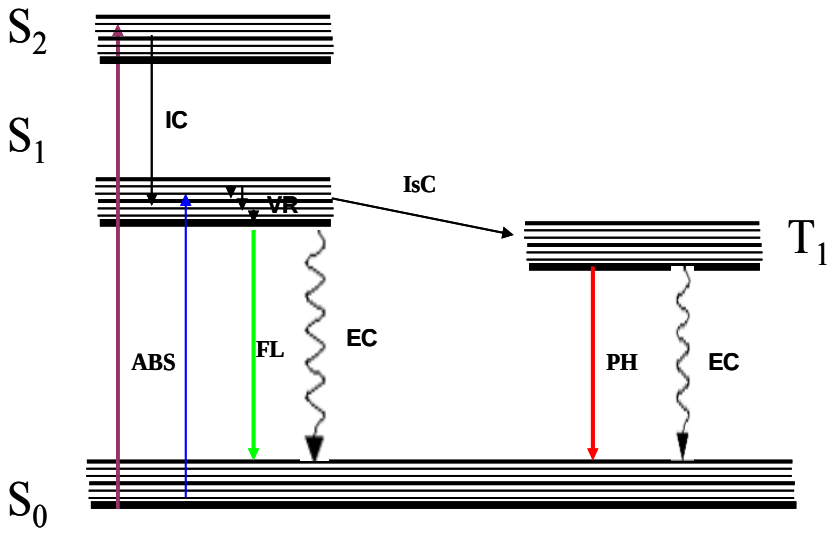

ABS - Absorbanc
FL – Fluorescence
PH - Phosphorescence

S_0- ground state
S_1 – Singlet first excited state
S_2- Singlet second excited state
T_1 - Triplet excited State

V.R.- Vibrational relaxation
IsC - Intersystem Crossing
I.C - Internal Conversion
E.C -Exteral conversion

Figure 1.1 Jablonski diagram

1.3.2 Characteristics of fluorescence emission

Florescence always occurs from the lowest vibrational level of the first singlet excited electronic state. Therefore, fluorescence emission spectra are generally independent of the absorption wavelength. Fluorescence emission spectra vary widely and are dependent upon the chemical structure of the fluorophore, pH, temperature and the solvent in which it is dissolved. Since the same transitions are involved in both absorption and emission, and due to the similarities of the vibrational levels of S_0 and S_1, the emission is the mirror image of absorption. The energy of emission is usually less than that of absorption. Thus, fluorescence occurs at longer wavelength. The energy difference is called the Stokes' Shift. The Stokes's Shifts can be caused by energy losses due to relaxation to ground vibrational states, solvent effects, excited state reactions, complex formation, and energy transfer. The fluorescence lifetime and quantum yield are important characteristics of a fluorophore. The quantum yield is defined as the number of emitted photons relative to the number of absorbed photons. The lifetime of the excited state is defined by the average time the molecule spends in the excited state prior to return to the ground state. A typical fluorescence lifetime is near 10 ns.

1.3.2 Fluorescence resonance energy transfer (FRET)

Fluorescence resonance energy transfer (FRET), a non-radiative energy transfer from the excited state of a donor (D) to an acceptor (A), is the result of long-range dipole-dipole interactions between the donor and acceptor (5, 7). As a result, the fluorescence intensity and lifetime of the donor is decreased and shortened, while the acceptor fluorescence is sensitized and its lifetime is increased. FRET donor/acceptor pairs satisfy

the following conditions: (i) spectral (or energy) overlap between the absorption spectrum of the acceptor and the fluorescence emission spectrum of the donor; (ii) the donor and acceptor molecules must be in close proximity (typically 10-100 Å). (iii) Donor and acceptor transition dipole orientations must be approximately parallel. The rate of energy transfer depends on the extent of spectral overlap between the emission spectrum of the donor and the absorption spectrum of the acceptor, the relative orientation of donor/acceptor transition dipoles and the distance between the donor and acceptor. The rate of energy transfer is given by the equation (1).

$$k_t = \tau_D^{-1} \left(\frac{R_0}{R} \right)^6 \qquad [1]$$

$\boldsymbol{\tau_D}$ is the measured lifetime of the donor in the absence of the acceptor. $\mathbf{R_0}$ is termed the critical radius of the transfer or the Forster distance, which is the distance at which the energy transfer efficiency is 50%. The Forster distance, $\mathbf{R_0}$, depends on the spectral characteristics of the donor-acceptor pair and is expressed in equation (2).

$$R_0 = \left(\frac{3000}{4\pi N |A|_{1/2}} \right)^{1/3} \qquad [2]$$

N is Avogadro number and $|A|_{1/2}$ is the concentration of the acceptor at which the energy transfer efficiency **E** is 50%. For a donor and acceptor pair that is covalently bound, the energy transfer efficiency, **E**, is expressed as:

$$E = \frac{R_0^6}{R_0^6 + R^6} \qquad [3]$$

The FRET efficiency can be experimentally measured by monitoring changes in the donor or/and acceptor fluorescence intensities, or changes in the fluorescent lifetimes of fluorophores.

FRET, incorporated with optical microscopy, is a powerful photophysical technique because of its high sensitivity to changes in distance and relative dipole orientations between donor and acceptor. FRET has been widely used in probing biological phenomena, including studying protein-protein interactions (binding affinity), diffusion dynamics, protein conformational changes, and detecting nucleic acid and peptides (8-12).

1.4 Quantum dots

1.4.1 Structural properties of quantum dots

Quantum dots are semiconductor nanoparticles of 1-10nm in diameter. Luminescent nanocrystals are composed of atoms from groups II–VI (CdS, CdSe, CdTe, ZnO, ZnSe), III–V (InP, InAs, GaN, GaP, GaAs), and IV-VI (PbS, PbSe, PbTe) of the periodic table. Quantum dots are neither atomic nor bulk semiconductors. They are spherical, crystalline particles of a given material consisting of hundreds to thousands of atoms. Quantum dots are smaller than the electron-hole pairs (exciton) Bohr radius. When the size of a semiconductor is small enough to approach the size of the materials exciton Bohr radius, the electron energy levels can no longer be treated as a continuum. They must be treated as discrete. This situation of discrete energy levels is called quantum confinement. Quantum confinement leads to increased stress on the exciton, which results in increased energy of the emitted photon. The smaller the quantum dots, the less room for exciton

separation, and more energy is required to form the exciton. The behavior of the excited electron can be described by a simple "particle-in-a-box" model (13). The Quantum confinement causes a blue shift in the band gap energy (figure 1.2) and increases the probability of overlap between the electron and hole which increases the rate of radiative recombination. This results in quantum dots with unique optical and electric properties (14-18). As the size of quantum decreases, the absorption onset shifts to higher energy, indicating an increase in bandgap energy. CdX (X= S, Se, Te) quantum dots have generated a great deal of interest due to their emission in the Ultraviolet-Visible to near infrared (NIR) range of the electromagnetic spectrum.

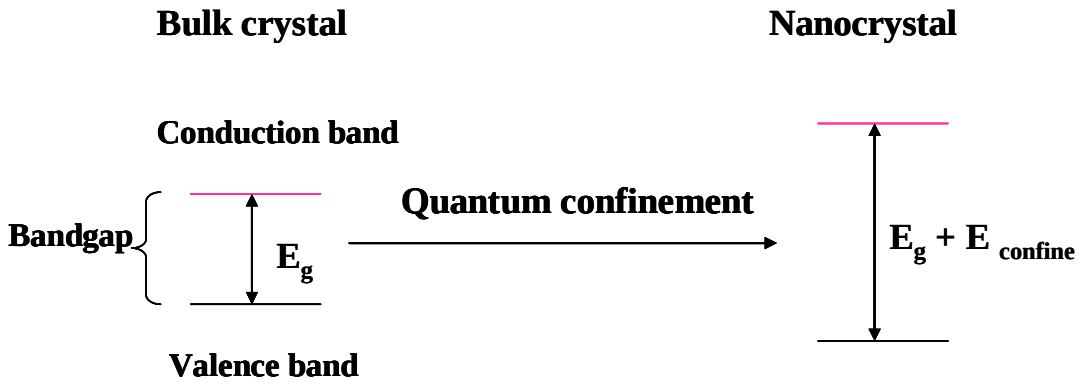

Figure 1.2 blue shift in the band gap energy in nanometer crystal compared to the bulk crystal.

1.4.2 Optical properties of quantum dots

In semiconductors, the electron in the valence band can be excited by photon absorption and promoted to the conduction band, creating a "hole" in the valence band. The excited electron will relax back to fill in the hole and emit light. This is conceptually the same as conventional fluorescence. However, quantum dots have several optical characteristics which distinguish them from conventional organic fluorophores because of the strong confinement of excitons in quantum dots in such small size (quantum confinement effect). (i) Size-tunable luminescence (2, 19); the wavelength of emitted light is determined by the band gap energy between valence and conduction band of quantum dots. As the size of the quantum dots decreases, the energy gap increases. Since the band gap energy of the quantum dots is size dependent, the emission color of the quantum dots is also size dependent. The emission peak changes from ultraviolet to infrared by varying the size and composition of quantum dots (20, 21). (ii) Organic fluorophores have narrow absorption. They can only be excited by a narrow range of wavelengths. On the other hand, the absorption of quantum dots has an increased probability at higher energies, which leads to broad absorption spectrum and enable quantum dots to be excited by a wide range of wavelengths. Quantum dots with different sizes can be excited with a single wavelength. This enables multiplexing or simultaneous detection of multiple signals of quantum dots (16). Additionally, the molar extinction coefficients of quantum dots are larger than that of organic dyes (22, 23) (iii) Quantum dots have symmetric and narrow emission spectra without a red tail. This reduces cross-talk between emission signals (24). (iv) The long fluorescence lifetime of quantum dots enable their use in time-gated detection to separate their signal from that of species with

shorter lifetime species, like autofluorescence encountered in cells. This increases the analytical sensitivity of quantum dots (25, 26). (v) A major advantage of quantum dots is their high photostability and chemical stability compared to organic dyes, which enables their use in imaging applications that require long exposure times (27-33).

1.4.3 Synthesis of quantum dots

The size and shape of quantum dots are controlled by altering the duration, temperature, and ligand molecules used in their synthesis. To date, quantum dots, such as CdSe, CdS, CdTe, have been synthesized in various media including aqueous solution (34, 35), reverse micelles (36), polymer films (37,38), sol-gel systems (39) and trioctylphosphine oxide (TOPO) / trioctylphosphine (TOP) (19, 40-42). High quality quantum dots have been achieved by pyrolysis of organometallic precursors in TOP/TOPO media, which was first reported by Murray in 1993 (19). The synthesis is carried out by injecting dimethylcadmium ($Cd(CH_3)_2$) and sulfur, selenium, or tellurium dissolved in TOP solution to hot TOPO media. However, dimethylcadmium is very toxic, pyrophoric, unstable and expensive. The synthesis procedure was later refined by Peng and coworkers who replaced the toxic cadmium precursor $Cd(CH_3)_2$ with CdO, $Cd(Ac)_2$ and $CdCO_3$ and lead to green synthesis (40-42). The method developed by Peng is used extensively for the synthesis of luminescent quantum dots with some quantum dot products already available commercially (Evident Technologies (NY), Quantum Dots Corporation (CA)).

Confining the electrons to the bulk of luminescent quantum dots is imperative to their bright luminescence. The excited electron or hole can be trapped by surface defects, such

as vacancies, local lattice mismatches, dangling bonds, or adsorbates at the surfaces, and lead to the nonradiative recombination, which will result in the low quantum yield (13). Additionally, the uncapped quantum dots are so reactive that they readily undergo photochemical degradation. To decrease the effect of surface defects and to protect surface atoms from oxidation and other chemical reactions, an additional thin layer made of a higher band gap semiconductor material, for example ZnS, is grown on the surface of the quantum dots(43-47). This process, often described in the literature as surface passivation, increases the emission quantum yield, improves chemical stability and photostablility, and reduces the toxicity by preventing leakage of Cd or Se to the surrounding environment. Due to the availability of precursors and the simplicity of crystallization, CdSe/ZnS core/shell quantum dots have been the most well-studied and popular for biological applications.

1.4.4 Surface modification of quantum dots

When high quality quantum dots are synthesized in organic solvents, they are insoluble in water, non-biocompatible and don't have functional groups for bioconjugation. To facilitate their application in aqueous biological systems, the hydrophobic TOPO molecules that serve as capping ligands of luminescent quantum dots must be replaced with bifunctional hydrophilic capping ligands or overcoated with amphiphilic protective layer to impart water-solubility and potential bioconjugation sites. To address this, various methods on the improvement of quantum dots biocompatibility and stability have been developed during the past few years. These solublization strategies can be divided into three primary categories.

(i) Ligand exchange is a process involving the replacement of hydrophobic ligands with bifunctional ligands in which one end that has anchoring groups can bind to the inorganic QD surface and an opposing end imparts water solubility via hydrophilic groups. Various ligand exchange methods were developed in recent years to form water soluble quantum dots. Thiols (-SH) are often used as anchoring groups on the ZnS surface. The TOPO ligands are often exchanged with thiol functionalized compounds like mercaptoacetic acid (MAA) (3), dihydrolipoic acid (DHLA) (48), dithiothreitol (DTT)(49), and dendrons (50). In our laboratory, we found that the amino acid cysteine is also an effective capping ligand to create hydrophilic quantum dots (51). Weiss and coworkers reported that cysteine containing peptides could also be used as effective capping ligands to facilitate the water miscibility of quantum dots (52). Since the bond between thiol and ZnS is not very strong, quantum dots will tend to aggregate over time, the solubility of quantum dots capped with thiol chemistry is limited (53). Also the ligand exchange processes usually disturbs the chemical and physical state of the surface atoms of quantum dot and reduce quantum efficiency (54).

(ii) Silica encapsulation involves growth of a silica layer on the surface of quantum dots. Also, functional organosilicone molecules are incorporated into the shell and provide surface functionalities for bioconjugation (2, 55-58). The silica coated quantum dots are extremely stable because the silica layer is highly cross-linked. However, the method is very laborious and the silica layer may be hydrolyzed (59).

(iii) Another approach is to coat quantum dots with amphiphilic polymer and phospholipids, which interleave with the hydrophobic TOPO ligands through hydrophobic attraction and provide a hydrophilic exterior to ensure aqueous solubility

(33, 60-62). This process maintains the native ligands (TOPO) on the surface of quantum dots to retain the high quantum yield of quantum dots and protect the quantum dots surface from deterioration in biological solution. However, the final size of quantum dots is larger, which could limit many biological applications (59).

Although several methods for solubilization of quantum dots in aqueous solution have been devised, each has its own benefits and liability. Progress on the synthesis of high quality water-soluble quantum dots is still playing a crucial role in the area of quantum dots based nanobiotechnology.

1.4.5 Biological Application of quantum dots

Because of unique properties, quantum dots have been promising tools in biological applications as an alternative to common organic fluorophores and have been a new generation of fluorescent probes. Water soluble quantum dots are widely used in protein assays (63-67), DNA and RNA hybridization assays (68-72), and fluorescence resonance energy transfer (FRET) (73-77). They are also used as labels in *in vitro* imaging of cells and tissues (78-82) and in *in vivo* imaging applications in whole animals (83-87).

1.4.5.1 Quantum dots as FRET donors

Fluorescent conventional organic molecules have been widely used as FRET donors and acceptors because of small size, compatibility with covalent coupling, and relatively large detectable optical signal. However, organic dyes have some problems as FRET agents: (i) The narrow absorption spectrum leads to direct excitation of the acceptor; (ii) The broad emission spectrum of the donor, with long tailing, overlaps with the emission

spectrum of the acceptor and results in spectral cross-talk; (iii) Low photobleaching thresholds prevent monitoring dynamics over long period. Quantum dots provide a potential solution to the above problems.

Quantum dots have been investigated as FRET donors as alternatives to traditional organic dyes because of their high photostability and their unique spectral properties (60, 88-90). (i) A broad absorption spectrum enables choosing an excitation wavelength that does not excite the acceptor molecules directly. This prevents "bleeding" of energy into the acceptor channel, which often increases the fluorescence intensity of the acceptor and therefore leads to over-estimation of the FRET efficiency between the donor and acceptor fluorophores. (ii) A narrow and symmetric emission spectrum makes it easier to distinguish the emission of the quantum dots from that of the acceptor and reduces the donor spectra leakage into the acceptor channel. (iii) The size-tunable spectrum enables control of the spectrum overlap between quantum dots and acceptor by controlling the size of quantum dots. (iv) Multiple acceptor sites can enhance FRET efficiency.

In 1996, Kagan and his coworker first reported energy transfer between quantum dots (91, 92). After a couple years of silence, in 2001, several research groups reported FRET between quantum dots and organic dyes (93-95). For example, Willard and his coworker developed quantum dots as a FRET donor in a protein-protein binding assay (93). Quantum dots were conjugated to BAS as FRET donors and tetramethylrhodamine was bound to the protein as the FRET acceptor. Medinta and coworkers first reported quantum dots based self-assembled nanoscale FRET biosensors for maltose in 2003 by coating CdSe/ZnS quantum dots capped with DHLA with maltose binding protein (MBP) molecules (96). The FRET assay was based on the interactions between MBP and the

acceptor molecules. Maltose molecules displaced the fluorescent acceptor molecules, which resulted in a maltose concentration dependent increase in the emission of the MBP coated quantum dots. Since that, quantum dots based FRET biosensor have been interesting fields for researchers. So far, the quantum dots based FRET biosensors have been reported to detect TNT (97), toxins (98), β-lactamase (99), collagenase(100), DNA(101), RNA (102) and protein(103), etc.. In these probes, the quantum dots are used as donors while the organic fluorophores serve as fluorescent acceptors. The FRET mechanism allows the quantum dots to respond to environmental changes while avoiding direct chemical interaction with the quantum dots that could negatively affect their photo-physical properties and decrease their brightness.

Although quantum dots based FRET measurements have great potential as biosensors, there are also a number of limitations with quantum dots for FRET. It must be noted that the Forester theory commonly used to describe energy transfer between molecular donor and acceptor molecules was never tested in heterogeneous systems consisting of a luminescent nanoparticle as a donor and fluorescent molecules as acceptors. The heterogeneity in quantum dots size can affect the precision of single-molecule FRET measurements. From a theoretical standpoint, this process is yet to be studied. The FRET efficiency between the luminescent nanoparticles and a fluorescent acceptor molecule is not as high as in molecular FRET due to the larger size of quantum dots. The presence of multiple acceptor molecules on the surface of the luminescent quantum dots leads to a substantial accumulative effect, which is easily observed using conventional spectroscopy and microscopy instrumentation. Quantum dots are not optimal for FRET acceptors.

1.4.5.2 Quantum dots in cellular studies

As previously mentioned, the objective of my PhD project is to develop quantum dot based sensors for cellular measurements. Due to their unique spectroscopic properties, luminescent quantum dots have been used in cellular studies. The broad excitation of quantum dots enables simultaneous detection of different quantum dots-tagged cells with a single excitation light source. The size dependent tunability of quantum dots facilitates their use in an emission spectral range which minimizes the effect of cellular auto-fluorescence. Most importantly, quantum dots are highly resistant to chemical and enzymatic degradation in living cells and photobleaching, which allows for real time monitoring of cellular dynamic events, such as cell migration, differentiation, and metastasis (104). Since the first report of quantum dots that were used to stain F-actin in fixed cells (2), quantum dots have been extensively used in the cell-based studies, including cellular labeling, cellular tracking, and cellular imaging.

Cellular membrane protein and receptors, such as prostate specific membrane antigen (PSMA) (60), mortalin (105), band 3 protein (106), Epidermal Growth Factor(EGF) (107), Glycine receptors (GlyRs) (108), serotonin (109), and membrane glycoprotein(110) can be labeled with quantum dots. For example, Wu and his coworker used quantum dots coated with an amphiphilic polymer linked to immunoglobulin G and streptavidin to localize the breast cancer marker Her2, cytoskeleton fibers, and nuclear antigens in fixed and live cancer cells (28). They compared the brightness and photostability of quantum dots labels to organic dyes. One of the challenges for using quantum dots in biological studies is to label cells selectively and specifically.

Quantum dots can be delivered into live cells by microinjection (33), electroporation (111), peptide mediated transport (112-115), receptor mediated transport (3), and nonspecific endocytosis (31, 32, 116). For example, Jaiswal and colleagues used quantum dots for the long term multiple color imaging of live cells (31). Quantum dots can be internalized by cells via nonspecific endocytosis and accumulated in vesicles in the perinuclear region. With endosome-specific marker Pgp-EGFP, quantum dots can undergo uptake to endosomes. The mechanism and pathway of incorporating quantum dots into cells via endocytosis is still not very clear. However, the high photostability of quantum dots enables long-term cell studies (i.e., up to two weeks), which can't be achieved with organic dyes (59).

Quantum dots have shown great potential as *in vivo* tumor imaging and targeting probes. Akerman first reported peptide-coated quantum dots used to target tumor vasculatures in mice (83). Gao and his coworker described encapsulating luminescent quantum dots in ABC tri-block copolymers for cancer cell targeting and imaging in live animals (60). The ABC tri-block copolymer addresses problem of aggregation and fluorescence loss that occurred when quantum dots were in physiological buffer or inside the live animal. Ballow and coworkers examined the in vivo behavior of injected PEG-coated quantum dots into the mouse blood stream (117). Cai and coworkers used RGD peptide conjugated quantum dots to target giloblastoma tumor vasculate in mice. The RGD peptide showed specific affinity for the angiogenic factor integrin $\alpha_v ß_3$, which is upregulated in growing tumors (87). Although there are some successful reports on quantum dots as tumor targeting and imaging probes on mouse model, more research work is needed before quantum dots can be used as *in vivo* imaging in human subjects.

The required advances include synthesis of high quality non-Cd based quantum dots, synthesis of high-efficiency NIR emitting quantum dots, and improvement of the stability of quantum dots in physiological buffers or inside the live animal via surface modification (118, 119).

1.5 References

1. Murcia, M. J.; Naumann, C.A. *Biofunctionalization of fluorescent nanoparticles* In Biofunctionalization of nanomaterials. By Kumar,Challa S. S. R. (Editor), **2005**:1-38.
2. Bruchez, M.; Moronne, M.; Gin, P.; Weiss, S.; Alivisatos, A. P. *Science*, **1998**, 281, 2013–2016
3. Chan, W. C. W.; Nie, S.M. *Science*, **1998**, 281, 2016–2018
4. Willard, D. M.; Mutschler, T.; Yu, M.; Jung, J.; Van Orden, A. *Anal. Bioanal. Chem.*, **2006**, 384, 564–571
5. Lakowicz, J.R., *Principles of Fluorescence Spectroscopy*, 3nd Edition; Springer: New York, **2006**
6. Skoog, D.A.; Holler, F.J.; Nieman, T.A.; Principles of Instrumental Analysis, 5th Edition, Sanders Golden Publishing, **1998**
7. Haugland, R.P., *Handbook of Fluorescent Probes and Research Products*, 9th Edition**, 2002**
8. O'Connell, P.J., Guilbault, G.G., *Anal. Lett.,* **2001**, 34, 1063-1078,
9. Bensin, D.E., Conrad, D.W., de Lorimer, R.M., Tranmel, S.A., Hllinga, H.W., *Science* **2001**, 293, 1641-1644,
10. Hellinga, H. W.; Marvin, J. S., *Trends Biotechnol.* **1998**, 16, 183-189
11. Looger, L. L.; Dwyer, M. A.; Smith, J. J.; Hellinga, H. W. *Nature* **2003**, 423, 185-190
12. Jares-Erijman, E. A.; Jovin, T. M., *Nat. Biotechnol.* **2003**, 21, 1387-1395
13. Murphy, C.J., *Anal. Chem*, **2002**, 74(19), 520A-526A
14. Alivisatos, A. P. *Science* **1996,** 271 (5251), 933-937
15. Efros, A.L.; Rosen, M. M., *Ann. Rev. Mater. Sci*, **2000**, 30, 475-521
16. Chan, W. C.W; Maxwell, D. J.; Gao, X.; Bailey, R. E.; Han, M.; Nie, S., *Curr. Opin. Biotechnol.* **2002**, 13, 40-46
17. Gao, X.H.; Yang, L.; Petrsos, J.A.; Marshall, F.F.; Simons, J.W.; Nie, S.M., *Curr. Opin. Biotechnol.* **2005**, 16, 63-72
18. Michalet, F. X.; Pinaud, F. ; Bentolila, L. A.; Tsay, J. M.; Doose, S.; Li, J. J.; Sundaresan, G.; Wu, A. M.; Gambhir, S.; Weiss, S. S., *Science*, **2005**, 307, 538-544
19. Murray, C.B.; Norris, D.J.; Bawendi, M.G.; *J. Am. Chem. Soc.*, **1993**, 115, 8701-15
20. Alivisatos, A.P., *J. Phys.Chem.*, **1996**, 100, 13226-29
21. Eailey, R.E.; Smith, A.M.; Nie, S.M., *Physica E,* **2004**, 25, 1-12,
22. Striolo, A.; Ward, J.; Prausnitz, J.M.; Parak, W.J.; Zanchet, D.; Gerion, D.; Milliron, D.; Alivisatos, A.P. *J. Phys. Chem. B.*, **2002**, 106, 5500-5505
23. Leatherdale, C.A., Woo, W.K.; Mikulec, F.V.; Bawendi, M.G., *J. Phys. Chem. B.*, **2002**, 106, 7619-7622
24. Parak, W.J.; Pellogrino, T.; Plank, C., *Nanotechnology*, **2005**, 16, R9-R25
25. Dahan, M.; Laurence, T.; Pinaud, F.; Chemla, D.S.; Alivisatos, A.P., *Opt. Lett,* **2001**, 26, 825-27
26. Hohng, S., Ha, T., *J. Am. Chem. Soc.*, **2004**, 126, 1324-25
27. Michalet, X.; Pinaud, F., Lacoste, T.D.; Dahan, M.; Bruchez, M., *Single Mol.* **2001**, 2, 261-276
28. Wu, X.; Liu, H.; Liu, J.; Haley, K.N.; Treadway, J.A., *Nat. Biotechnol.*, **2003**, 21, 41-46
29. Xiao, Y.; Barker, P.E.; *Nucleic Acids Res.*, **2004**, 32, e28

30. Ness, J.M.; Akhtar, R.S.; Latham, C.B.; Roth, K.A.; *J. Histochem. Cytochem.*, **2003**, 51, 981-87
31. Jaiswal, J.K.; Mattoussi, H.; Mauro, J.M.; Simon, S.M.; *Nat. Biotechnol.,* **2003**, 21, 47-51
32. Hanaki, K., Momo A., Oku, T., Komoto, A., Maenosono, S., *Biochem. Biophys. Res. Commun.*, **302**, 496-501
33. Dubertret, B., Skourides, P., Norris, D.J., Noireaux, V., Brivanlou, A.H., Libchaber, A., *Science*, **2002**, 1759-62
34. Gaponik, N.; Talapin, D. V.; Rogach, A. L.; Eychmuller, A.; Weller, H.; *Nano Lett.* **2002**; *2(8);* 803-806
35. Ni, T.; Nagesha, D. K.; Robles, J.; Materer, N. F.; Mussig, S.; Kotov, N. A.; *J. Am. Chem. Soc.* **2002;** *124*(15); 3980-3992
36. Hirai, T.; Watanabe, T.; Komasawa, I. *J. Phys. Chem. B.* **1999**, 103 (46). 10120-10126
37. Farmer, S. C.; Patten, T. E.; *Chem. Mater.* **2001**; 13(11); 3920-3296
38. Mansur, HS, Vasconcelos WL, Grieser F, Caruso F. J. *Mater. Sci*. **1999**, 34 (21), 5285-5291
39. Zelner M, Minti H, Reisfeld R, Cohen H, Tenne R. *Chem. Mater*. **1997**, 9 (11), 2541-2543
40. Peng, Z. A.; Peng, X.; *J. Am. Chem. Soc.* **2001**; 123(1), 183-184
41. Peng, Z. A.; Peng, X. *J. Am. Chem. Soc.* **2001**; 123(7), 1389-1395
42. Yu, W. W.; Qu, L.; Guo, W.; Peng, X.; *Chem. Mater.* **2003**; 15(14); 2854-2860
43. Hines, M. A.; Guyot-Sionnest, P. *J. Phys. Chem*. **1996**, *100*, 468-471.
44. Dabbousi, B. O.; Rodriguez-Viejo, J.; Mikulec, F. V.; Heine, J. R.; Mattoussi, H.; Ober, R.; Jensen, K. F.; Bawendi, M. G. *J. Phys. Chem*. B **1997**, *101*, 9463-9475.
45. Li, J. J.; Wang, Y. A.; Guo, W.; Keay, J. C.; Mishima, T. D.; Johnson, M. B.; Peng, X.; *J. Am. Chem. Soc*. **2003**, *125*, 12567-12575
46. Mekis, I.; Talapin, D. V.; Kornowski, A.; Haase, M.; Weller, H. *J. Phys. Chem*. B **2003**,107, 7454-7464
47. Malik, M. A.; O'Brien, P.; Revaprasadu, N. *Chem. Mater*. **2002**, 14, 2004-2010
48. Mattoussi, H.; Mauro, J. M.; Goldman, E. R.; Anderson, G. P.; Sundar, V. C.; Mikulec, F. V.; Bawendi, M. G.; *J. Am. Chem. Soc.* **2000**, 122, 12142-12150 .
49. Pathak, S., Choi, S. K., Arnheim, N., Thompson, M. E., *J. Am. Chem. Soc.* **2001**, 123, 4103-4104 .
50. Guo, W.; Li, J.J.; Wang, Y.A.; Peng, X.; *Chem. Mater.,* **2003**, 15, 3125-3133
51. Chen, Y., Rosenzweig, Z.; *Anal. Chem.;* **2002**; *74*(19); 5132-5138
52. Pinaud, F., King, D., Moore, H.P., Weiss, S., *J. Am. Chem. Soc.* **2004**, 126, 6115.
53. Aldana, J.; Wang, Y.A.; Peng, S., *J. Am. Chem. Soc.*, **2001**, 123, 8844-8850
54. Yu, W.W.; Chang, E.; Drezek, R.; Colvin, V.L, *Biochem. Biophys. Res. Commun.*, **2006**, 348, 781-786
55. Mulvaney, P.; Liz-Marzan, L.M.; Giersig, M.; Ung, T., *J. Mater. Chem.,* **2000**, 10, 1259-1270
56. Gerion, D.; Pinaud, F.; Williams, S.C.; Parak, W.J.; Zanchet, D.; Weiss, S.; Alivisatos, A.P.; *J. Phys. Chem. B.*; **2001**, 105, 8861-8871
57. Nann, T.; Mulvaney, P.; *Angew. Chem. Int. Ed.*; **2004,** 43, 5393-5396

58. Rogach, A.L.; Nagesha, D.; Ostrander, J.W.; Giersig, M.; Kotov, N.A.; *Chem. Mater.*,**2000**, 12, 2676-2685
59. Alivisatos, A.P.; Gu, W.W.; Larabell, C., *Annu. Rev. Biomed. Eng.*, **2005**, 7, 55-76
60. Gao, X.; Cui, Y.; Levenson, R.M.; Chung, L.W.; Nie, S.; *Nat. Biotechnol.,* **2004**, 22, 969-976
61. Pellegrino, T.; Manna, L.; Kudera, S., Liedl, T.; Koktysh, D.; Rogach, A.L. Keller, S.; Raedler, J.; Natile, G.; Parak, W.J.; *Nano. Lett.,* **2004,** 4, 703-707
62. Fan, H.; Leve, E.W.; Scullin, C.; Gabaldon, J.; Tallant, D.; Bunge, S.; Boyle, T.; Wilson, M.C.; Brinker, C.J.; *Nano. Lett.*; **2005**, 5, 645-648
63. Goldman, E. R.; Balighian, E. D.; Mattoussi, H.; Kuno, M. K.; Mauro, J. M.; Tran, P. T.; Anderson, G. P. *J. Am. Chem. Soc.;* **2002**; *124*(22); 6378-6382.
64. Lingerfelt, B. M.; Mattoussi, H.; Goldman, E. R.; Mauro, J. M.; Anderson, G. P. *Anal. Chem.,* **2003**, *75*(16), 4043-4049.
65. Aoyagi, S.; Kudo, M.; *Biosens Bioelectron.* **2005** 15; 20(8):1680-4.
66. Ravindran, S.; Kim, S.; Martin, R.; Lord, E. M.; Ozkan, C. S.; *Nanotechnology* **2005**, 16(1), 1-4.
67. Zhang, Y.; So, M.-k.; Loening, A. M.; Yao, H.; Gambhir, S. S.; Rao, J. *Angewandte Chemie, International Edition* **2006,** 45(30), 4936-4940.
68. Tholouli, E. ; Hoyland, J. A.; Di Vizio, D.; O'Connell, F.; MacDermott, S. A.; Twomey, D.; Levenson, R.; Yin, J. A. Liu; G., Todd R.; Loda, M.; Byers, R. *Biochem. Biophys. Res. Commun.*, **2006**, 348(2), 628-636.
69. Srinivasan, C.; Lee, J.; Papadimitrakopoulos, F.; Silbart, Lawrence K.; Zhao, M.; Burgess, D. J. *Molecular Therapy*, **2006**, 14(2), 192-201.
70. Crut, A.; Geron-Landre, B.; Bonnet, I.; Bonneau, S.; Desbiolles, P.; Escude, C., *Nucleic Acids Research*, **2005**, 33(11), e98/1-e98/9.
71. Gill, R.; Willner, I.; Shweky, I.; Banin, U., *J. Phys. Chem. B* **2005**, *109*, 23715-23719.
72. Zhang, C.Y.; Yeh, H.C.; Kuroki, M.T.; Wang, T.H. *Nature Materials* **2005**, *4*, 826-831.
73. Medintz, I.L.; Goldman, E.R.; Lassman, M.E.; Mauro, J.M. *Bioconj. Chem.* **2003**, *14*, 909-918.
74. Patolsky, F.; Gill, R.; Weizmann, Y.; Mokari, T.; Banin, U,; Willner, I. *J. Am. Chem. Soc.* **2003**, *125*, 13918-13919.
75. Kim, J.H.; Morikis, D.; Ozkan, M. *Sensors Actuators B-Chemical* **2004**, *102*, 315-319.
76. Medintz, I.L.; Clapp, A.R.; Melinger, J.S.; Deschamps, J.R.; Mattoussi, H. *Adv. Mat.* **2005**, *17*, 2450-2455.
77. Pons, T.; Medintz, I.L.; Wang, X.; English, D. S.; Mattoussi, H., *J. Am. Chem. Soc.*, **2006**, 128(47), 15324-15331
78. Dubertret, B.; Skourides, P.; Norris, D. J.; Noireaux, V.; Brivanlou, A. H.; Libchaber, A. *Science* **2002**, 298(5599), 1759-1762.
79. Wu, X.; Liu, H.; Liu, J.; Haley, K.N.; Treadway, J.A.; Larson, J. P.; Ge, N.; Peale, F.; Bruchez, M. P. *Nature Biotechnology* **2003**, 21(1), 41-46
80. Fu A.; Gu W.; Larabell C.; Alivisatos A. P. *Current opinion in neurobiology*, **2005**, 15(5), 568-75.
81. Smith, A. M.; Dave, S.; Nie, S.; True, L.; Gao, X. *Expert Review of Molecular Diagnostics* **2006**, 6(2), 231-244.

82. Weng, J.; Song, X.; Li, L.; Qian, H.g; Chen, K.; Xu, X.; Cao, C.i; Ren, J.. *Talanta* **2006**, 70(2), 397-402
83. Akerman, M. E., Chan, W. C. W., Laakkonen, P., Bhatia, S. N., Ruoslahti, E., *P. N. A. S. U. S. A.* **2002,** 99, 12617-12621
84. Larson, D.R.; Zipfel, W. R.; Williams, R. M.; Clark, S. W.; Bruchez, M.l P.; Wise, F. W.; Webb, W. W.; *Science* **2003**, 300(5624), 1434-1437.
85. Hoshino, A.; Hanaki, K.; Suzuki, K.; Yamamoto, K. *Biochemical and Biophysical Research Communications* **2004**, 314(1), 46-53.
86. So, M.-K.; Xu, C.; Loening, A.M.; Gambhir, S. S.; Rao, J. *Nature Biotechnology* **2006**, 24(3), 339-343.
87. Cai, W.; Shin, D.-W.; Chen, K.; Gheysens, O.; Cao, Q.; Wang, S..; Gambhir, S.S.; Chen, X.. *Nano Letters* **2006**, 6(4), 669-676.
88. Clapp, A.R.; Medintz, I.L., Mattoussi, H., *Chemphyschem*. **2006**; 7:47-57
89. Clapp, A. R.; Medintz, I. L.; Mauro, J. M.; Fisher, B. R.; Bawendi, M. G.; Mattoussi, H., *J. Am. Chem. Soc.*; **2004;** 126(1); 301-310
90. Willard, D.M.; Van Orden, A.; *Nat. Mater.*, **2003**, 2 (9): 575-576
91. Kagan, C.R.; Murra, C.B.; Bawendi, M.G. *solids. Phys. Rev. B-Condens. Matt.* **1996**; 54, 8633-8643
92. Kagan, C.R.; Murray, C.B.; Nirmal, M, Bawendi, M.G. *Phys.Rev.Lett.* **1996**; 76, 1517-1520
93. Willard, D.M., Carillo, L.L., Jung, J., Orden, A.V. *Nano Lett.*, **2001;** 1, 469-474.
94. Finlayson, C.E., Ginger, D.S., Greenham, N.C. *Chem.Phys.Lett.* **2001**; 338, 83-87
95. Mamedova, N.N., Kotov, N.A., Rogach, A.L., Studer, J. *Nano Lett.* **2001**; 1, 281-286
96. Medintz, I.L.; Clapp, A.R.; Matoussi, H.; Goldman, E.R.; Fisher, B.; Mauro, J.M., *Nat. Mater.* **2003**, 2, 630-638
97. Goldman, E.R.; Medinta, I. L.; Whitley, J. L., *J. Am. Chem. Soc.***, 2005**; 127, 6744-6751.
98. Goldman, E. R.; Clapp, A. R.; Anderson, G. P.; Uyeda, H. T.; Mauro, J. M.; Medintz, I. L.; Mattoussi, H. *Anal. Chem.;* **2004**; 76(3), 684-688
99. Xu, C.; Xing, B.; Rao, J.; *Biochem. Biophys. Res. Commun.,* **2006**; 344, 931-935
100. Chang, E.; Miller, J.S.; Sun, J., et al. *Biochem. Biophys. Res. Commun.* **2005**; 334(4), 1317-1321.
101. Zhang, C.Y.; Yeh, H.C.; Kuroki, M.T.; Wang, T.H., *Nat. Mater.,* **2005**; 4,826-831.
102.Bakalova, R.; Zhelev, Z., Ohba, D.; Baba, Y., *J. Am. Chem. Soc.,* **2005**, 127,11328-11335.
103. Medintz, I.L.; Konnert, J.H.; Clapp, A.R.; *Proc. Natl. Acad. Sci. U.S.A.* **2004**, 101, 9612-9617
104. Nie, S.M.; Xing, Y.; Kim, G.J.; Simons, J.W., *Annu. Rev. Biomed. Eng.,* **2007**, 9: 12.1-12.32
105. Kaul, Z.; Yaguchi, T.; Kaul, S.C.; Hirano, T.; Wadhwa, R.; Taira, K.; *Cell Res.*, **2003**, 13, 503-7
106. Tokumasu, F.; Dvorak, J.; *J. Microsc.,* **2003**, 211, 256-61
107. Lidke, D.S.; Nagy, P.; Heintzmann, R.; Arndt-Jovin, D.J.; Post, J.N.; Grecco, H.E.; Jares-Erijman, E.A.; Jovin, T.M.; *Nat. Biotechnol.,* **2004**, 222, 198-203
108. Dahan, M.; Levi, S.; Luccardini, C.; Rostaing, P.; Riveau, B.; Triller, A.; *Science,* **2003**, 302, 442-45

109. Rosenthal, S.J.; Tomlinson, A.; Adkins, E.M.; Schroeter, S.; Adams, S.; *J.Am. Chem. Soc.,* **2002**, 124, 4584-94
110. Minet, O.; Dressler, C.; Beuthan, J.; *J. Fluoresc.*, **2004**, 14, 241-47
111. Ramachandran, S.; Merrill, N.E.; Blick, R.H.; Van der Weide, D.W.; *Biosens. Bioelectron.*, **2005,** 20, 2173-2176
112. Mattheakis, L.C.; Dias, J.M.; Choi, Y.J.; Gong, J.; Bruchez, M.P.; Liu, J.; Wang, E.; *Anal. Biochem.*, **2004**, 327, 200-8
113. Delehanty, J.B.; Medintz, I.L.; Pons, T.; Brunel, F.M.; Dawson, P.E.; Mattoussi, H.; *Bioconjugate Chem.,* **2006**, 17, 920-927
114. Chen, F.; Gerion, D.; *Nano Lett.*, **2004**, 4, 1827-1832
115. Rozenzhak, S.M.; Kadakia, M.P.; Caserta, T.M.; Westbrook, T.R.; Stone, M.O.; Naik, R.R., *Chem. Commun.*, **2005**, 2217-2219
116. Parak, W.J.; Boudreau, R.; LeGros, M.; Gerion, D.; Zanchet, D.; *Adv. Mater.* , **2002**, 14, 882-85
117. Ballou, B.; Lagerholm, B.C.; Ernst, L.A.; Burchez, M.P.; Waggoner, A.S.; *Bioconju.Chem.*, **2004**, 15, 79-86
118. Rhyner, M.N.; Smith, A.M.; Gao, X.H; Mao, H.; Yang, L.; Nie, S.M.; *Nanomedicine,* **2006**, 1, 209-217
119. Cai, W.B.; Hsu, A.R.; Li, Z.B.; Chen, X.Y.; *Nanoscale Res. Lett*, **2007**, 2(6), 265-281

CHAPTER 2 EXPERIMENTAL

This chapter describes the general experimental information, which includes chemicals and supplies, instrumentation for characterization, and the cell culture procedures. The specific and detailed experimental procedures will be discussed in the appropriate chapter.

2.1 Chemicals and supplies

Cadmium oxide (CdO, Sigma), lauric acid (Sigma), trioctylphosphine (TOP, Sigma), trioctylphophine oxide (TOPO, Sigma), hexadecylamine (HDA, Sigma), selenium powder (Sigma), diethylzinc ($Zn(Et)_2$, Sigma), hexamethyldisllathiane ($(TMS)_2S$, Sigma), chloroform (Sigma), methanol (Sigma), peptide RGDC (American Peptide Company), dimethyl sulfoxide (DMSO, Sigma), tetramethylammonium hydroxide pentahydrate (TAMOH, Sigma), pyridine (Sigma), Rhodamine Red^{TM}-X, succinimidyl ester 5-isomer (Rhodamine, Invitrogen), trypsin from porcine pancreas (trypsin, Sigma), collagenase (Sigma), urease (Sigma), 1,10-phenantroline (Sigma), 4-(2-Aminoethyl) benzene-sulfonyl fluoride hydrochloride (Sigma), 4-Amidinophenylmethane-sulfonyl fluoride hydrochloride (Sigma), Dulbecco's PBS buffer solution at pH 7.4 (1X) (2.67 mM KCl, 1.47 mM KH_2PO4, 137.93 mM NaCl, and 8.06 mM $Na_2HPO_4{\cdot}7H_20$) (Invitrogen), HTB126 breast cancer cells (ATCC), HTB125 normal breast cells (ATCC), Dulbecco's modified Eagle's medium (Invitrogen), Dulbecco's PBS buffer (Invitrogen), Fetal bovine serum (Invitrogen), Trypsin-EDTA (Invitrogen), L-glutamine (Invitrogen), sodium

pyruvate (Invitrogen), Epidermal Growth Factor(EGF, Invitrogen), Sodium Bicarbonate(sigma), Bovine Insuline(invitrogen), Hybri-care cell culture media(ATCC), trypan blue (invitrogen), Mercaptohexadecanoic acid (MHDA, Sigma), Metallothionein(MT, Sigma), Aminobenyl-EDTA(Sigma), Glutaraldehyde(Sigma), Sodium cyanoborohydride(Sigma) , manganese chloride (Sigma), Calcium chloride (J.T. Barker), ferrous ammonium sulfate (Mallinckrodt), Zinc chloride(E.M), cupric sulfate pentahydrate (E.M), ferric chloride (Sigma), Sodium Chloride(E.M), Sodium fluoride (E.M.), ethylenediaminetertaacetic acid disodium salt dehydrate (EDTA, J. R. Barker), 3-hydroxy-1,2-dimethyl-4(*1H*)-pyridone(HPO, Sigma), 3-(N-Morpholino) propanesulfonic acid (MOPS, USB), sodium hydroxide (sigma), hydrogen chloride acid (sigma),

All aqueous solutions were prepared with 18 MΩ deionized water produced by a water purification system (Barnstead Thermolyne Nanopure) and all chemicals were used as received without further purification. Amicon Centricon YM30 spin dialysis tubes were purchased from Microcon. Microscope glass cover slips used for microscopy and Lab-Tek II chambered coverglass were purchased from VWR.

2.2. Characterization

2.2.1. Absorption Spectra

Absorption spectra of free quantum dots in solution and their nanoassemblies were obtained in two systems: a Varian UV-VIS-NIR spectrophotometer system (CARY 500 Scan), and a SpectraMax M2 microplate reader (Molecular Devices, Inc.).

2.2.2. Fluorescence Emission Spectra

Emission spectra of free quantum dots solution and their nanoassemblies were taken in a quartz cuvette using a spectrofluorometer (PTI International, Model QM-1), or LS 55 Luminescence spectrometer (Perkin Elmer), both equipped with a 75-W continuous Xe arc lamp as a light source.

2.2.3. Digital Fluorescence Imaging Microscopy and Spectroscopy

Emission spectra and images of free quantum dots solution and their nanoassemblies were obtained using digital luminescence imaging microscopy and spectroscopy system, equipped with a 100 W mercury lamp as a light source. Emission spectra were measured by Olympus (IX-71) inverted fluorescence microscope equipped with a 250 mm spectrograph and a high performance 16-bit back-illuminated CCD camera (Roper Scientific) The Roper Scientific software Win Spec/32 was used for spectral analysis. Images were monitored by Olympus (IX-71) inverted fluorescence microscope equipped with a high performance color CCD camera (Olympus DP 70). The software Image-pro Plus was used for image analysis. A filter cube containing a 425 ±20 nm band-pass excitation filter, a 465 nm dichroic mirror, and a 475nm long pass emission filter was used to ensure spectral purity. The spectra and images were taken through 10X, 20X, and 40X objectives with numerical apertures of 0.3, 0.5, and 0.9, respectively.

2.3. Cell culture of HTB 125 and HTB 126

2.3.1. Cell maintenance

HTB 125 is a normal breast cell line and HTB 126 is one type of breast cancer cells. These two cell lines were used to study extracellular MMPs activity. The cells were maintained following protocols provided by the American Type Tissue Culture Collection (ATCC). For HTB125, the media was specially prepared by Hyclone in order to have the same composition as the Hybri-care cell culture media used by ATCC but without phenol red. The basic media was supplemented by adding 30 ng/mL of EGF, 1.5 g/L of Sodium Bicarbonat,e and 10% of Fetal Bovine Serum Qualified. For HTB126, 4 mM of L-glutamine, 0.01 mg/mL of Bovine Insuline, and 10% of Fetal Bovine Serum were added to DMEM supplemented media used as growth media. The cells were grown at 37^0C under 5% CO_2. The medium was renewed every 3 days. Cell cultures were planted in a 4-well chamber. The following procedures describe the cell preparation steps of trypsinizing the cells, counting the cells, and planting the cells.

2.3.2 Trypsinization

5 mL of Trypsin-EDTA was added to the confluent 75 cm^2 T-culture flask and, after a brief washing of the cells surface, the trypsin was removed and discarded. Thus, 5 mL of Trypsin-EDTA was added to the flask. The flask was put in the incubator (37 ^{0}C) for 10-15 minutes, or until we see the cells detached from the flask surface. The trypsinized cell suspension were homogenized with a 5 mL pipette and 1-2 mL of this cell suspension were transferred for a new 75 cm^2 T-culture flask, The cells were dispersed in 25 mL of culture growing media and incubated at 37 ^{0}C and 5% CO_2.

2.3.3 Counting

200 μL of the cell suspension solution was mixed very well with 200 μL of trypan blue, and then 12 μL of the mixed solution was injected into the hemacytometer. The hemacytometer was placed under the microscope to count the number of cells. If the number of cells counting on the hemacytometer is X, the number of the cells/mL is 20,000 times of X.

2.3.4 Planting

Cell suspension (10^6 cells/mL) was seeded onto a glass slide chamber. Then, 1 mL of growth media was added to the chamber it was incubated at 37 ^{0}C under 5% CO_2 for 48 hours to reach 90% confluence in order to realize a fully-developed extracellular matrix.

CHAPTER 3 QUANTUM DOTS FRET BASED PROTEASE SENSOR

3.1 Introduction

My PhD study targets a unique family of enzymes called matrix metalloproteinases (MMPs). MMPs are nautral proteinases that share a common modular domain structure and are capable of degrading the extracellular matrix (ECM) components (1-3). The main components of ECM are various glycoproteins, proteoglycans and hyaluronic acid. The most abundant glycoproteins in the ECM are collagens. There are over 20 different enzymes in the MMP family. Most MMPs appear to be secreted from cells in their inactive form, making their activation a key step in regulating the amount of degradative activity outside the cells. MMPs have the following functions: i) they regulate the level of ECM degradation and remodelling; ii) they participate in mechanisms enabling cell migration, wound healing, and angiogenesis; iii) they activate other MMPs; iv) they release or activate growth factors and other bioactive molecules. The motivation to target MMPs and develop sensors to detect their activity arises from their largely higher level in tumors compared to normal tissues. Numerous studies have shown a correlation between the expression of MMPs and the invasive behavior and metastasis potential of tumors (4, 5). For example, MCF-7 breast cancer cells in culture produce both soluble and membrane-bound factors that stimulate the production of pro-MMPs (6). A higher level of MMP1 was found in the breast cancer cell lines MDA-MB-231 and MCF-7 compared to normal breast cell lines (7). Clearly, it is of high importance to develop tools for the measurement of MMPs as a mean for the detection of breast cancer cells in biopsies. A variety of methods and probes were previously developed to detect and enable better

understanding of the functions of MMPs in cancer development. These include the design of biocompatible near infrared fluorochromes, novel imaging probes specific to MMPs, fluorescent nanoparticles and fluorescence molecular tomography (FMT) (8, 9). Recently Bremer and co-workers described a probe which is based on FRET between organic fluorophore donor and acceptor molecules via a peptide linker that is amenable to cleavage by MMPs (10). Here, we take advantage of quantum dots as FRET donors in place of organic dyes and we have designed quantum dot FRET based probes to real time monitoring of MMPs in cell cultures and effectively discriminate between MMPs activity in normal and cancerous breast cell cultures.

As we discussed in the chapter 1, quantum dots based FRET biosensors have been devised over the past few years. Recently, quantum dots were linked to peptide molecules that were labeled with quenchers or molecular acceptors were used probes for proteolytic activity (11-13). West and her coworkers first developed protease probes for collagenase based on the FRET between quantum dots and gold nanoparticles via a proteolytically degradable peptide linker (11). They reported a 52% rise in luminescence of quantum dots over 47 hours of exposure to 0.2 mg/mL collagenase. The quenching mechanism is still not clear. Possibly, the response time of these probes was long due to aggregation of the quantum dots-gold nanocrystals clusters that do not involve peptide linking and steric hindrances that decrease the rate of enzymatic cleavage of molecular peptides trapped between the larger nanoparticles. Also, the use of gold as FRET acceptor will not allow the use of ratiometric detection due to the absence of re-emission of gold nanoparticle. Mattoussi and coworkers recently developed a modular peptide structure that allowed the attachment of dye-labeled substrates for proteases to the surface of luminescent quantum

dots. The researchers used these dye-labeled quantum dots in proteolytic assays that were carried out under both excess enzyme and excess substrate conditions. The assays provided quantitative data including enzymatic velocity, Michaelis-Menten kinetic parameters, and mechanisms of enzymatic inhibition (12). Mattoussi and co-workers also reported a detailed mechanistic study that aimed to understand the mechanism of fluorescence resonance energy transfer between quantum dots and linked molecular acceptors (13). The researchers concluded that FRET between quantum dots and linked molecular acceptors could be described using the Forester FRET theory. It seems that due to their nanometric dimensions, quantum dots can be described, at first approximation, as point dipoles. Therefore, the distance between quantum dots and linked molecular acceptors can be measured from the center of the quantum dots to the molecular acceptors adsorbed to the quantum dot surface. It should be mentioned however, that other factors like the shape of the quantum dots and the nature of the shell separating the quantum dots and molecular acceptors could affect the distance dependence of the FRET efficiency in this system. More studies are needed to fully understand the mechanism of FRET between nanoparticle donors like quantum dots and molecular acceptors.

Here, we developed a quantum dots based FRET protease sensor with the capability to monitor the enzyme activity in real time. In these probes, rhodamine molecules are attached to the surface of the quantum dots and used as molecular acceptors. Quantum dots-molecular acceptor systems are advantageous because of the simultaneous emission increase and decrease of the emission of quantum dots and molecular acceptors, which enables a ratiometric analysis method and results in high quantitative power. A schematic diagram of the quantum dot FRET based protease probes is shown in scheme 3.1. To

fabricate the quantum dots FRET based probes CdSe/ZnS quantum dots capped with tri-octyl phosphine oxide (TOPO) molecule were modified by exchanging the TOPO ligands with tetra peptide RGDC (Arginine-Glycine-Aspartic acid-Cysteine) molecules to form water-soluble quantum dots. The peptide molecules were bound to the ZnS shell of the CdSe/ZnS quantum dots through the thiol group of cysteine (C). The peptide-coated quantum dots were labeled with Rhodamine Red™-X succinimidyl ester through the formation of amide bonds with the amino terminals of the coating peptides to form the quantum dots based FRET probes. In these FRET probes the quantum dots served as donors and the attached rhodamine molecules as acceptors. The emission of the quantum dots was quenched and the emission of the attached rhodamine molecules increased due to FRET between the quantum dots and the rhodamine molecules. Upon cleavage by enzymes the rhodamine molecules were removed from the surface of the quantum dots, which resulted in an increase in the emission peak of the quantum dots and a corresponding decrease in the emission of the displaced rhodamine molecules due to a decrease in FRET efficiency between the quantum dots and rhodamine molecules. The quantum dots based probes were first applied for detecting enzyme activity and for screening enzyme inhibitors in solution. Then, they were also used for the measurement of extracellular matrix metallproteinases (MMPs) activity in normal and cancerous breast tissue. The probes were able to discriminate between normal and cancerous cells primarily because of the difference in the proteolytic activity of their extracellular matrices.

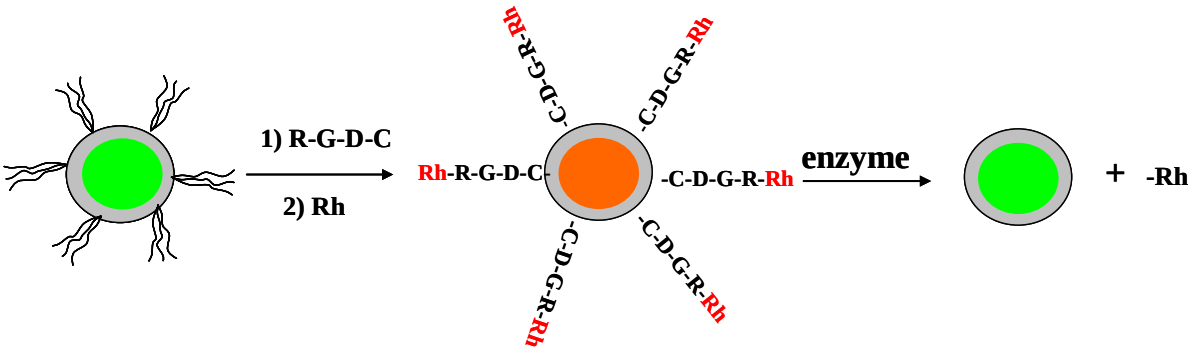

Scheme 3.1 Schematic representation of quantum dots FRET based protease sensor

3.2 Experimental

3.2.1 Synthesis of TOPO coated quantum dot

TOPO capped CdSe/ZnS quantum dots were prepared following a method developed by Peng with slight modifications (14, 15). Briefly, 12.7 mg CdO and 160 mg lauric acid were mixed under nitrogen for half hour. The mixture was heated to >200 °C to fully dissolve the cadmium oxide until a clear colorless solution was formed. Then, 1.94 g TOPO and 1.94 g hexadecylamine (HDA) were added to the solution under stirring and the temperature was increased to 280°C. Then, 80 mg selenium powder dissolved in 2ml solution of trioctylphosphine (TOP) was rapidly injected into the solution under vigorous stirring. The mixture was cooled to ~200 °C and kept at this temperature for 3 minutes. Then, a 2 ml TOP solution containing 250 µl hexamethyldisilathiane ($(TMS)_2S$) and 1 ml diethylzinc ($Zn(Et)_2$) was premixed well under nitrogen and gradually injected into the

solution. The injection took about 1 minute to complete. The reaction mixture was kept at 180°C for one hour. The solution was then cooled to room temperature and the resulting sample of CdSe/ZnS quantum dots was washed three times with methanol and re-dissolved in chloroform.

3.2.2 Synthesis of peptide coated quantum dots

The ligand exchange reaction used to replace the TOPO ligands with RGDC was carried out in a mixture of pyridine and dimethyl sulfoxide following a method first reported by Pinaud and coworkers (16). 1mL of 1μM TOPO coated CdSe/ZnS quantum dots were precipitated with methanol and re-dissolved in 2ml 9:1(V/V) pyridine:DMSO cosolvent. The use of this co-solvent effectively prevented aggregation of quantum dots during the reaction. Then, 200ul 5mg/mL peptide in DMSO was added to the reaction mixture. The pH was adjusted to 10 by adding tetra-methyl ammonium hydroxide (TAMOH) 20% (w/v) in methanol to the reaction mixture. The TAMOH molecules were used to form anionic cysteine thiolates to facilitate binding of the peptide to the CdSe/ZnS quantum dots through the cysteine residues (17). The peptide coated quantum dots were vortexed for 30 minutes, centrifuged, and re-suspended in DMSO. Then the solution was centrifuged and redissolved in Dulbecco's PBS buffer solution at pH 7.4. Unbound peptide molecules were removed by two repeated cycles of spin dialysis using an Amicon Centricon spin dialysis tube with a cutoff molecular weight of 30kDa (Microcon YM30, Millipore Corp.). In each spin dialysis cycle, the sample was centrifuged at 2000 rpm for 20 minutes and washed with the Dulbecco's PBS buffer

solution at pH 7.4. The peptide coated quantum dots were kept at 4°C in the Dulbecco's PBS buffer solution at pH 7.4 until used.

3.2.3 Conjugation of Rhodamine to the peptide coated quantum dots

Rhodamine labeled peptide-coated quantum dots were prepared by adding 150 μL of 0.1 μM peptide coated quantum dots and varying volumes (0 μL to 150 μL) of 4.8 μM Rhodamine Red™-X, succinimidyl ester to a PBS buffer solution of pH 7.4 to a final volume of 1.5 mL. Succinimidyl ester is a good leaving group and it undergoes nucleophilic attach by the amine group in a peptide. The reaction mixture was incubated for 1 hour at room temperature.

3.2.4 Enzyme activity and inhibition assays of trypsin

Rhodamine-labeled peptide-coated quantum dots that were prepared in solution containing a rhodamine:quantum dots ratio of 48:1 were used as our FRET-based enzymatic activity probes. 500 μL of 10nM quantum dot FRET based probes and varying volumes ranging from 0 μl to 500 μL of 1 mg/mL trypsin were added to Dulbecco's PBS buffer solution at pH 7.4 to a final volume 1.0 mL. Time dependent spectral measurements were carried out following the addition of trypsin using a fluorescence spectrometer or a digital fluorescence spectral imaging system. Inhibition assays were performed in a chambered cover glass (LabTek) and were monitored using digital fluorescence imaging microscopy and spectroscopy. To carry out the inhibition assay, 250 μL of 1 mg/mL trypsin were added to Dulbecco's PBS buffer solution at pH 7.4 that contained inhibitors of various concentrations to a total volume of 500 μL. Following 30

minutes incubation 500μL of 10nM quantum dot FRET-based probes were added to the mixture and FRET measurements were carried out to monitor the enzymatic reaction.

3.2.5 Enzyme activity of collageanse

500 μL of 10nM quantum dot FRET based probes and varying volumes ranging from 0 μl to 50 μL of 100 μg/mL collgenase were added to Dulbecco's PBS buffer solution at pH 7.4 to a final volume 1.0 mL. Time dependent spectral measurements were carried out following the addition of collagenase using a fluorescence spectrometer.

3.2.6. Cell analysis

Qualified 10^6 cells/mL were seeded and cultured on glass slides for 48 hours to reach 90% confluence in order to realize a fully developed extracellular matrix. The cells were kept at 37^0C under 5% CO2. The cells were washed with Dulbecco's PBS buffer, and then quantum dots protease probes were added and analyzed by digital fluorescence microscopy.

3.2.7 Fluorescence Spectroscopy Measurements

Emission spectra of TOPO coated quantum dots, peptide coated quantum dots and quantum dots-peptide-rhodamine conjugates were measured using a spectrofluorometer (PTI International, Model QM-1), equipped with a 75-W continuous Xe arc lamp as a light source. All samples were excited at 445 nm, which is near the minimum of the rhodamine absorption spectrum in order to reduce interference from direct excitation of rhodamine. Emission scans were measured from 480nm to 700nm in a 1-cm cell.

3.2.8. Digital Fluorescence Imaging Microscopy and Spectroscopy

Emission spectra of the quantum dot FRET probes were carried out using an Olympus (IX-71) inverted fluorescence microscope equipped with a 250 mm spectrograph and a high performance 16-bit back illuminated CCD camera (Roper Scientific). The Roper Scientific software Win Spec/32 was used for spectral analysis. Emission images of quantum dots FRET probes were obtained using an Olympus (IX-71) inverted fluorescence microscope equipped with a high performance color CCD camera (Olympus DP 70). The software Image-pro plus was used for image. The spectra and images were taken through 10X and 20X objectives with numerical apertures of 0.3 and 0.5, respectively. A filter cube containing a 425 ±20 nm band-pass excitation filter, a 505 nm dichroic mirror, and a 515-nm long pass emission filter was used.

3.3 Results and discussion

3.3.1 Peptide coated quantum dots

Peptide coated quantum dots were synthesized as described in the experimental section. Figure 3.1a shows the emission spectra of 100nM solutions of TOPO and peptide coated quantum dots when excited at 445 nm. It can be seen that the emission intensity of the peptide coated quantum dots was four times lower than the emission intensity of TOPO coated quantum dots. Normalized emission spectra of TOPO and peptide coated quantum dots are shown in figure 3.1b. The emission spectra show negligible changes in the peak emission wavelength and bandwidth following the ligand exchange process.

Despite the significant reduction in emission quantum yield, which is typical to quantum dots when dispersed in aqueous media, the quantum dots were sufficiently luminescent to successfully prepare quantum dots based enzymatic activity probes. The ligand exchange method that was used in our experiments to coat the quantum dots with peptide molecules is a simple, one-step reaction that resulted in high-quality peptide coated quantum dots. As seen in figure 3.1b the photophysical properties of the quantum dots were not affected by the peptide coating. Additionally, the attachment of peptide molecules to the quantum dots enabled further conjugation of rhodamine to the amino terminals of the peptides.

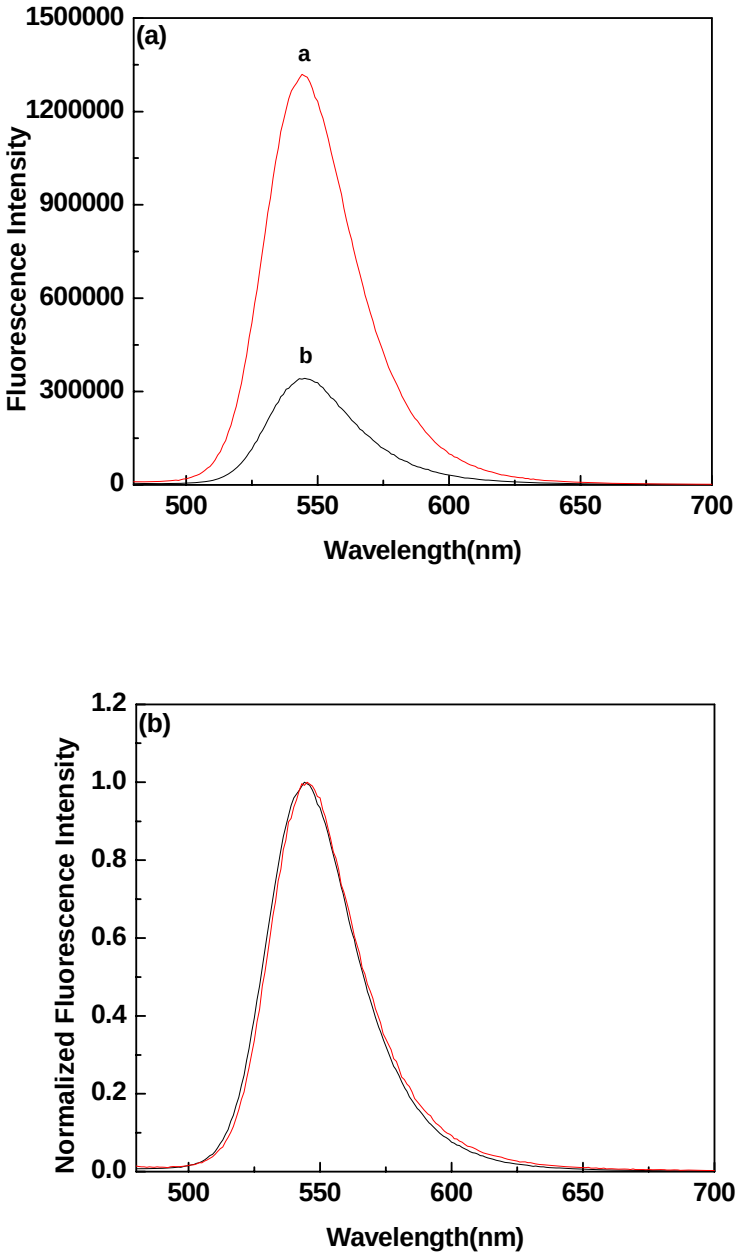

Figure 3.1 a) Emission spectra and b) normalized emission spectra of TOPO coated quantum dots (red) and peptide-coated quantum dots (black) (λex = 445 nm).

3.3.2 Conjugation of Rhodamine to the peptide coated quantum dots

Rhodamine molecules were conjugated to the peptide coated quantum dots as described in the experimental section. The effect of increasing concentration of rhodamine in the reaction mixture on the fluorescence resonance energy transfer (FRET) efficiency of the rhodamine labeled quantum dots is shown in figure 3.2a. When excited at 445 nm the emission spectra of the rhodamine labeled quantum dots show two clearly separated emission peaks of the quantum dots and the rhodamine molecules at 545 nm and 587 nm respectively. The emission peak of the quantum dots decreases with increasing rhodamine concentration indicating the occurrence of FRET between the quantum dots and the rhodamine molecules. The FRET efficiency increased with increasing rhodamine concentration and the effect leveled of at a rhodamine:quantum dots molar ratio of 48:1. Luminescent quantum dots that were prepared under this ratio conditions were later used as our FRET-based protease sensors. Control experiments showed that the emission intensity of solutions of similar rhodamine concentration in the absence of peptide coated quantum dots was 10 times lower than the intensity of the red emission peak at 587 nm of the rhodamine labeled quantum dots (shown in figure 3.2b). This is another indication that the large emission signal at 590 nm of quantum dot-rhodamine conjugate is a result of FRET between the quantum dots and bound rhodamine molecules.

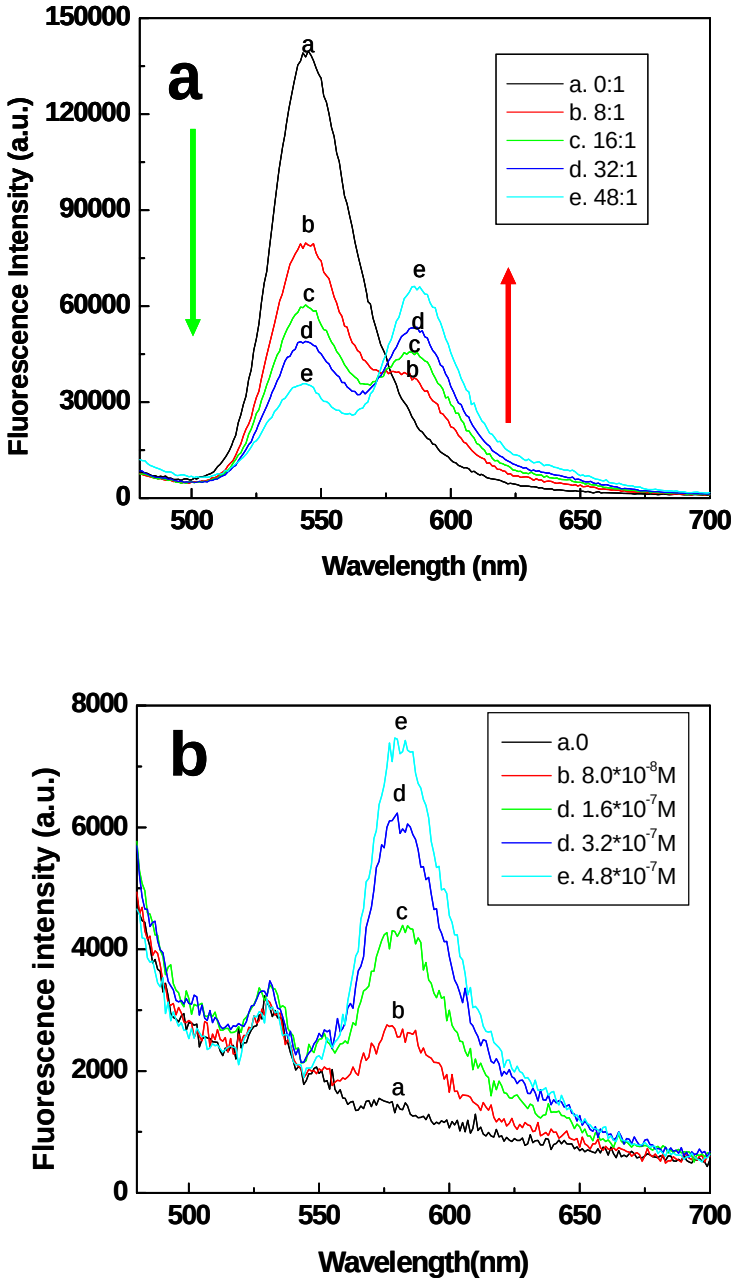

Figure 3.2 a) Emission spectra of rhodamine-labeled peptide-coated quantum dots at increasing the rhodamine to peptide coated quantum dots ratio: (a)0:1 (black),(b) 8:1 (red), (c)16:1 (green), (d)32:1 (dark blue), e)50:1 (light blue). b) Control experiments-the fluorescence spectra of a rhodamine solution of the same concentration used in a. (λex = 445 nm)

Figure 3.3 depicts the emission intensity of quantum dots decay percentage as a function of the rhodamine/quantum dots ratio. Here, F_{d0} is the emission intensity of quantum dots without labeling rhodamine and F_d is the emission intensity of quantum dots in rhodamine-labled-quantum dots conjugate. It was clearly shown that F_d/F_{d0} decrease as the increase of rhodamine/quantum dots ratio. For a 48:1 ratio of rhodamine: quantum dots, it indicates 75% quenching of quantum dots signal compared to unlabeled quantum dots. These results strongly suggest that FRET is the primary mechanism for the reported observations.

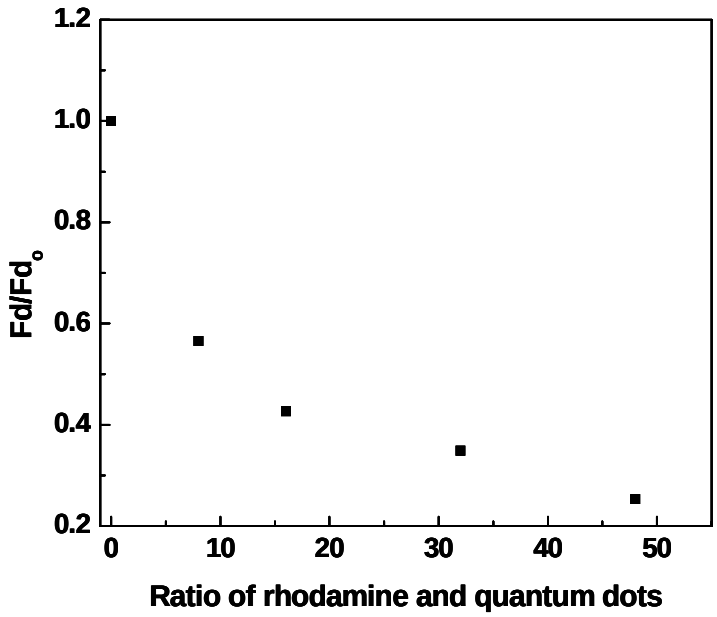

Figure 3.3 The emission intensity of peptide coated quantum dots decay percentage (F_d/F_{d0}) versus the ratio of rhodamine and quantum dots. F_{d0} is the emission intensity of quantum dots without labeling rhodamine and F_d is the emission intensity of quantum dots in rhodamine-labled-quantum dots conjugate.

FRET interactions between quantum dots and fluorescent acceptor molecules are not fully understood. Unlike FRET between donor and acceptor molecules, the distance between quantum dots and molecular acceptors is not well-defined. Our study shows that the FRET efficiency is high even when a short tetra-peptide links the quantum dots and the acceptor molecules. It is possible that the accumulative interaction between a single quantum dot and multiple acceptor molecules compensates for the low FRET efficiency between quantum dots and individual acceptor molecules when these are bound through a short linker.

3.3.3 Enzyme activity measurements

The quantum dots FRET-based enzymatic probes were used to determine the activity of the enzyme trypsin. Trypsin is a proteolytic enzyme with a molecular weight of 23,800 Daltons that cleaves proteins and peptides at the carboxyl end of lysine (K) and arginine (R). Emission spectra showing the effect of trypsin at increasing concentration on the emission of the quantum dot FRET probes are shown in figure 3.4a (λex = 445nm). The spectra were recorded 15 minutes after adding trypsin to the quantum dots solution. An increase in the quantum dots emission peak at 545 nm and a decrease in the rhodamine emission peak at 590 nm were clearly seen indicating a significant decrease in the FRET efficiency. Figure 3.4b describes the trypsin concentration dependence of the ratio F_d/Fa. F_d and F_a were the peak emission intensities of the quantum dot FRET-based probes when excited at 445 nm at 545 nm (quantum dot donors) and 590 nm (rhodamine

acceptors) respectively. The F_d/F_a ratio was normalized to $(F_d/F_a)_0$ which is the value of F_d/F_a prior to the addition of trypsin to the quantum dot FRET-based solutions. The trypsin concentration dependent FRET signal changes were attributed to the enzymatic cleavage of the peptide molecules which led to the expected release of rhodamine molecules from the quantum dots to the solution.

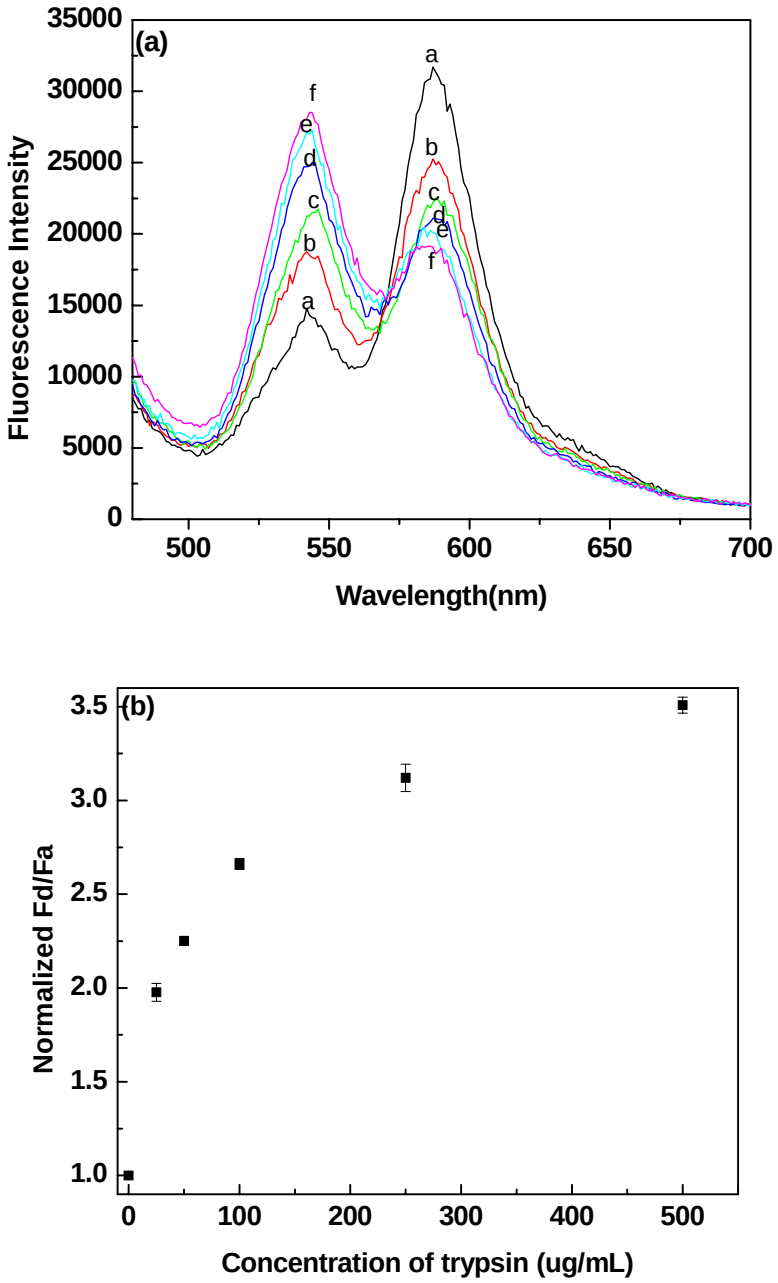

Figure 3.4 a) Emission spectra of the quantum dot FRET-based probes at increasing trypsin concentration: (a) 0µg/mL, (b) 25µg/mL, (c) 50µg/mL, (d) 100µg/mL, (e) 250µg/mL, (f) 500µg/mL. (λex = 445 nm). b) Trypsin concentration dependence of Fd/Fa , 15 minutes following the addition of trypsin to solutions of quantum dot based probes. Fd/Fa values were normalized to $(Fd/Fa)_0$, which is the ratio Fd/Fa prior to adding trypsin to the quantum dot probes solutions.

Time dependent measurements of the FRET signal at increasing trypsin levels were carried out to demonstrate the ability of the quantum-dots based probes to provide dynamic information over long observation times. Figure 3.5 shows the temporal dependence of the ratio F_d/F_a at increasing trypsin concentration ranging from 0 to 500 μg/ml (λex = 445 nm). The F_d/F_a ratio was normalized to $(F_d/F_a)_0$ which is the value of F_d/F_a prior to the addition of trypsin to the quantum dot FRET-based solutions. It can be seen that the ratio F_d/F_a increased faster at higher trypsin concentrations. For a concentration of 250 μg/ml trypsin the enzymatic reaction was completed in less than 15 minutes. As expected, the duration of the enzymatic assays increased with decreasing enzyme concentrations. It was possible to detect as low as 0.1 μg/mL, (4 picomol), in a 2-hour assay. The short assay time is a significant advantage over previously reported FRET based quantum dot probes in which longer reaction times were reported (11). Control experiments using solutions of quantum dots based probes in the absence of trypsin indicated insignificant changes in the FRET signal (F_d/F_a) over several hours. This supported our conclusion that the quantum dot FRET-based probes only responded to the proteolytic activity of trypsin.

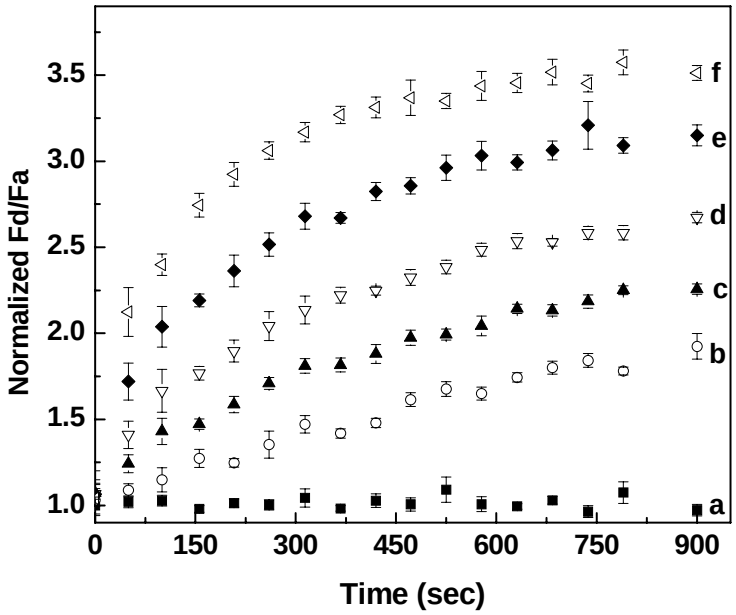

Figure 3.5 Temporal dependence of the rhodamine-labeled peptide-coated quantum dots at increasing trypsin concentration: (a) 0μg/mL, (b) 25μg/mL, (c) 50μg/mL, (d) 100μg/mL, (e) 250μg/mL, (f) 500μg/mL. The ratio F_d/F_a was normalized to $(F_d/F_a)_0$, which is the ratio F_d/F_a prior to adding trypsin to the quantum dot probes solutions.

Furthermore, to examine selectivity of these probes, we monitored the enzymatic activity of urease in the quantum dots based probes. We used the enzyme urease as a negative control to demonstrate the specificity of the quantum dots based enzyme probes. The enzyme ability comparison between trypsin and urease under the same concentration (50μg/mL) and under the same condition are showed in figure 3.6a (emission spectra) and figure 3.6b (temporal dependence). As a result, with a concentration of 50ug/mL trypsin, the emission intensity of quantum dots increases and the emission intensity of rhodamine decreases with time, after 15mins, the F_d/F_a increase from 0.4 to 0.90. On the other hand, with a concentration of 50ug/mL urease, the emission intensity of quantum

dots and rhodamine hardly change over 15mins. Both of the spectra and temporal dependence clearly demonstrated that the quantum dots based probe FRET efficiency is affected by trypsin and is not affected by urease or in the absence of proteases (Dulbecco's PBS buffer solution at pH 7.4).

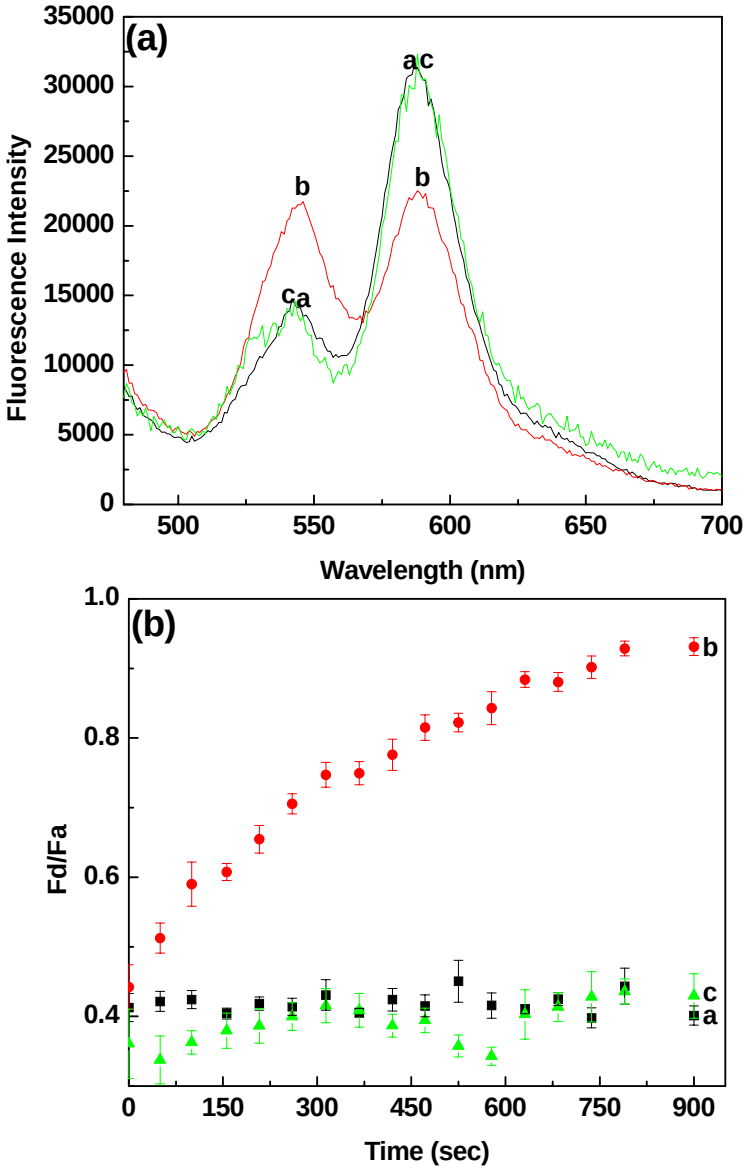

Figure 3.6 (a) Emission spectra and (b) Temporal dependence of the rodamine-labeled peptide-coated quantum dots with different enzyme: a) buffer (black), b) 50μg/mL trypsin(red), c) 50μg/mL urease(green).

Digital fluorescence images shown in figure 3.7 provided clear visual evidence of FRET between the quantum dots and the attached rhodamine and of the effect of trypsin on the FRET signal. Image 3.7a shows a digital fluorescence image of peptide coated quantum dots with their characteristic green emission. Image 3.7b shows the fluorescence image of the peptide coated quantum dots when labeled with rhodamine. The quantum dots emit yellow-orange light due to FRET between the quantum dots and rhodamine molecules. Image 3.7c shows the fluorescence image of the quantum dot FRET-based probes 15 minutes following the addition of 250 μL of 1 mg/mL trypsin. It can be seen that the emission color of the quantum dots turned green due to enzymatic cleavage of the RGDC peptide linker, which released rhodamine molecules to the solution and restored the green emission color of the quantum dots. It must be noted that the rate of enzymatic cleavage of a substrate consisting of a target peptide linking a quantum dot as a donor and a molecular acceptor would be lower than the rate of enzymatic cleavage of a target peptide linking between a molecular donor and a molecular acceptor. This is due to steric hindrances in the quantum dot/molecular acceptor system. However, the application of luminescent quantum dots as donors in FRET assays is advantageous due to the ability to link multiple acceptors to a single quantum dot, which, in turn, leads to larger FRET signal changes in enzymatic assays. Additionally, the high photostability of quantum dots enables highly sensitive real-time enzymatic assay in volume-limited samples and eventually in single cells.

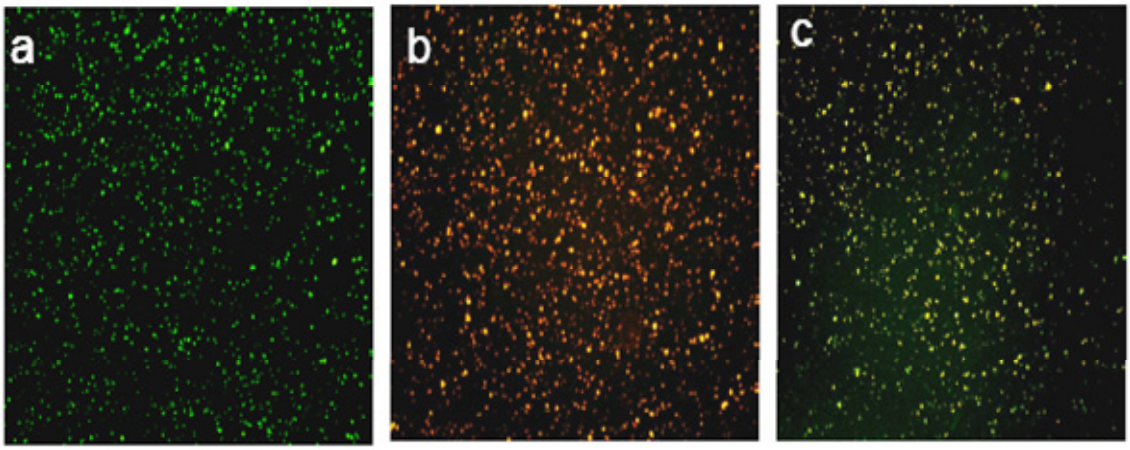

Figure 3.7 Digital fluorescence images of (a) peptide coated quantum dots showing green emission, (b) rhodamine-labeled peptide coated quantum dots showing yellow-orange emission due to FRET between the quantum dots and rhodamine molecules, (c) quantum dot FRET-based probes when incubated for 15 minutes in a solution of 250μg/mL trypsin showing green emission.

3.3.4 Screening enzyme inhibitors

To further demonstrate the utility of the quantum dots FRET-based enzymatic probes, we measured the inhibition efficiency of the trypsin inhibitors 4-(2-aminoethyl) benzene-sulfonyl fluoride hydrochloride, 4-amidinophenylmethane-sulfonyl fluoride hydrochloride and 1, 10-phenanthroline. 4-(2-Aminoethyl) benzene-sulfonyl fluoride hydrochloride and 4-amidinophenylmethane-sulfonyl fluoride hydrochloride are water-soluble, relatively non-toxic irreversible inhibitors of serine proteases (18, 19). 1, 10-phenanthroline is a reversible inhibitor of metallo-proteinases and metal activated proteinases (20). The structures of inhibitors are shown in figure 3.8.

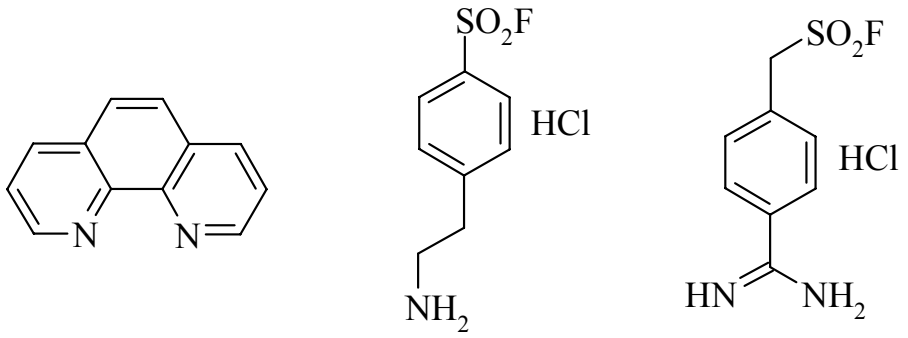

(1) **(2)** **(3)**

Figure 3.8 Structure of 4-(2-Aminoethyl) benzene-sulfonyl fluoride hydrochloride (**1**), 4-Amidinophenylmethane-sulfonyl fluoride hydrochloride (**2**) and 1,10- phenantroline (**3**) used for inhibition assay.

Figure 3.9 shows the temporal dependence of the ratio F_d/F_a of quantum dot FRET-based enzymatic probes in the presence of 250μg/mL trypsin and 4-(2-Aminoethyl) benzene-sulfonyl fluoride hydrochloride at increasing concentrations from 0 to 2.5 mg/mL. In the inhibition assays, the trypsin inhibitor was first incubated with 250 μL of 1 mg/mL trypsin for 30 minutes at room temperature. 500μL of 10nM quantum dot FRET-based probes were added to the solution and the fluorescence of the quantum dots was monitored using digital fluorescence spectroscopy. The rate of increase of the ratio F_d/F_a was found to be dependent on the concentration of the enzyme inhibitor. A level of 2.5

mg/mL 4-(2-aminoethyl) benzene-sulfonyl fluoride hydrochloride led to a 75% inhibition of trypsin activity.

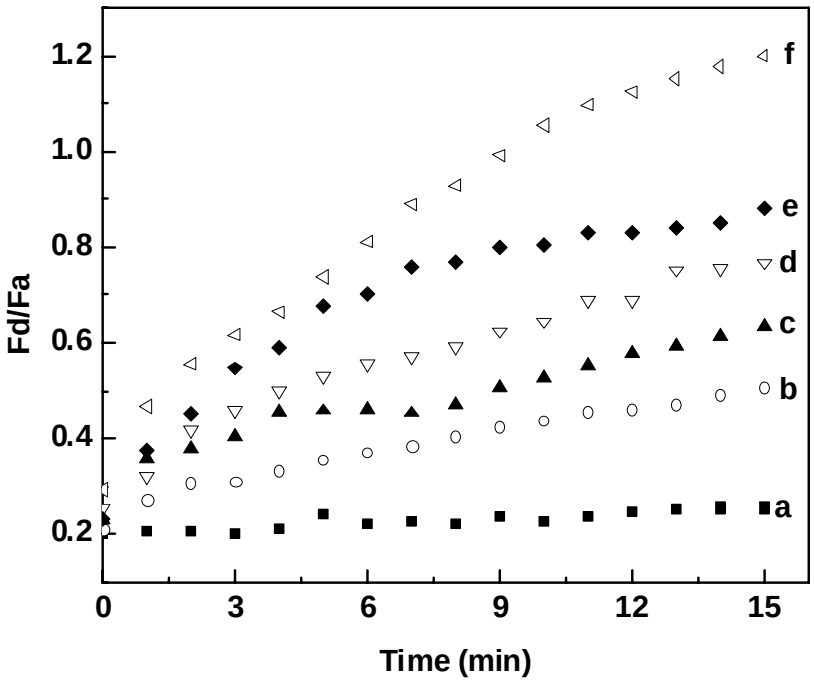

Figure 3.9 Temporal dependence of F_d/F_a in the presence of 250µg/mL trypsin and increasing concentrations of the trypsin inhibitor 4- (2-Aminoethyl) benzene-sulfonyl fluoride hydrochloride. a) a control experiment in the absence of trypsin and trypsin inhibitor, b) 2.50 mg/mL, c) 1.25 mg/mL, d) 250µg/mL, e) 50µg/mL, f) 0µg/mL.

A comparison between the inhibition efficiency of 4-(2-aminoethyl) benzene-sulfonyl fluoride hydrochloride, 4-amidinophenylmethane-sulfonyl fluoride hydrochloride and 1, 10-phenanthroline at 250 µg/mL is shown in figure 3.10, which describes the temporal

dependence of the FRET efficiency (F_d/F_a) of the quantum dot FRET-based probes in the presence of the tested inhibitors. It can be seen that, at this level, 1,10-phenanthroline completely inhibits trypsin activity. It can also be seen that the inhibition efficiency of 4-(2-aminoethyl) benzene-sulfonyl fluoride hydrochloride is 2.3-fold higher than the inhibition efficiency of 4-Amidinophenylmethane-sulfonyl fluoride hydrochloride.

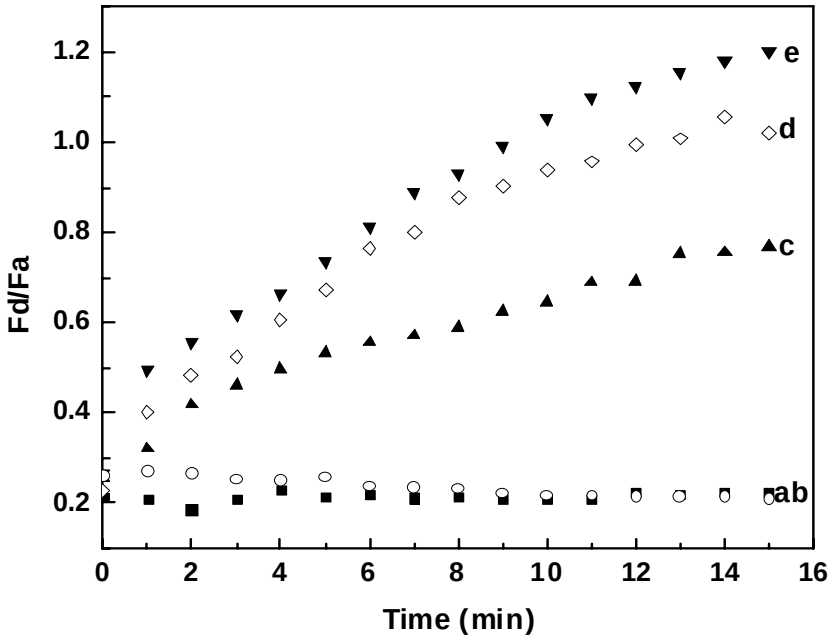

Figure 3.10 Real time monitoring of the inhibition efficiency of 250µg/mL trypsin inhibitor in the presence of 250µg/mL trypsin. a) A control experiment in the absence of trypsin and trypsin inhibitor (■), b)1,10 phenantroline (○), c) 4-(2-Aminoethyl)benzene-sulfonyl fluoride hydrochloride (▲), d) 4-Amidinophenylmethane-sulfonyl fluoride hydrochloride (◊) and e) in the absence of trypsin inhibitor (▼).

Figure 3.11 show the inhibition ability of trypsin inhibitors. The inhibition ability was calculated using equation [4].

$$Inhibition = \frac{\left[\left(\frac{F_d}{F_a}\right)_0 - \left(\frac{F_d}{F_a}\right)_I\right]}{\left[\left(\frac{F_d}{F_a}\right)_0 - \left(\frac{F_d}{F_a}\right)_b\right]} \qquad [4]$$

$(F_d/F_a)_0$ is the ratio of emission intensity of quantum dots and rhodamine with trypsin (without inhibitor) after adding the quantum dots based probes for 15mins. $(F_d/F_a)_I$ is the ratio of emission intensity of quantum dots and rhodamine with trypsin and different concentrations of inhibitor after adding quantum dots based probes for 15mins. And, $(F_d/F_a)_b$ is the ratio of emission intensity of quantum dots and rhodamine in Dulbecco's PBS buffer solution at pH 7.4 without trypsin and inhibitors. The inhibition efficiency of 4-(2-aminoethyl) benzene-sulfonyl fluoride hydrochloride is higher than that of 4-amidinophenylmethane-sulfonyl fluoride hydrochloride. It is clearly seen that 1,10-phenanthroline is the best performing inhibitors. With a concentration of 250µg/mL, 1,10-phenanthroline inhibits 100% of enzymatic activity of trypsin, while 4-(2-aminoethyl) benzene-sulfonyl fluoride hydrochloride and 4-amidinophenylmethane-sulfonyl fluoride hydrochloride inhibit trypsin by 45% and 20% respectively.

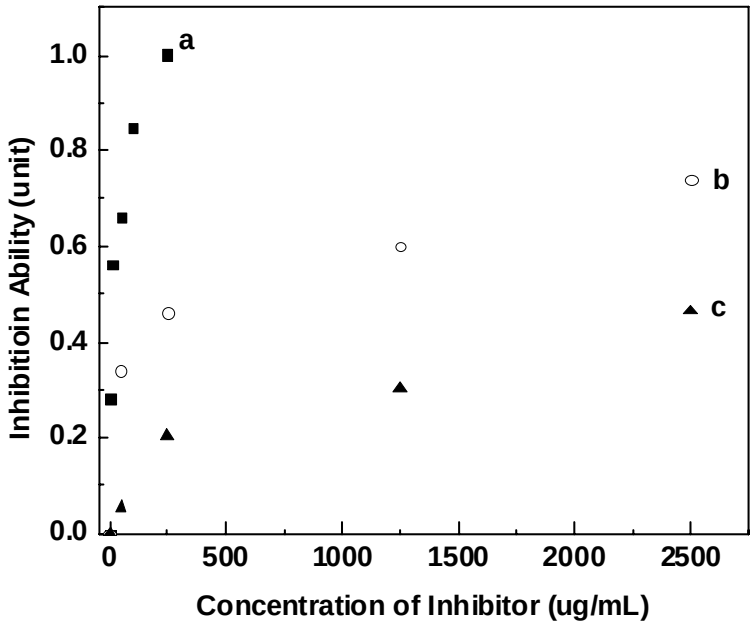

Figure 3.11 Inhibition ability of trypsin inhibitors: a) 1,10-phenanthroline, b) 4-(2-Aminoethyl) benzene-sulfonyl fluoride hydrochloride and c) 4-Amidinophenylmethane-sulfonyl fluoride hydrochloride.

3.3.5 Monitoring the proteolytic activity of MMPs in normal and cancerous breast cells

Collagenase is an extracellular matrix metalloproteinase (MMP). The quantum dots FRET-based enzymatic activity probes were first used to determine the activity of collagenase in solution to test the analytical capabilities of the quantum dots FRET based probes in a model system. We hypothesized that since collagenase has a wide range of proteolytic activity, it would be at least as effective as trypsin in cleaving the RGDC peptide that was attached to our quantum dots. FRET measurements of the quantum dots

at increasing levels of collagenase in solution are shown in figure 3.12. Similarly to trypsin, the fluorescence intensity of the quantum dots at 545 nm increased while the fluorescence intensity of the rhodamine molecules decreased due to the enzymatic cleavage of the peptide by collagenase. It should be noted, however, that a 20-fold lower level of collagenase compared to trypsin was needed to similarly affect the FRET signal of the quantum dots. As mentioned previously, the higher cleavage rate by collagenase could be attributed to its non-selective peptide cleavage activity. The temporal dependence of the ratio F_d/F_a of the quantum dots at increasing collagenase concentration ranging from 0 to 5μg/mL provided information on the rate of the enzymatic reaction. The ratio F_d/F_a was collagenase concentration dependent and time dependent. With a concentration of 5μg/mL collagnase the enzymatic reaction was completed in 15 minutes.

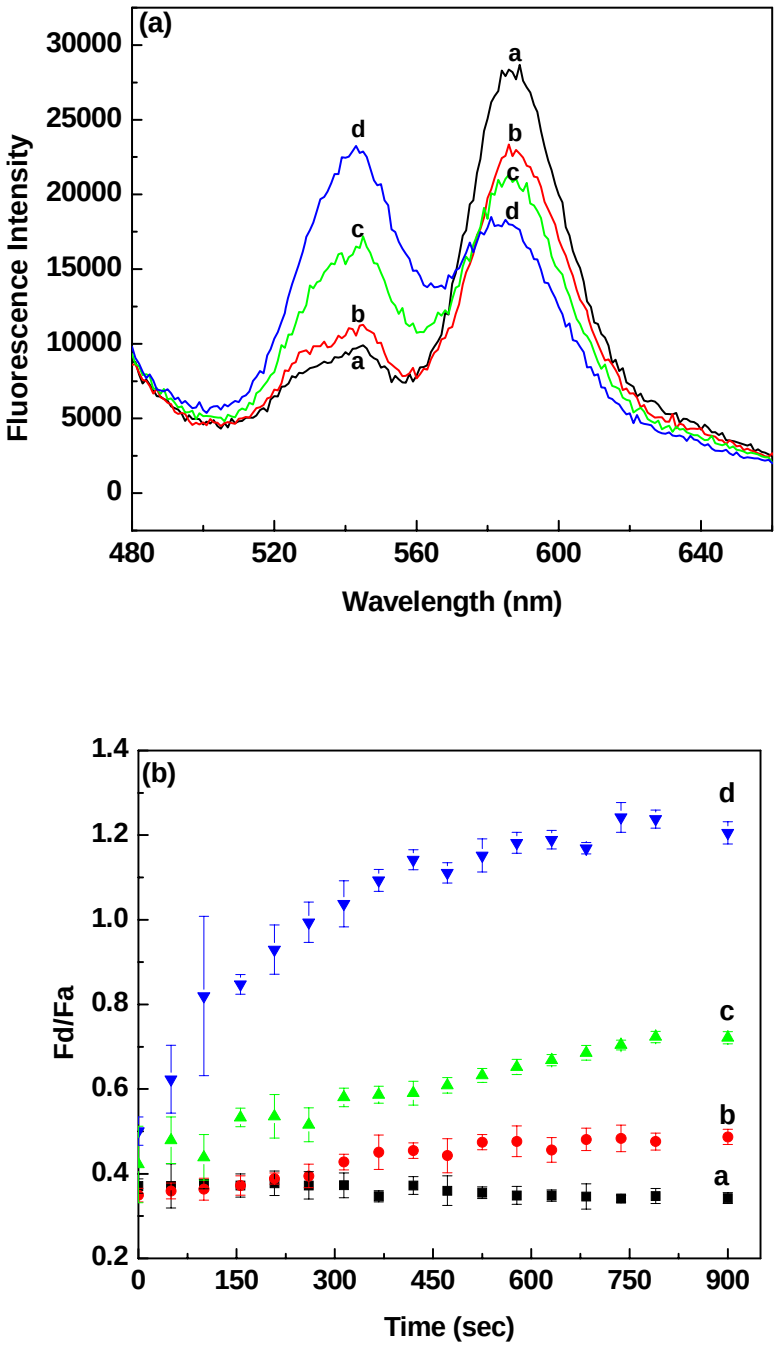

Figure 3.12 (a) Emission spectra of rhodamine labeled peptide-coated quantum dots 15 minutes following the addition of collagenase of increasing concentration. (b) Time dependence of the ratio Fd/Fa of the rhodamine-labeled peptide-coated quantum dots at increasing collagenase concentration. The ratio F_d/F_a was normalized to $(F_d/F_a)_0$, which is the ratio F_d/F_a prior to adding collagenase to the quantum dot probes solutions. a) 0μg/mL (black), b) 0.5μg/mL (red), c) 2.5μg/mL (green), d) 5.0μg/mL (blue)

Following the successful demonstration of using quantum dot FRET based probes to monitor the activity of collagenase, we measured in real time the activity of MMPs in cell cultures. Digital fluorescence microscopy images were used to measure the FRET between quantum dots and rhodamine and the effect of MMPs in normal and cancerous breast cells on the FRET signal. The experiments were carried out using the cell lines HTB 125 (normal breast cells) and HTB 126 (breast cancer cells). The cells were maintained following protocols provided by the American Type Tissue Culture Collection (ATCC). 10^6 cells/ml were seeded and cultured on glass slides for 48 hours to reach 90% confluence in order to realize a fully developed extracellular matrix. The quantum dot FRET probes were added to the cultures and covered with cover slips to enable close proximity of the probes to the extracellular matrix. Figure 3.13 shows images of the quantum dot FRET probes in normal (images a, b) and cancerous (images c, d) breast cells when taken at t = 0 and t = 15 minutes following the addition of the probes. It can be seen that the emission color of the quantum dots (orange) did not change when incubated with normal breast cells. Whereas there was a significant change of emission color from orange to green when the quantum dot probes were incubated with breast cancer cells, which is attributed to the over expression of MMPs in breast cancer cells. The quantum dots probes could be used to discriminate normal and cancerous breast cells based on the different lever of MMPs expressions between normal and cancerous breast cells.

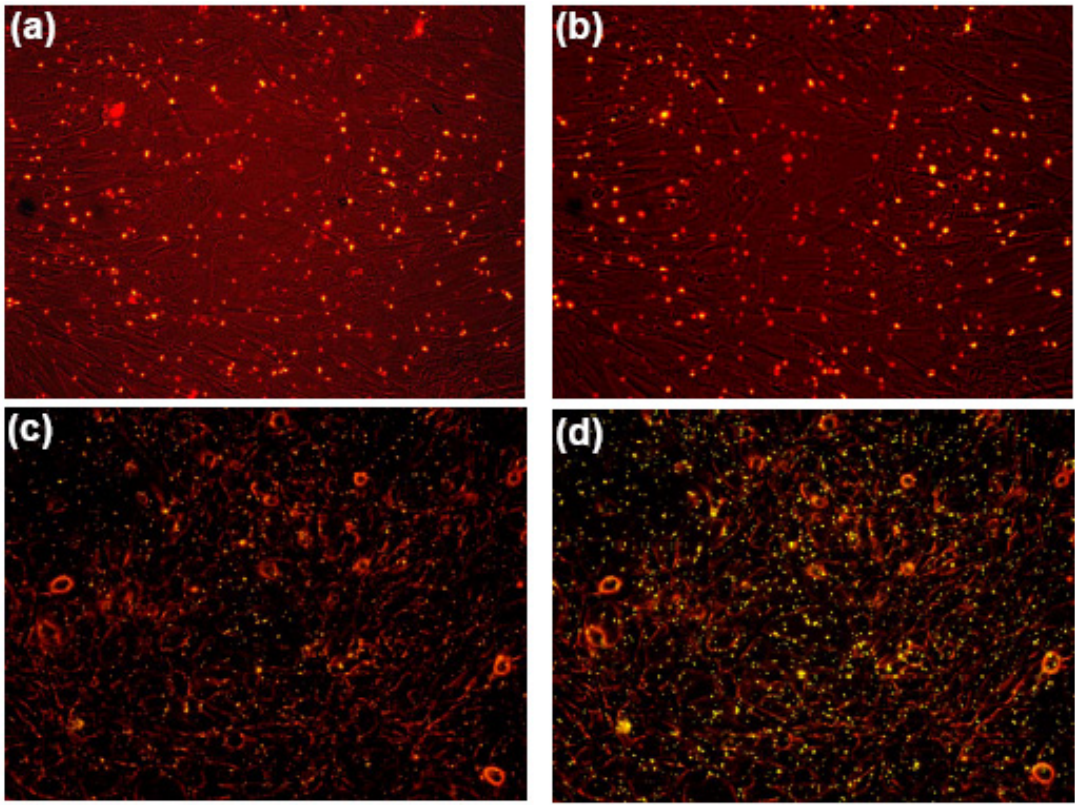

Figure 3.13 Digital fluorescence microscopy images of rhodamine labeled peptide-coated quantum dots in cell culture. (a) Incubated in HTB 126 cell line for 0 minute, (b) incubated in HTB 126 cell line for 15 minutes; (c) incubated in HTB 125 cell lines for 0 minutes, (d) incubated in HTB 125 cell lines for 15minutes.

Figure 3.14 describes the temporal dependence of the FRET signal of the quantum dot FRET probes in normal and cancerous breast cultures. Curve (a) shows the results of a control experiment in which quantum dot FRET probes were observed in the absence of cells. No change in the emission properties of the quantum dots was detected. Curves (b) and (c) follow the response of the quantum dot FRET probes in normal (b) and cancerous

(c) breast cells. It can be seen that the MMPs activity in breast cancer cultures is significantly higher compared to normal cells. The change in FRET signal is completed in about 10 minutes.

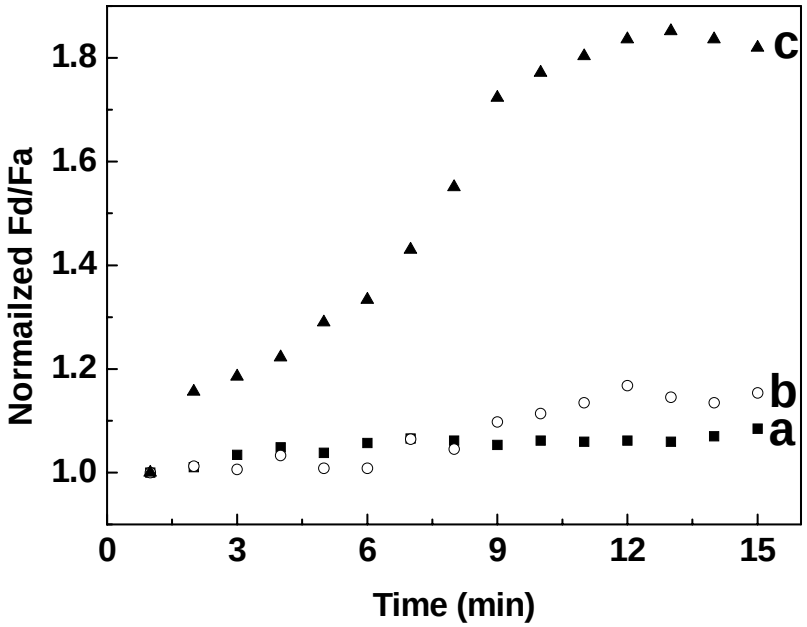

Figure 3.14 Temporal dependence of FRET signal (F_d/F_a) of quantum dot FRET-based protease sensors in the absence of cells (a) and when attached to the extracellular matrix of normal breast cells (b) and cancerous breast cells (c).

3.4 Conclusions

We have successfully synthesized peptide coated CdSe/ZnS quantum dots. The peptide coated quantum dots were water-soluble, biocompatible, and maintained their original photophysical properties. We designed and developed new quantum dots based

FRET probes in which rhodamine molecules were bound to the quantum dots through a peptide linker that contained selective cleavage sites to proteolytic enzymes. The quantum dots FRET-based enzymatic probes were first used to test the enzymatic activity of trypsin in solution. The FRET signal changes were found to be trypsin concentration dependent and time dependent. The rapid response time of the probes enabled real time monitoring of trypsin activity in assay times that lasted less than 15 minutes. The enzymatic assays could be performed at picomol trypsin levels. However, the assay times increased with decreasing trypsin concentration. The probes were used to determine the inhibition efficiency of the three organic compounds 4-(2-Aminoethyl) benzene-sulfonyl fluoride hydrochloride, 4-Amidinophenylmethane-sulfonyl fluoride hydrochloride and 1, 10 phenanthroline. We also have successfully applied rhodamine-labeled peptide coated CdSe/ZnS quantum dots to monitor the proteolytic activity of MMPs in normal and cancerous cell cultures. We were able to discriminate between a normal and cancerous tissue in less than 15 minutes. The method can be extended to other applications involving over expression of proteolytic activity. Changing the peptide sequence would enable measuring the activity of specific proteolytic enzymes. It could also enable high throughput screening of protease inhibitors and activators in an array format. In their current form it was difficult to determine the inhibition efficiency of larger trypsin inhibitors, for example protein molecules. It is possible that protein molecules could displace the peptide molecules from the quantum dots. This would release rhodamine molecules to the solution even in the absence of trypsin. To overcome this difficulty, we are currently synthesizing CdSe/ZnS quantum dots that are capped with the protein metalothionein (MT) following a method recently developed by Benson and

coworkers (21). This would improve the stability of the quantum dots in biological media due to MT binding to the quantum dots through multiple cystein residues. Additionally, it would be possible to link rhodamine labeled to the MT capped quantum dots, which in turn would result in more stable quantum dot FRET-based probes. The effect of MT coating on the FRET efficiency and on the ability to monitor enzymatic cleavage of peptide molecules using FFRET between the quantum dots and rhodamine residues remained to be determined. We are also developing a lithographic technique to fabricate quantum dot FRET-based arrays for high throughput screening of enzyme inhibitors and activators.

3.5 References

1. Mandal, M., Mandal, A., Das, S., Chakarborti, T., Chakraborti, S., *Molecular and cellular biochemistry*, **2003**, 252; 305-329,
2. Kahari, V.M.; Saarialho-Kere, U., *Ann Med.,* **1999**, 31 (1), 34-45
3. Nawrocki, B., Ploette, M., Marchand, V., Monteau, M., Gillery, P., Tournier, J.M., Birembaut, P., *Int. J. Cancer,* **1997**, 72, 556-564
4. Pham, W., Choi, Y., Weissleder, R., Tung, C. H., *Bioconjugate Chem.*. **2004**, 15, 1403-1047,
5. Balduyck, M., Zerimech, F., Gouyer, V., Lemaire, R., Hemon, B., Grard, G., Thiebaut, C., Lemaire, V., Dacquembronne, E., Duhem, T., Lebrun, A., Dejonghe, M.J., Huet, G., *Clin. Exp. Metastasis*, **2000**, 18, 171-178
6. Ito, A., Nakajima, S., Sasaguri, Y., *Br. J. Cancer* , **1995**, 71, 1039-1045
7. Nutt, J.E., Lunec, J., *Eur. J. Cancer*, **1996**, 32A, 2127-2135
8. Ntziachristos, V., Tung, C.H., Bremer, C., Weissleder, R., *Nature Med*, **2002**, 8, 757-761
9. Weissleder, R., Ntziachristos, V., *Nature Med,* **2003**, 9 (1), 123-128,
10. Bremer, C., Tung, C. H., Weissleder, R., *Nature Med.*, **2001**, 7, 743-748
11. Chang, E., Miller, J. S., Sun, J., Yu, W. W., Colvin, V. L., Drezek,R., West, J. L., *Biochem Biophys Res Commun.,* **2005**, 9; 334(4), 1317-1321
12. Medintz, I. L.; Clapp, A. R.;. Brunel, F. M.; Tiefenbrunn, T.; Uyeda, H. T.; Chang, E. L.; Deschamps, J. R.; Dawson, P. E.; Mattoussi, H. *Nat. Mater.* **2006**, 5(7), 581-589.
13. Clapp, A. R.; Medintz, I. L.; Mattoussi, H. *ChemPhysChem* **2006**, *7* (1), 47-57.
14. Peng, Z. A.; Peng, X.; *J. Am. Chem. Soc.* **2001**; 123(1); 183-184
15. Wang, D.; He, J.; Rosenzweig, N.; Rosenzweig, Z.; Nano Lett.; **2004**; 4(3), 409-413.
16. Pinaud, F.; King, D.; Moore, H.P.; Weiss, S. *J. Am. Chem. Soc.* **2004**, *126*, 6115-6123
17. Rosenthal, S. J.; Tomlinson, I.; Adkins, E. M.; Schroeter, S.; Adams, S.; Swafford, L.; McBride, J.; Wang, Y.; DeFelice, L. J.; Blakely, R. D.;*J. Am. Chem. Soc.* **2002**, 124, 4586-4594.
18. Hahm, B.; Han, D.S.; Back, S.H.; Song, O.K.; Cho, M.J.; Kim, C.J.; Shimotohno, K.; Jang, S.K.*; J. Virol.*, **1995**, *69*, 2534-2539
19. Laura, R.; Robison, D.J.; Bing, D.H.; *Biochemistry*, **1980**. *19*, 4859-4864
20. Brannstrom, M.; Woessner Jr, J.F.; Koos, R.D,; Sear, C.H.; LeMaire, W.J.; *Endocrinology*, **1988**, 122, 1715-1721
21. Sandros, M. G.; Gao, D.; Benson, D. E. *J. Am. Chem. Soc.* **2005**; *127*, 12198-12199

CHAPTER 4 QUANTUM DOTS FRET BASED PH SENSOR

4.1 Introduction

A sensor that has the capability to measure cellular pH change can be used to probe biological processes in cells. Measurement of pH in cells has indicated that there is a difference between tumor and normal tissues (1-3). Water-soluble sensor systems capable of detecting pH changes through fluorescence resonance energy transfer (FRET) between organic dyes have been developed because of high sensitivity and high specificity for pH variation in intracellular environments. Meanwhile, color change according to pH can be monitored by microscopy. For example, Hong and coworkers designed a FRET based pH sensor via a polymeric linker containing a sulfonamide group which undergoes the coil-globule transition at pH 7.0 and induces the distance change between pyrene (donor) and coumarin 343 (acceptor)(4). Ohmichi and coworker reported a DNA-based pH sensor to detect pH changed between pH 5.0-7.0 in living cells (5).

In recent years, the unique photophysical properties of luminescent quantum dots make them more popular than organic dyes in imaging and sensing applications. The luminescence of quantum dots is sensitive to the presence and characteristics of ligands or molecules at surfaces or environments. Especially for quantum dots based sensors, it is very important to understand what factors affect the optical properties of quantum dots. Recently, some researchers have been working on studying pH effects on the luminescence of quantum dot. For example, Tomasulo and coworkers demonstrated pH induced transformations of chromogenic ligands on the surface of quantum dots, which would activate the energy transfer from quantum dots to ligand and cause the quenching

of the fluorescence intensity of quantum dots (6, 7). Liu and coworkers use mercaptoacetic acid capped CdSe/ZnSe/ZnS quantum dots as intracellular pH sensor in SKOV-3 human ovarian cancer cells (8). They reported that quantum dots aggregated and quenched in acidic environments. The fluorescence intensity of quantum dots increased as the pH increased in both fixed and living cells. However, only a single color was found that did not change effectively with the pH. Thus, more effective methods for monitoring the pH change in biological media are needed. Here we take advantage of quantum dots and FRET to investigate how pH affects quantum dots and show quantum dots FRET based systems as a potential pH sensor in buffer solution.

Previous work with peptide RGDC coated quantum dots has shown small aggregate quantum dots in PBS buffer at pH 7.4 due to the instability of disulfide bond between quantum dots and peptide containing a single cysteine amino acid (9, 10). Benson and his coworker have reported on cysteine-rich peptide MTs as capping ligands to improve the stability of quantum dots via multiple thiol bonds (11, 12). MT is a collective name for a superfamily of ubiquitous low molecular weight (6-7 kDa), cysteine-rich, metal-binding proteins or polypeptides (13, 14). MT contains 61 or 62 amino acid residues, 20 of which are cysteines which have high capacity of binding metal through sulfhydryl groups and from metal-thiolate complexes (15). MT is also a lysine-rich peptide. The MT coated quantum dots, full of amine groups on the surface of quantum dots for further bioconjugation, were labeled with Rhodamine Red™-X succinimidyl ester through the formation of amide bonds with ε -amine group of lysine in MT peptide to form the quantum dots based FRET probes. FRET signal responded differently to pH values could be monitored by the alternation on emission spectra and emission color of the probes.

4.2 Experimental

4.2.1 Synthesis of mercaptohexadecanoic acid (MHDA)-coated quantum dots

MHDA coated quantum dots were prepared following a procedure for the synthesis of lipoic acid capped CdSe/ZnS core-shell quantum dots developed by Bawendi (16), with a slight modification. 25mg MHDA was heated up to 70-80°C until dissolved then 3mL ~ 1μM TOPO-Qdots and 3mL chloroform was added and stirred for 2-3 hours at 50-60°C. Then 6mL of H_2O (containing tetramethylammonium hydroxide pentahydrate) was added to the mixture and stirred for another half hour at room temperature after which it was allowed to settle down for a few minutes. This resulted in a two-phase mixture with the aqueous MHDA coated quantum dots layer above the organic chloroform layer. The aqueous layer was collected and centrifuged several times to remove TOP/TOPO until clear solution was observed. Then the clear suspensions were collected and spin dialyzed 2 times with a cutoff molecular weight of 30kDa to remove the excess MHDA. In each spin dialysis cycle, the sample was centrifuged at 3000 rpm for 20 minutes and washed with DI water. MHDA coated quantum dots were kept at 4°C in DI water until used.

4.2.2 Synthesis of Metallothionein (MT) coated quantum dots

MT coated quantum dots were prepared following the protocol development by Benson and his coworkers (16). MHDA capped quantum dots were mixed with MT (the mole ratio of MT/MHDA-quantum dots is 10) in DI water for 1 hour. Then the solutions were spin-dialyzed to remove the unbound MT. In each spin dialysis cycle the sample

was centrifuged at 3000 rpm for 20 minutes and washed with DI water. MT coated quantum dots were kept at 4°C in DI water until used.

4.2.3 Conjugation of Rhodamine to MT coated quantum dots

Rhodamine labeled MT-coated quantum dots were prepared by adding 20μL of 0.30 MT coated quantum dots and varying volumes ranging from 0 μL to 80μL of 3.0 Rhodamine Red™-X, succinimidyl ester to a 20mM MOPS buffer solution at pH 6.5 to a final volume of 1.0 mL. The reaction mixture was incubated for one hour at room temperature, and then the spectra and image were measured under digital microscopy. The spectra and images were taken through 40X objectives with numerical apertures of 0.9. A filter cube containing a 425 ±20 nm band-pass excitation filter, a 465 nm dichroic mirror, and a 475nm long pass emission filter was used to ensure spectral purity. The emission peaks of the quantum dot FRET probes were observed at 525 nm (quantum dots) and 590 nm (rhodamine).

4.2.4 Effect of pH on the conjugation between Rhoamine and MT coated quantum dots

20μL of 0.3μM MT coated quantum dots and 40μL of 3.0μM Rhodamine were added to 940μL of MOPS at different pH values (4.5, 5.5, 6.5, 7.5, 8.5, and 9.5) and incubated at room temperature for half hour. FRET measurements were carried out by digital microscopy and spectroscopy.

4.2.5 Effect of pH on the FRET efficiency of Rhodamine labeled MT coated quantum dots

200µL of 0.3µM. MT coated quantum dots and 400µL of 3.0µM. rhodamine were added to 400µL of MOPS at pH 6.5 and incubated at room temperature for one hour. Then 50µL of the quantum dots-MT-rhodamine conjugate was diluted with 450µL of MOPS buffer at different pH values (4.5, 5.5, 6.5, 7.5, 8.5, and 9.5). Imaging and spectra were taken at half hour, one hour, one and half hours, and two hours.

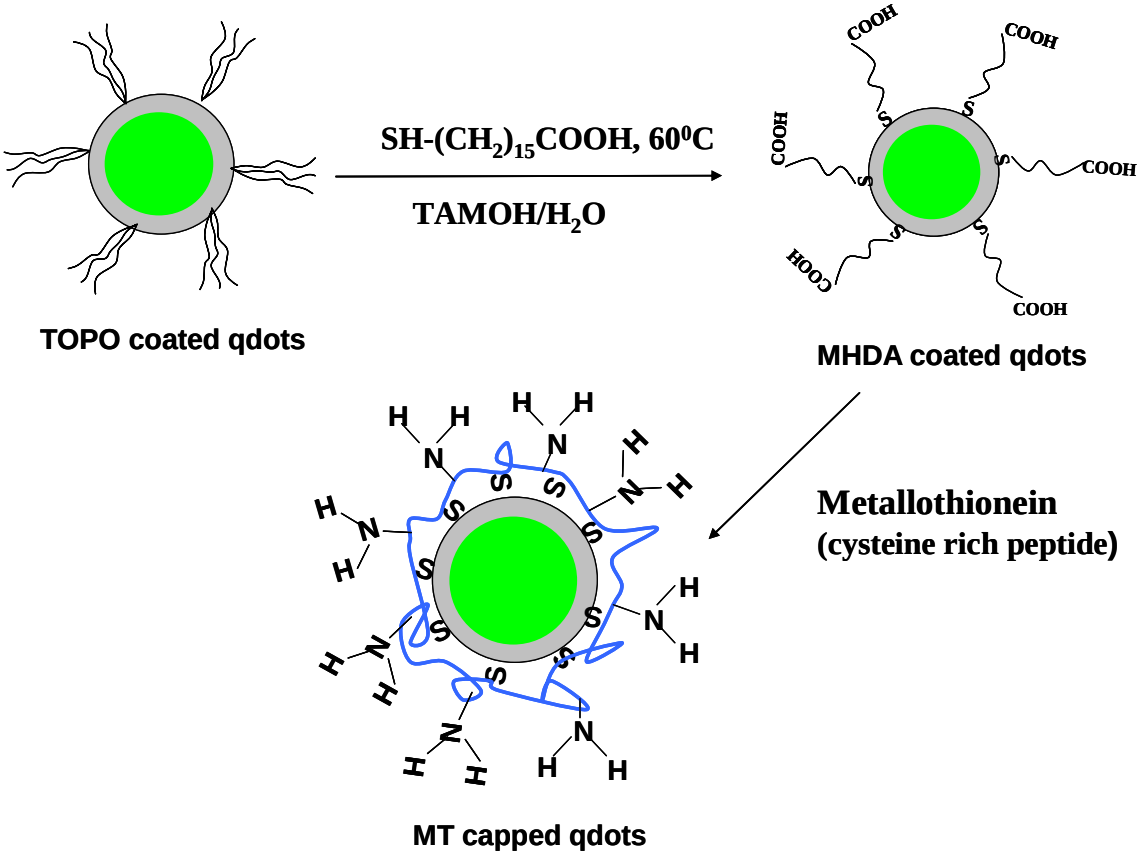

Scheme 4.1 The synthesis of MT coated quantum dots

4.3 Results and discussion

4.3.1. Effect of pH on the stability of MT coated quantum dots on buffer solution

Previous work with peptide RGDC coated quantum dots has shown small aggregate quantum dots in PBS buffer at pH 7.4 due to the instability of the disulfide bond between quantum dots and peptide containing a single cysteine amino acid (14, 15). Here we utilize cysteine-rich-peptide MT as a capping ligand to improve the stability of quantum dots. First, the TOPO coated quantum dots exchanged with MHDA to form the water-soluble quantum dots. Then MHDA coated quantum dots further exchanged with MT to improve stability via multiple thiol bonds between cysteine in MT and quantum dots (Scheme 4.1). MT is also a lysine-rich peptide. The MT coated quantum dots are decorated with amine groups that are available for labeling with rhodamine succinimidyl ester. As Figure 4.1 shows, the stability of MT coated quantum dots is dependent on pH. At low pH, MT dissociates from the surface of quantum dots, which results in aggregation and loss of solubility. At neutral or basic pH ($\geq$6.5), the solitions are very clear and there is no quantum dot aggregation. The solution can be stored over 1 month.

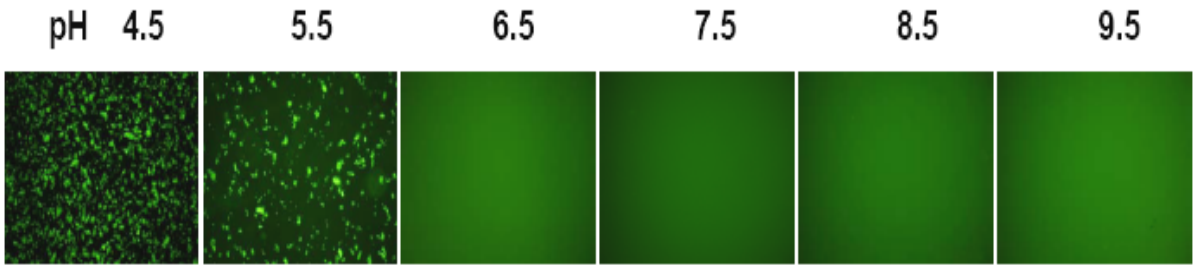

Figure 4.1 Effect of pH on the emission images of MT coated quantum dots

4.3.2 Conjugation of Rhodamine to the MT coated quantum dots

Since MT coated quantum dots show high aqueous solubility at nearly neutral or basic pH condition, the conjugation between MT coated quantum dots and rhodamine were carried out in MOPS buffer at pH 6.5. Figure 4.2a shows the fluorescence spectra of the quantum dot-MT-rhodamine conjugate at increasing ratio between the rhodamine and quantum dots. The emission of the quantum dots at 525 nm decreased while the emission of rhodamine at 590 nm increased with increasing rhodamine to quantum dots ratio. This indicated the occurrence of FRET between the MT coated quantum dots and the rhodamine molecules. The FRET efficiency increased with increasing rhodamine concentration. Figure 4.2b depicts that the emission intensity of quantum dots decays as a function of the rhodamine/quantum dots ratio. Here, F_{d0} is the emission intensity of unlabeled MT coated quantum dots and F_d is the emission intensity of rhodamine-labled MT-coated-quantum dots. It was clearly shown that F_d/F_{d0} decreases as the ratio of rhodamine/quantum dots increases. For a 20:1 ratio of rhodamine to quantum dots, it

indicates 70% quenching of quantum dots signal compared to unlabeled MT-coated quantum dots.

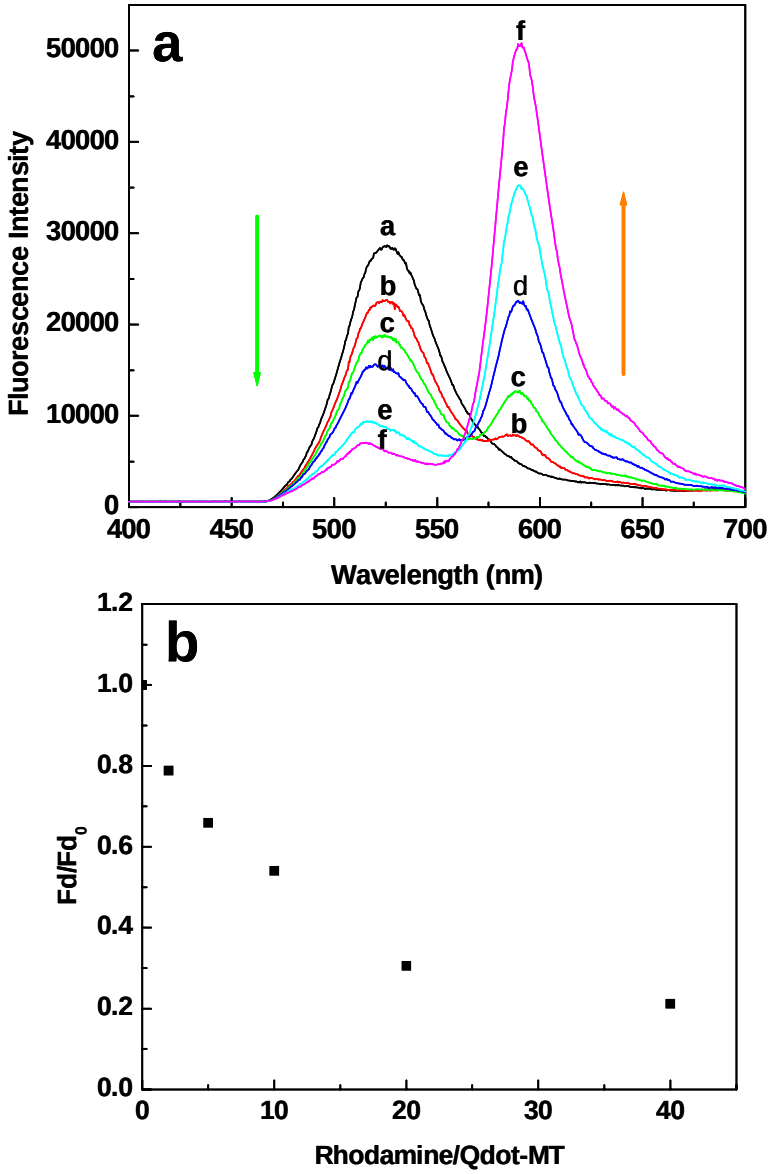

Figure 4.2 a) Emission spectra of rhodamine-labeled MT-coated quantum dots at increasing the rhodamine to peptide coated quantum dots ratio: (a)0:1 (black),(b) 2:1 (red), (c)5:1 (green), (d)10:1 (dark blue), e)20:1 (light blue), f) 40:1 (pink); b) The emission intensity of MT coated quantum dots decay percentage versus the ratio of rhodamine and quantum dots in MOPS buffer at pH 6.5; F_{d0} is the emission intensity of quantum dots without labeling rhodamine and F_d is the emission intensity of quantum dots in rhodamine-labled-quantum dots conjugate.

Digital fluorescence images provide more visual evidence of FRET between the MT coated quantum dots and the attached rhodamine. Figure 4.3 describes the images of quantum dots-MT-rhodamine as a function of the rhodamine/quantum dots ratio. It can be clearly seen that the emission color changes from green to orange progressively as the ratio of rhodamine/quantum dots increases. The change of emission color also indicates that there is FRET between MT coated quantum dots and rhodamine.

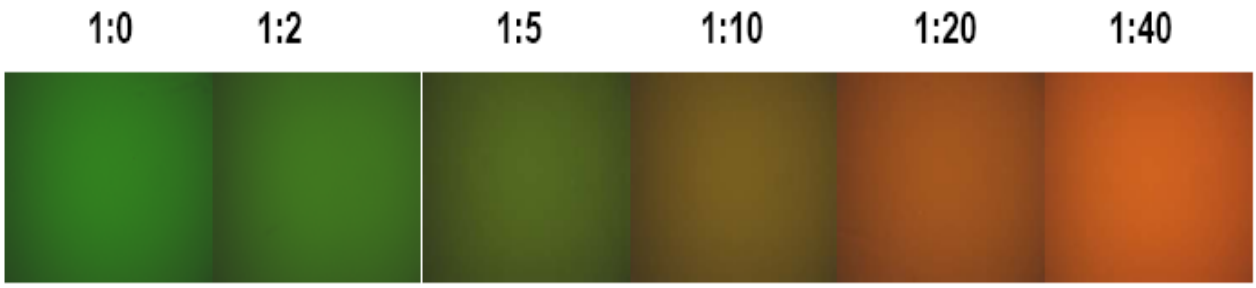

Figure 4.3 Digital fluorescence images of quantum dots-MT-Rhodamine at the different ratio of rhodamine/quantum dots.

Figure 4.4 shows spectra and imagse of rhodamine-labeled MT-coated quantum dots probes with a ratio of 20:1 of rhodamine to quantum dots. The fluorescence intensity of MT-coated quantum dots decreases by 3.3 times when labeled with rhodamine, whereas the fluorescence intensity of rhodamine increases by 5.1 times when bound to MT-coated quantum dots. This is another indication that the large emission signal at 590 nm of rhodamine conjugate is a result of FRET between the quantum dots and bound rhodamine

molecules, and not due to self-excitation of rhodamine molecules. The emission color of MT-coated quantum dots and rhodamine were green and dark red, respectively. Whereas the emission color of rhodamine labeled MT coated quantum dots were orange. The emission color change indicates that rhodamine bound to quantum dots and result in the FRET occurrence between MT coated quantum dots and rhodamine. Later luminescent quantum dots based pH probes were prepared under this ratio conditions.

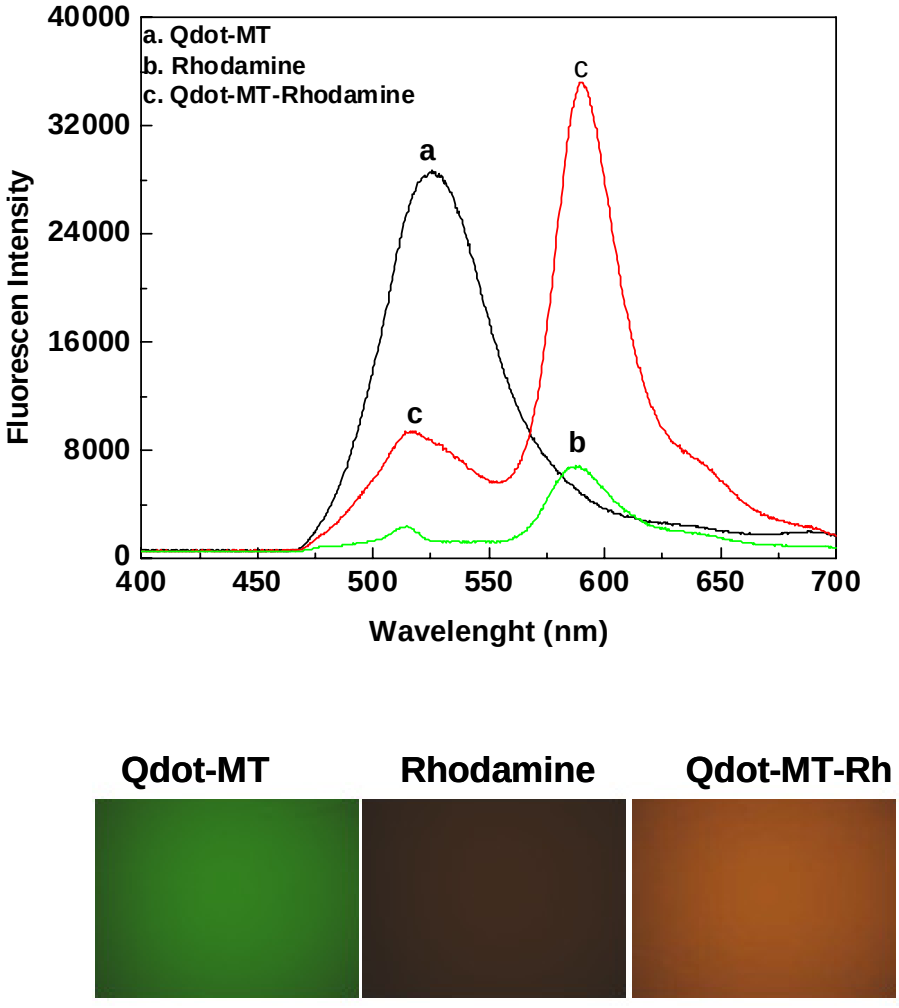

Figure 4.4 The emission spectra and fluorescence images of a) MT coated quantum dots, b) rhodamine and c) rhodamine labeled MT coated quantum dots in MOPS buffer at pH 6.5 with the ratio 20:1 of rhodamine:quantum dots

4.3.3 Effect of pH on the conjugation between Rhoamine and MT coated quantum dots

First, we examined the effect of pH on the conjugation between rhodamine and MT-coated quantum dots. MT-coated quantum dots and rhodamine were mixed under different pH MOPS buffer for 1hour. The image and spectra of MT-coated quantum dots mixed with rhodamine at different pH are shown in figure 4.5a. At low pH, the emission color of the mixture is yellowish-green. The quantum dots are aggregated and not available for conjugating with rhodamine. The emission color turns to orange as the pH increases to 6.5 and quantum dots are very clear with no aggregation. Then, the solution tends to turn back to green as the pH increases to 9.5. The fluorescence intensity of quantum dots decreases and the fluorescence intensity of rhodamine increases as pH increases from 4.5 to 6.5, then the emission spectra of quantum dots and rhodamine tend to recover its original spectra as the pH is raised from pH 6.5 to pH 9.5. The fluorescence intensity ratio of MT-coated quantum dots to rhodamine is plotted against pH values, as shown in figure 4.5b. Here, F_d is the fluorescence intensity of quantum dots at 525nm, F_a is the fluorescence intensity of rhodamine at 590nm. It can be clearly seen that the intensity ratio F_d/F_a decreases quickly from 1.5 to 0.3 as pH increase from 4.5 to 6.5 and reach the minimum at pH 6.5, indicating the FRET from quantum dots to rhodamine occurs. As the pH is raised from pH 6.5 to 9.5, the intensity ratio increases from 0.3 to 0.9 which indicating the FRET efficiency decrease.

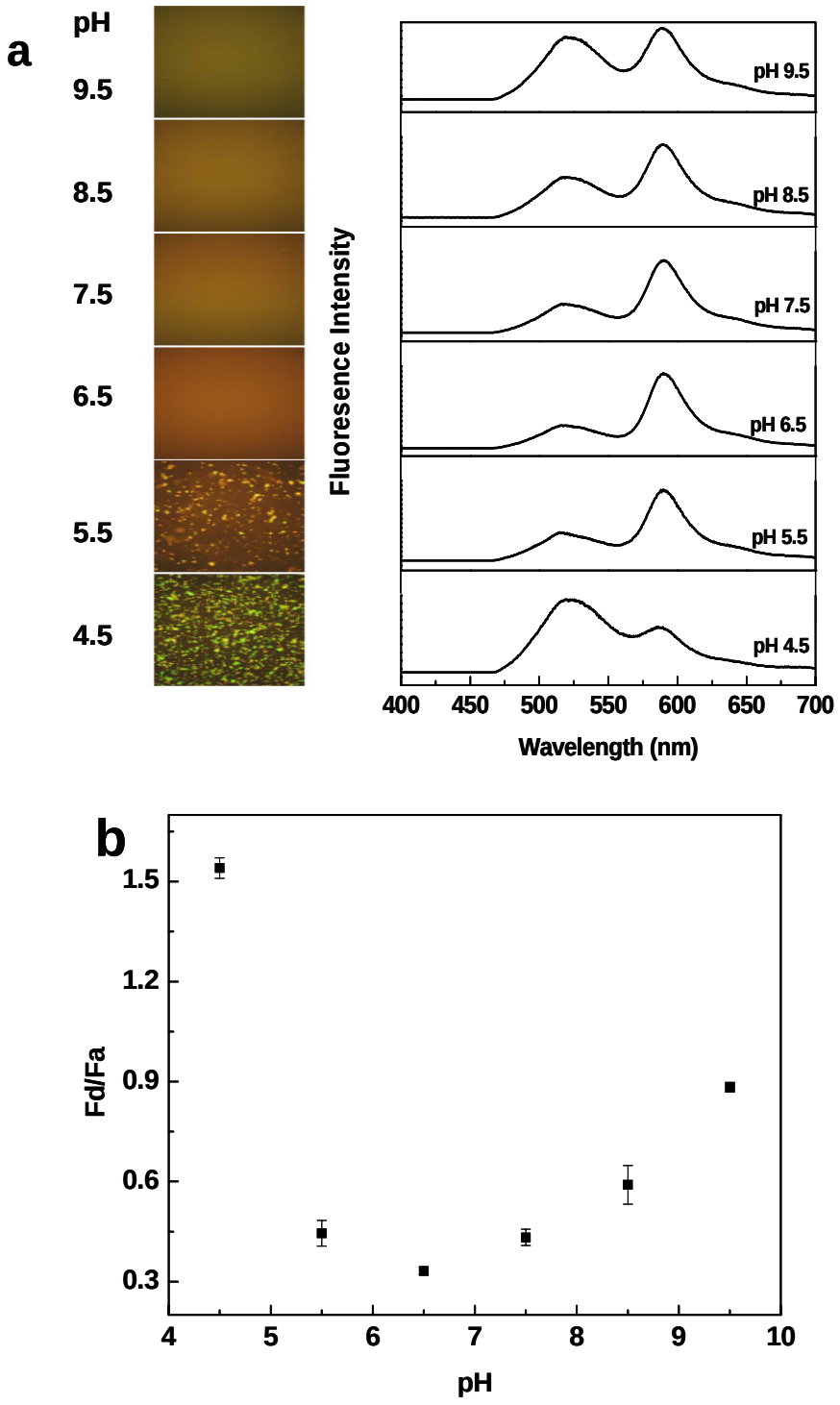

Figure 4.5 pH effect on conjugatioin between MT coated quantum dots and rhodamine. a) Images and fluorescence emission spectra of MT coated quantum dots and rhodamine at different pH values; b) Plot of intensity the ratio of MT coated quantum dots (F_d) and rhodamine (F_a) as a function of pH.

The above phenomena could be explained by the schematic model shown in scheme 4.2. At low pH, the amine terminus and ε-amine group of lysine in MT peptide will be protonated and also MT probably dissociates from the surface of the quantum dots, which results in the aggregation of quantum dots. Rhodamine will not be able to bind to the surface of quantum dots and it remains far away from quantum dots in the solution, and quantum dots will maintain their fluorescence and green emission color. At nearly neutral and slight basic condition, the amino group is maintained in the non-protonated form then amine-reactive rhodamine dye will react and the fluorescence intensity of quantum dots will be quenched by rhodamine due to FRET. This results in the emission color of quantum dots drastically changing from green to red as the pH increases. However, at even higher pH, rhodamine succinimidyl ester hydrolysis could compete with conjugation between rhodamine and MT-coated quantum dots, which would decrease the FRET signal.

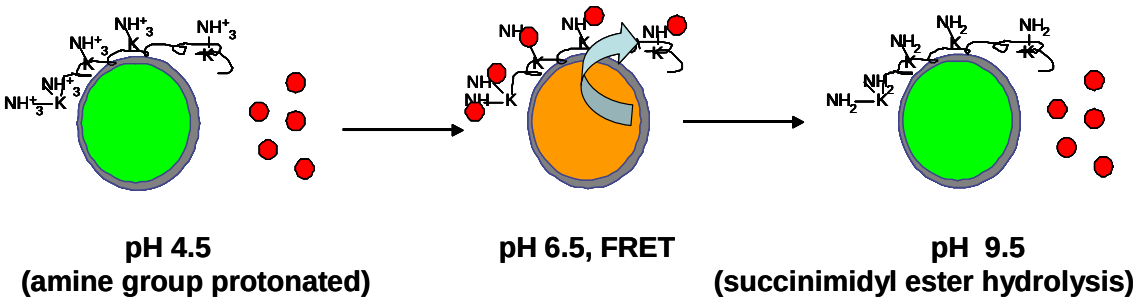

Scheme 4.2 A schematic representation of the mechanism of signal response to the change of pH

4.3.4 Effect of pH on the FRET efficiency of rhodamine labeled MT coated quantum dots

Here we further investigate the possibility of using rhodamine-labeled MT-coated quantum dots system as pH sensor. Quantum dots FRET based pH probes were first formed in MOPS buffer at pH 6.5 for half hour, and then diluted 10 times in MOPS buffer at different pH values. The fluorescence intensity ratio (F_d/F_a) and image of quantum dots FRET probes under different pH values were measured over time. The fluorescence intensity ratio F_d/F_a is pH dependent and time dependent, as shown in figure 4.6a. First, as pH increases from 4.5 to 6.5, F_d/F_a decrease was observed. Then pH continuity rises from 6.5 to 9.5, F_d/F_a increased. F_d/F_a increases over times and increase faster in pH 4.5 and pH 9.5. Figure 4.6b shows the images of quantum dots probes under different pH values over time. In acidic pH (4.5), the quantum dots aggregate over time with emission color turning green. Likely, at low pH, MT dissociates from the surface of quantum dots, which will cause the aggregation of quantum dots and rodamine far away from quantum dots, resulting in low FRET efficiency. At pH 6.5, the quantum dots are clear and orange emission color, which indicates the FRET occurred. At higher pH (9.5), quantum dots turn green without aggregation. It is possible that the amide bond between MT and rhodamine hydrolyzes over time and releases rhodamine from the surface of quantum dots, which decreases FRET efficiency.

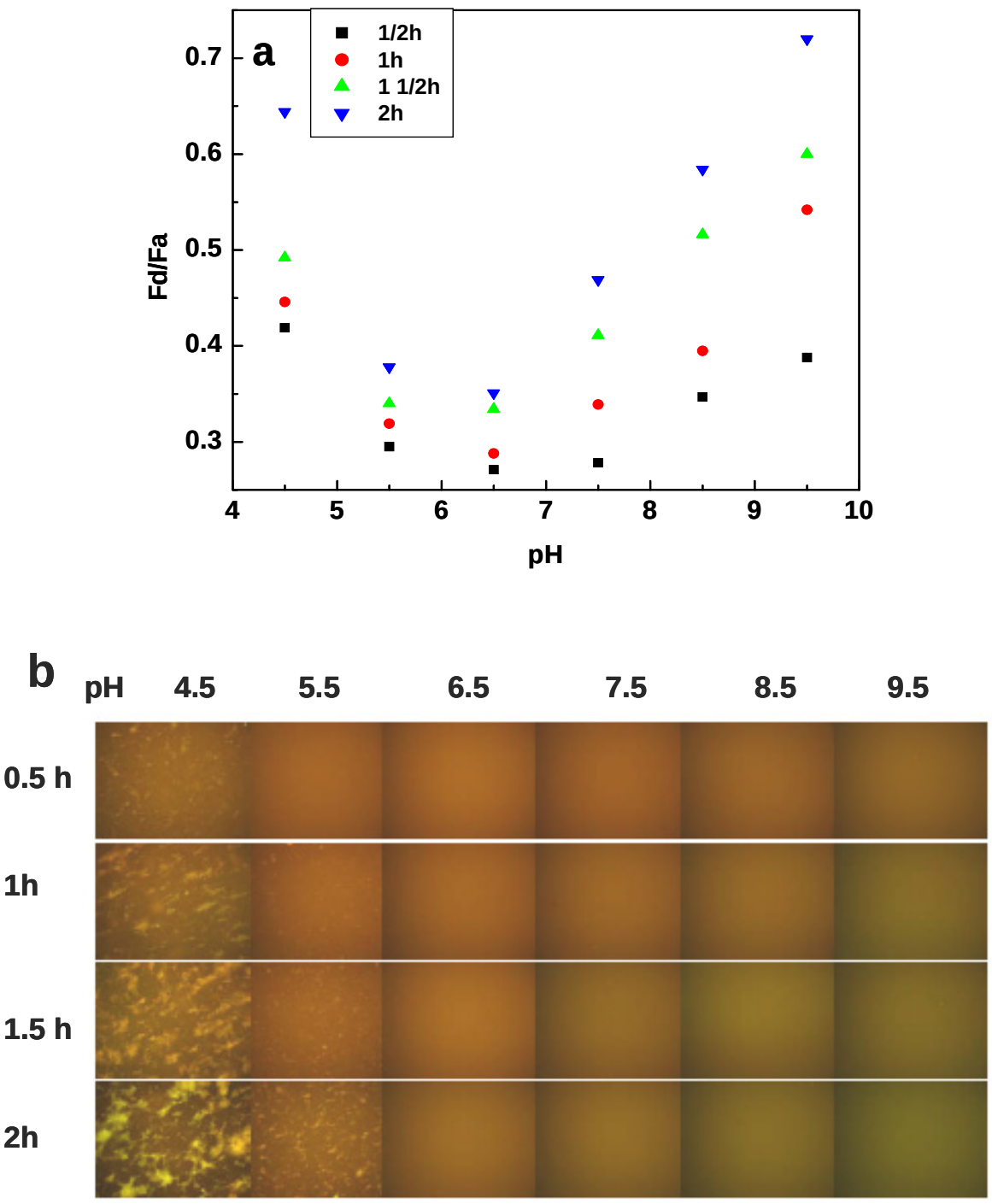

Figure 4.6 pH effect on rhodamine labeled MT coated quantum dots. a) Plot of the intensity ratio F_d/F_a of MT coated quantum dots (F_d) and rhodamine (F_a) as a function of pH over time; b) Images of rhodamine labeled MT coated quantum dots at different pH over time.

4.4 Conclusions

A quantum dots FRET based pH sensor was synthesized via labeling MT coated quantum dots with rhodamine. The stability of MT coated quantum dots is pH dependent in MOPS buffer solution. Quantum dots aggregated at low pH. FRET efficiency was pH dependent and time dependent, which could be confirmed by the fluorescence emission spectra and images. The FRET signal between quantum dots and rhodamine responded to pH changes. This was confirmed by emission spectra and images. FRET efficiency was pH dependent and time dependent. The FRET efficiency reached maximum at pH 6.5 and decreased either in lower or higher pH. MT dissociates from the surface of quantum dots at low pH, which will cause aggregation and rhodamine would be far away from quantum dots, which decreases FRET efficiency. The amide bond between MT and rhodamine would hydrolyze over time at high pH, releasing rhodamine from the surface of quantum dots, which results in low FRET efficiency. It is expected that this quantum dots FRET based pH sensor could be used for investigating biological phenomena. Continued studies will involve surface modification of quantum dots to improve their stability and biocompatibility in the cellular environment. It is also important to design quantum dot based sensors which specifically respond to pH changes in the cellular environment, but are not affected by other factors, such as ionic species, temperature, and electric field. Design method for effective intracellular delivery of quantum dots will be carried out.

4.5 References

1. Gerweck, L.E.; Seetharaman, K.; *Cancer Res* **1996**, 56, 1194–1198.
2. Wike-Hooley, J.L.; Haverman, J.; Reinhold, H.S.; *Radiother Oncol* **1997**, 2,343–366.
3. Thistlethwaite, A.J.; Leeper, D.B; Moylan, D.J III; Nerlinger, R.E.; *Int J Radiat Oncol Biol Phys* **1985**, 11, 1647–52.
4. Hong, S.W.; Kim, K.H.; Huh, J.; Ahn, C-H.; Jo, W.H.; *Chemistry of materials,* **2005**, 17, 6213-6215
5. Ohmichi, T.; Kawamoto, Y.; Wu, P.; Dasuke, M.; Karimata, H.; Naoki, S.; *Biochemistry*, **2005**, 444, 7125-7130
6. Tomasulo, M.; Yildiz, I.; Raymo, F.M., *J. Phys. Chem. B.*, **2006,** 110, 3853-3855
7. Tomasulo, M.; Yildiz, I.; Kaanumalle, S.L.; Raymo, F.M., *Langmuir*, **2006**, 22, 10284-10290
8. Liu, Y-S.; Sun, Y.; Vernier, P.T.; Liang, C-H.; Chong, S. Y. C.; Gundersen, M.A., *J. Phys. Chem. C* **2007**, 111, 2872-2878
9. Shi, L.; De Pauli, V.; Rosenzweig, N.; Rosenzweig, Z.； *J. Am. Chem. Soc.;* **2006**, 128,
10378-10379
10. Shi, L.; Rosenzweig, N.; Rosenzweig, Z. *Anal. Chem.*; **2007,** 79(1); 208-214.
11. Sandros, M. G.; Gao, D.; Benson, D. E. *J. Am. Chem. Soc.* **2005**; 127, 12198-12199
12. Aryal, B. P.; Neupane, K. P. ; Sandros, M. G.; Benson, D. E. *Small*, **2006**, 2(10), 1159-1163
13. Nordberg, G.F.; Nordberg, M.; Piscator, M.; Vesterberg, O.; *Biochem. J.*, **1972**, 126, 491-498
14. Sanz-Nebot, V.; Andon, B.; Barbosa, J., *J. Chromato.*, **2003**, 796, 379-393
15. Klaassen, C.D.; Liu, J.; Choudhuri, S.; *Annu. Rev. Pharmacol, Toxicol.* **1999**, 39, 267-94
16. Mattoussi, H.; Mauro, J. M.; Goldman, E. R.; Anderson, G. P.; Sundar, V. C.; Mikulec, F. V.; Bawendi, M. G. *J. Am. Chem. Soc.,* **2000**, 122, 12142–12150

CHAPTER 5 REVERSIBLE QUANTUM DOTS BASED IRON SENSOR

5.1 Introduction

Iron is associated with cell growth, cell division and cellular differentiation (1). In biological systems the most of cell iron is protein bound; only a minor fraction is labile iron (2). Cell damage associated with iron overload (IO) has been attributed to the emergence of excessive levels of cell labile iron. The labile iron can catalyze the formation of reactive oxygen species (ROS), such as hydroxyl radical ($OH^{\cdot}$) via Fenton reaction. The highly reactive hydroxyl radical attacks lipid, proteins and DNA, which result in DNA oxidation, mitochondrial damage, and the peroxidation of membrane lipids (3, 4). Also, the excess labile iron can react with unsaturated lipids to form alkoxyl and peroxyl radicals, which result in the impairment of cellular functions and lead to damage of cells beyond the cellular defense capacities (5, 6). A major objective of researchers in this area is to develop the method to detect the labile iron and understand the mechanisms of chelator access routes to cellular sites of labile iron accumulation in model cells relevant to IO and design drug for the treatment of IO disease (7). The detection and quantification of labile iron in intracellular or extracellular compartments can be achieved by physical or chemical methods. However, the physical method (AES, ICP) will destruct the sample and chemical methods (ESR, colorimetric) are not sensitive and not easy adaptable to high throughput assays. Fluorescence detection of iron is the most favorable due to simplicity and sensitivity (8).

Cabantchik is a world expert in the area of iron cellular biology and published extensively in this area (9-16). Recent studies in the Cabantchik laboratory focused on the design of fluorescent probes with iron chelation capability, which allow targeting specific cell compartments and response to metal binding by signal change. These probes change their emission properties upon binding to cellular iron. The Cabantchik research group often uses H9C2 cardiomyocytes as a cell model. However, it is also important to measure labile iron in brain tissue since abnormally high iron level was found in brain tissue of Parkinson patients (17). The poor photostability of organic fluorophores prevented long term cellular studies. The objective of the study is to design quantum dots based cellular probes to labile iron in iron-rich astrocytes with increased photostability over previously used organic fluorophore based probes.

Luminescent quantum dots have been a promising approach to fluorescent chemical sensing and they have attracted great interest in recent years among biological researchers since they provide solutions to problems associated with use of organic fluorophores in cellular studies due their unique optical properties. The most important feature is their photostability, which can be 100 times better than that of organic fluoreophores. Our research group first demonstrated the development of quantum dots based ion probe for Zn^{2+} and Cu^{2+} ions by CdS quantum dots capped with L-cysteine and triglycerol as selective probes in aqueous media (18). Since then, different quantum dots based ion probes have been devised over the past few years (19-27). For example, Leblanc and his coworker reported the peptide (Gly-His-Leu-Leu-Cys)-coated CdS quantum dots for the detection of Cu^{2+} and Ag^{+} in the micromolar level (19). CdSe functionalized with L-cysteine exhibited strong specific affinity for Hg^{2+} through quantum dots interface

functional group were reported by Zhu's research group (22). Sanz-Mendel and co-workers made an important contribution to introduce quantum dots into the area of anionic detection (23, 24). Zhao and his coworker use mercaptoacetic acid coated CdS quantum dots as fluorescence probes for sensitive and selective detection of highly reactive HSe^- ions in aqueous solutions (25). However, the mechanisms for the quenching or enhancement of luminescence of quantum dots are still not clearly understood (28). In some cases, the fluorescence change is due to electron transfer between Cd^{2+} and metal ions (18). Chiu's research group reported a fluorogenic sensor for K^+ sensors in aqueous solution based on 15-crown-5 functionalized CdSe/ZnS quantum dots via the Forster type energy transfer between two different color quantum dots. The detection limit is around uM. To a certain extent, the core/shell can avoid the electron transfer from CdSe core to the metal ions (27). Cu^+, Pb^{2+}, Ag^+ ions also can quench luminescence of quantum dots by replacing the Cd^{2+} ions in the nanocrystals' lattice (29). The quenching is permanent, not easy reversible, and usually not analyte specific, which is not practical as a sensing probe (30). CdSe is overcoated with ZnS shell to improve the stability, which will enable the detection of target analytes to be reversible.

To our best knowledge, there is no report on reversible quantum dots based selective iron ion sensing. If the response of quantum dots to ions is reversible, they can be used for real-time monitoring fluctuations in iron concentration. Here, this chapter first reports the development of reversible quantum dots based sensor for iron. A schematic diagram of the quantum dot iron ion probes is shown in scheme 5.1. First, CdSe quantum dots were overcoated with ZnS shell to improve the stability of CdSe core. To fabricate the quantum dot-based iron probes, they were functionalized with metallothionein (MT).

Then the surface of the MT coated quantum dots was modified with EDTA. EDTA was selected as a capping ligand because of relatively low binding affinity (mM level) to iron ions. When captured by the EDTA molecules, iron ions quenched the emission intensity of the quantum dots. Removal of iron from the quantum dot surface by free EDTA or other iron chelators with higher binding affinity resulted in a rise in the quantum dots' luminescence. The analytical properties of the probes including sensitivity, selectivity, and reversibility were characterized.

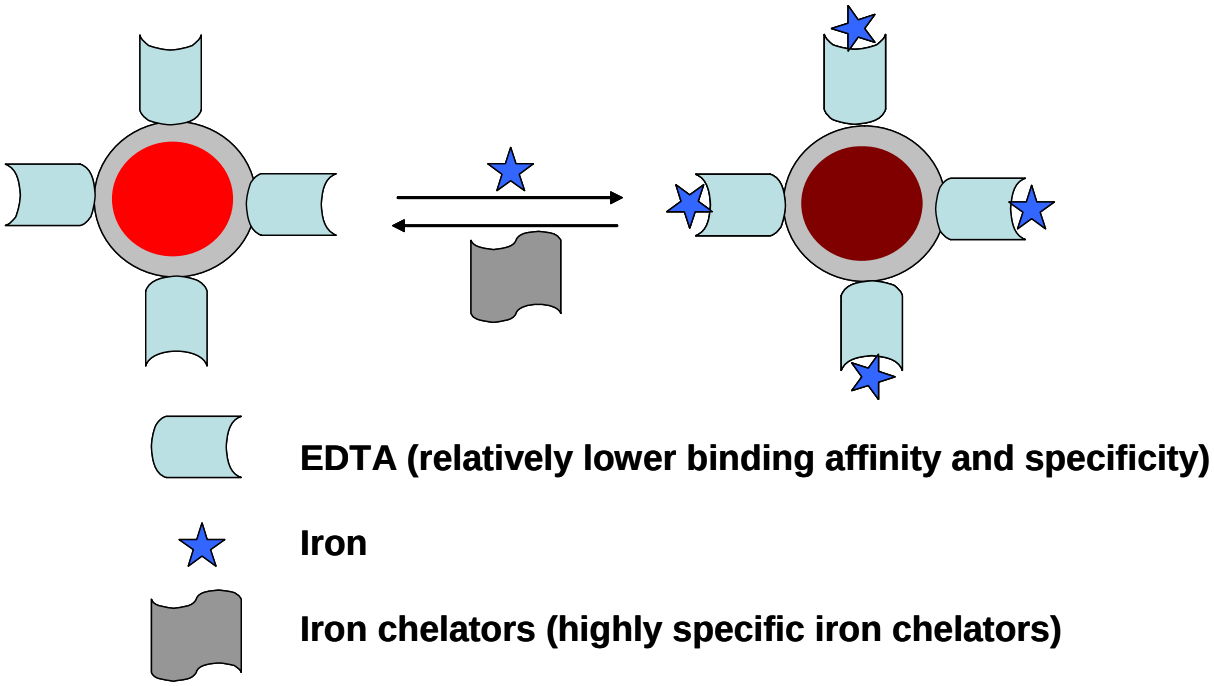

Scheme 5.1 Schematic representation of reversible quantum dots based iron sensor.

5.2 Experimental

5.2.1 Synthesis of EDTA coated quantum dots

Excess amount of glutaraldehyde was added to MT capped quantum dots in MOPS 7.0 buffer for 1-2 hours at room temperature with continuous mixing, then spin dialysis to remove the unbound glutaraldehyde. An excess amount of aminobenzyl-EDTA was added to the above resulting solution and incubated for 2-4 hours at room temperature with continuous stirring, which followed by spin dialysis to remove excess aminobenzyl-EDTA. The bond formed between an amino group and an aldehyde from a reversible Schiff base is not stable and it must be reduced by a process called reductive alkylation in order for the bond to be covalent. Sodium cyanoborohydride was added the above solution and mixed gently for 30 minutes. The product was spin dialyzed and resuspended in MOPS 7.0 buffer to a desired storage concentration, then stored at 4°C until used.

5.2.2 Iron response

200 µL of 30nM EDTA capped quantum dots and 200µL of varying concentration iron ranging from 1µM to 1mM were added to MOPS buffer solution at pH 7.0 to a final volume 1.0 mL. Response time measurements were carried out following the addition of iron using a fluorescence spectrometer. Emission spectra were recorded 3 minutes after adding iron solution (λex =400nm).

5.2.3 Selectivity

The EDTA capped quantum dots were tested for their response to other biologically relevant ions such as Na^{+}, K^{+}, Ca^{2+}, Mg^{2+}, Mn^{2+}, and Cu^{2+}. 200 µL 30nM EDTA capped quantum dots and 200µL of 1mM cations were added to MOPS buffer solution at pH 7.0 to a final volume 1.0 mL. Emission spectra were recorded 3 minutes following adding iron solution (λex =400nm).

5.2.4 Reversibility

Reversibility was measured by monitoring the change in fluorescence intensity upon the addition of iron chelator to the solution of EDTA capped quantum dots with iron suspended in a MOPS buffer solution at pH 7.0. The fluorescence intensity was measured as a function of time using excitation wavelength of 400nm and an emission wavelength of 605nm. To conduct the measurement, 200µL 30nM EDTA capped quantum dots in 600µL MOPS buffer solution at pH 7.0 was placed in the fluorometer and the emission was monitored. Then, 200µL of 1mM iron solution was injected into the cuvette until the signal reached saturation, and 100µL of 50mM iron chelators were injected to the above solution. The emission measurement was continuously carried out to monitor the reversibility.

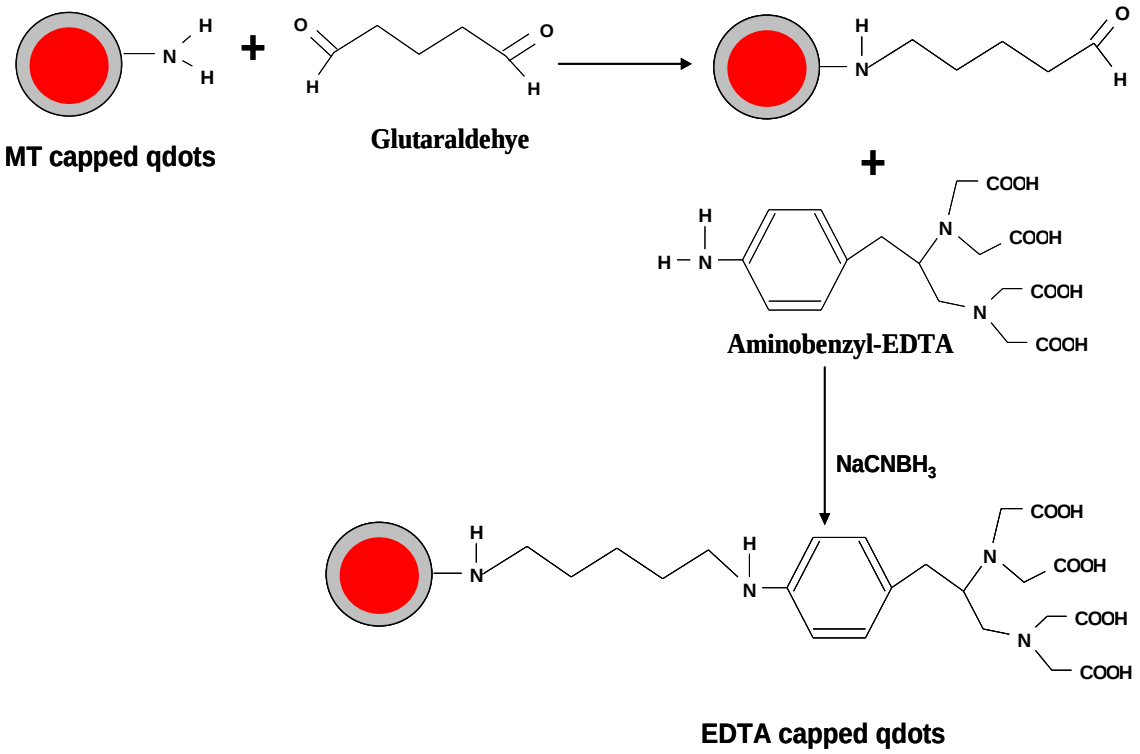

Scheme 5.2 The synthesis of quantum dots based iron sensor

5.3 Results and discussion

5.3.1 Effect of capped ligands on the Fluorescence of quantum dots

The synthesis of quantum dots iron probes was described in the experimental section. MT is also a lysine-rich peptide. The MT coated quantum dots, full of amine groups on the surface of quantum dots, conjugated with aminobenzyl-EDTA via glutaraldehyde to form the quantum dots iron probes (EDTA coated quantum dots) (see scheme 5.2). The normalized emission spectra of quantum dots capped with TOPO, MHDA, MT and EDTA are shown in figure 5.1 (excitation at 400nm). All samples were excited at 400nm Emission scans measured from 480nm to 700nm. It can be clearly seen in figure 5.1a that emission intensity of the MHDA coated quantum dots was 3 times lower than the emission intensity of TOPO coated quantum dots. Figure 5.1b showed that MT as capped ligands would increase 20% of the emission intensity of quantum dots. Whereas, the EDTA as capped ligands would decrease the emission intensity of quantum dots by 50% (figure 5.1c). These results showed that the surface ligands have intense effects on fluorescence emission of quantum dots. Surface chemistry would affect the photophysical properties of quantum dots. This is very crucial for development of quantum dots based probes. More research work need to done to form fully stable water-soluble quantum dots.

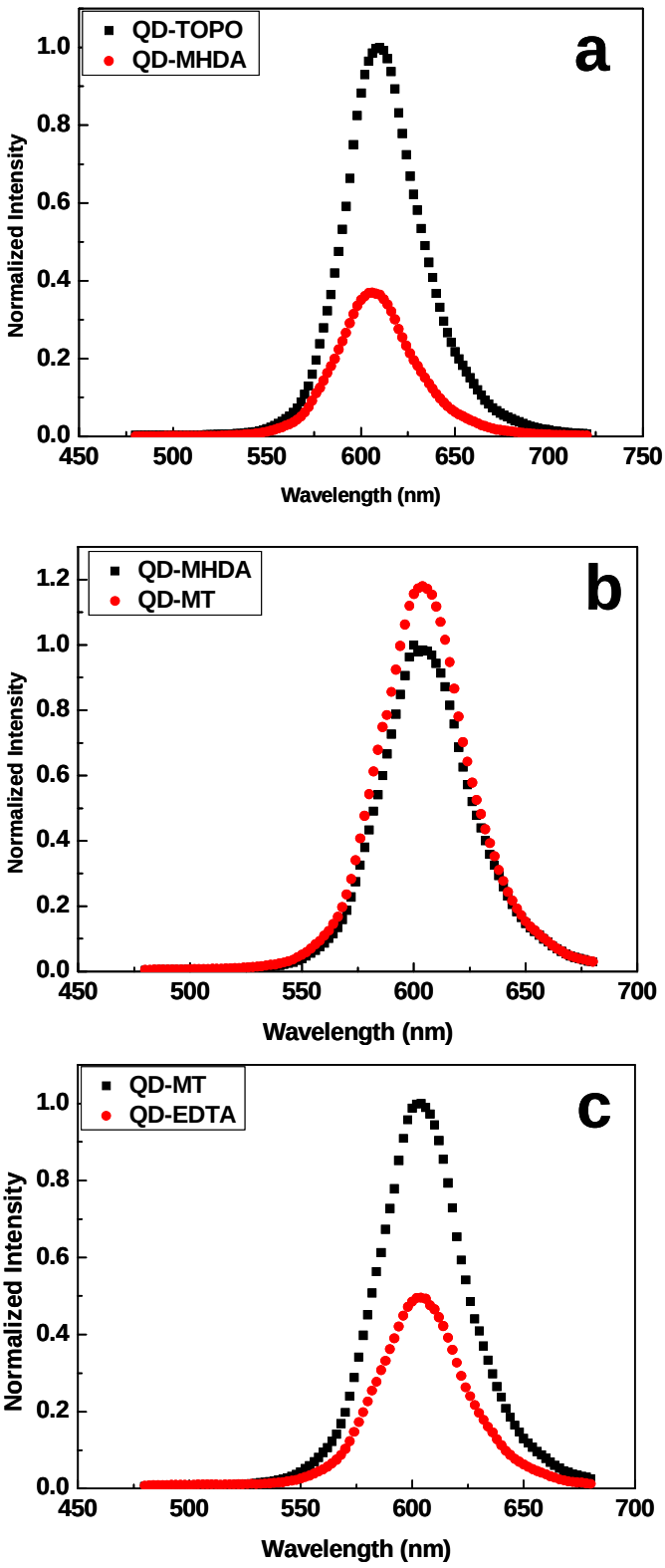

Figure 5.1 Effect of capped ligands on the fluorescence intensity of quantum dots

5.3.2 Iron response

First, we measured the response time of EDTA capped quantum dots to Fe^{2+} in MOPS buffer solutions at pH 7.0 (figure 5. 2). Here, F_0 is fluorescence intensity of the EDTA capped quantum dots in an iron free solution and F is fluorescence intensity of EDTA capped quantum dots following adding iron ion. It can be clearly seen that Fe^{2+} in the form of ferrous ammonium sulfate added to EDTA coated quantum dots in ambient conditions evoked a rapid and robust quench of the fluorescence intensity of quantum dots. As reported by the Cabanchik research group, Fe^{2+} rapidly oxidized to Fe^{3+} when Fe^{2+} was bound to EDTA (8).

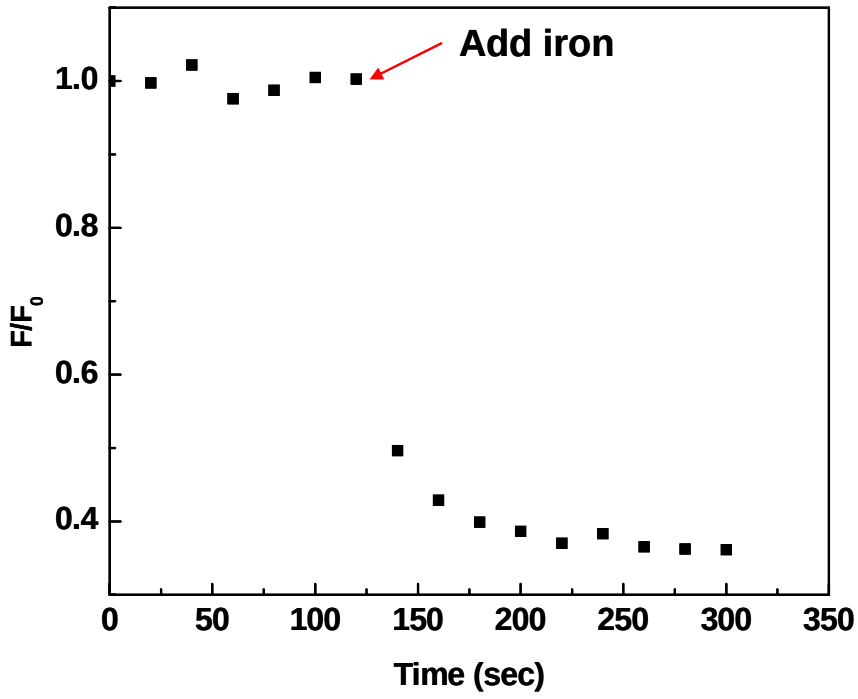

Figure 5.2 Characterization of the response time of the quantum dots iron sensor- the fluorescence intensity of the EDTA coated quantum dots prior and following the injection of an aliquot of concentrated Fe^{2+} solution (ferrous ammonium sulfate) is shown.

The iron concentration dependence of the fluorescence intensity of EDTA capped quantum dots is shown in figure 5.3a. It can be clearly seen that the fluorescence intensity of EDTA capped quantum dots decreases with the increasing Fe^{2+} concentration. We found that the quenching effect of iron on the fluorescence emission of EDTA capped quantum dots could be best described by a Stern-Volmer-type equation [5]:

$$\frac{F_{\max}}{F} = 1 + K_{sv}[Q] \qquad [5]$$

F and F_{max} are the fluorescence intensities of the EDTA capped quantum dots at a given iron concentration and in an iron free solution. Q is the iron concentration. Figure 5.3b showed a Stern-Volmer quenching curve describing F_{max}/F as a function of iron concentration. The Stern-Volmer quenching constant, K_{sv} , was determined to be 6710 M^{-1}. A good linear relationship ($r > 0.993$) was observed up to iron concentrations ranging from 0 to 200 μM, which allows the development of a method for the detection of iron. However, converse to typical Stern-Volmer quenching behavior, which is driven by collisions between quenchers and luminescent molecules, the quench of luminescence of EDTA capped quantum dots is attributed to iron binding followed by a charge transfer process on the surface of quantum dots. The experimental data can be explained in terms of the strong affinity of iron with EDTA, the surface ligands of quantum dots.

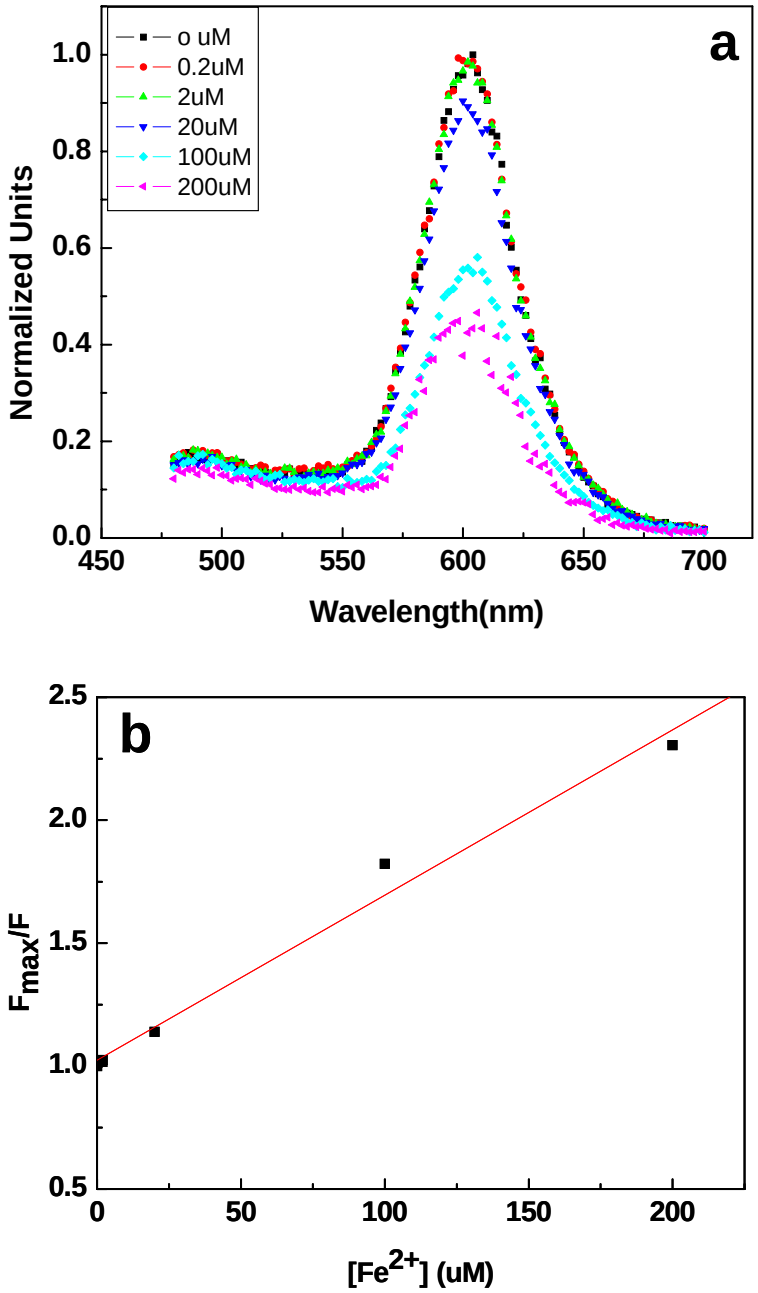

Figure 5.3 Effect of Fe^{2+} ion concentration on the emission of EDTA capped quantum dots. a) Fluorescence emission spectra; b) A stern-Volmer plot effectively describes the iron concentration dependence of the luminescence intensity of EDTA capped quantum dots with a Stern-Volmer constant Ksv=6710 M^{-1}.

We observed that there was a rapid and intense quenching on fluorescence of quantum dots between Fe^{2+} and EDTA coated quantum dots. On the other hand, we also observed that Fe^{3+} in the form of ferric chloride only evoked a slower and lower quenching on fluorescence of quantum dots in figure 5. 4. This result is probably due to the poor solubility of $FeCl_3$. Even with quantum dots based probes, these results also agreed with that of fluorophore from Cabanchik's research group (8). They have already extensively discussed that the rate and extent of Fe^{2+} and Fe^{3+} binding to the probes in ambient conditions is associated with the solubility and stability constant of the iron-anion salt complex and the capacity of the chelator to shift the oxidation state of the metal to that of higher affinity to a certain extent.

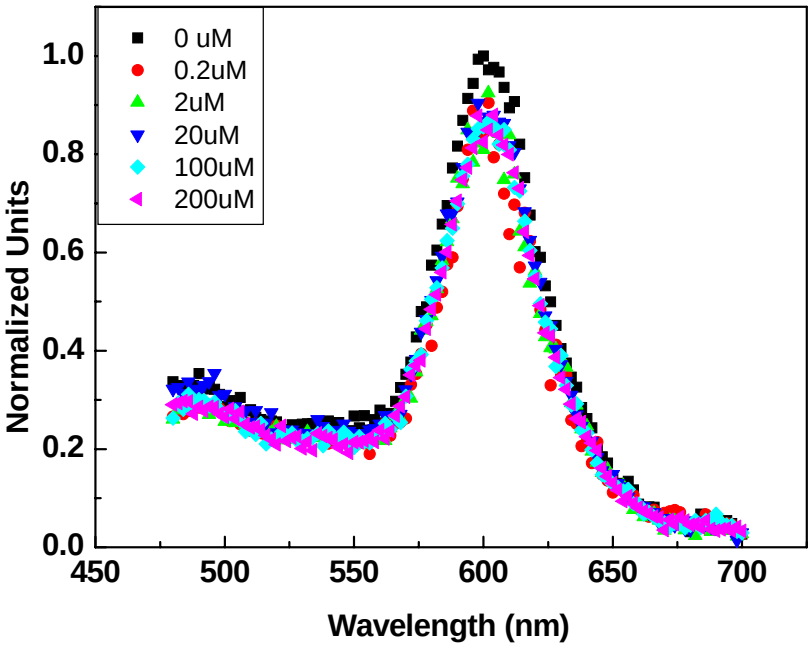

Figure 5.4 Effect of Fe^{3+} ion concentration on the emission of EDTA capped quantum dots.

Digital fluorescence images are shown in figure 5 and they show clear visual evidence of the effect of iron on fluorescence of EDTA capped quantum dots. It can be seen that the emission color of the quantum dots in iron free solution is red (emission wavelength 605nm). It should be mentioned that there is no aggregation on EDTA capped quantum dots. These results suggested that using cysteine-rich peptide MT as capped ligands improves the stability of quantum dots via multiple thiol bonds. The emission color of quantum dots get darker with the increasing iron concentration. This result suggests that iron quenches the fluorescence emission of EDTA capped quantum dots.

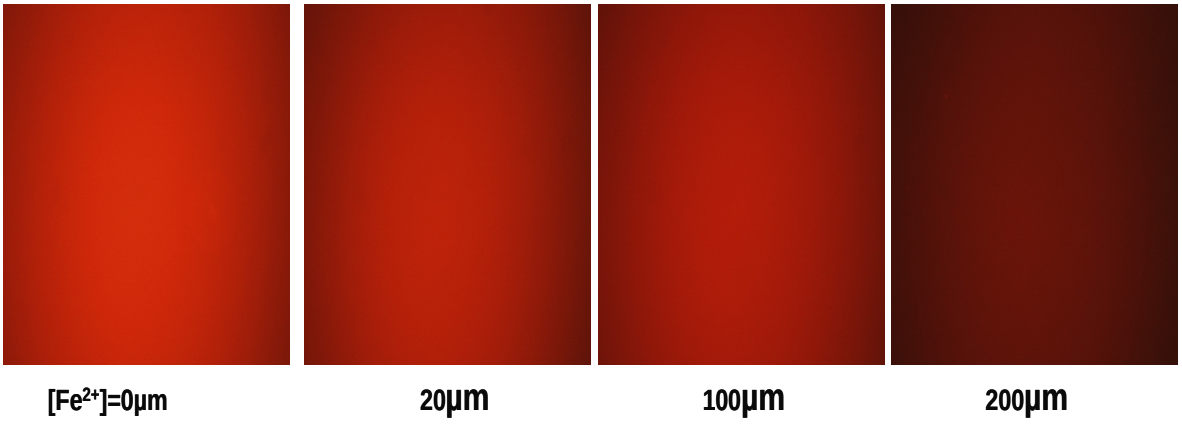

Figure 5.5 Digital fluorescence images of EDTA capped quantum dots with increasing concentration of iron, the images were taken through 40X objectives with numerical apertures of 0.9.

.

To further understand the mechanism of the quenching effect of iron on EDTA capped quantum dots, first control measurements that involved iron effect on MT capped quantum dots were carried out. Figure 5.6 describes the normalized fluorescence spectra of quantum dots with 200 μM iron level. Figure 5.6a shows that the fluorescence intensity of EDTA capped quantum dots decreases by 60% when exposed to 200 μM iron. However, Figure 5.6b reveals that this iron level hardly affects the fluorescence emission of the MT capped quantum dots. These results indicated that the quenching effect of iron on EDTA capped quantum dots is due to the specific binding between iron and EDTA molecules on the surface of quantum dots and not due to non-specific adsorption on the surface of quantum dots.

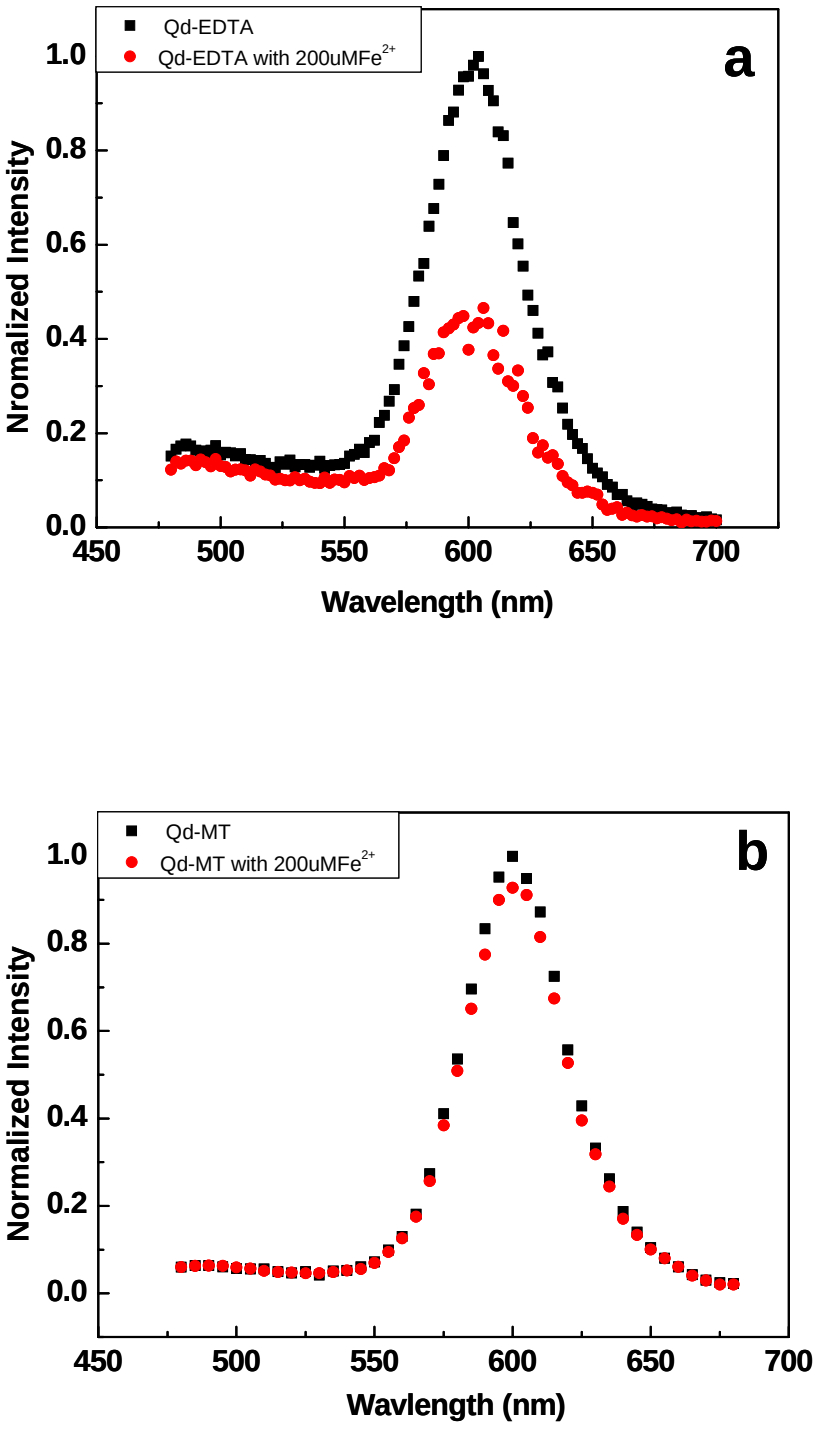

Figure 5.6 Normalized Fluorescence spectra of a) EDTA capped quantum dots and b) MT capped quantum dots with 200μM iron solution

Since Fe^{2+} rapidly oxidizes to Fe^{3+} when Fe^{2+} binds to EDTA, one should also be aware of inter filter effects of Fe^{3+} that may quench the fluorescence of quantum dots. Additionally, we further study whether inner filter resulting from the strong absorption of the excitation wavelength by iron is the factor of the quenching effect of iron on the luminescence of EDTA coated quantum dots. Since Fe^{2+} rapidly oxidizes to Fe^{3+} when Fe^{2+} binds to EDTA, Fe^{3+} would react with fluoride ion to form the colorless complex FeF_6 and eliminate the inner filter effect (18). Figure 5.7 shows the emission of EDTA-quantum dots complex did not change in the presence of 200 mM of F ions. It is still quenched by iron ions. This result suggests that the quenching effect of Fe^{2+} on luminescence of EDTA coated quantum dots is not due to an inner filter.

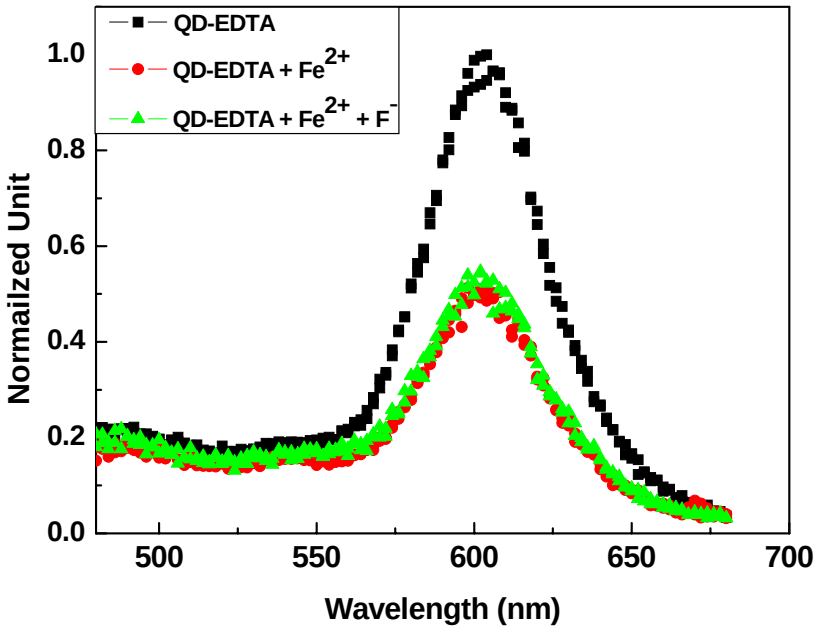

Figure 5.7 The emission of EDTA coated quantum dots with 200mM fluoride ion ([iron] =200μM)

5.3.3 Selectivity

The above result shows that the fluorescence emission of quantum dots is quenched by 60% in a solution containing 200μM iron. To better understand selectivity of EDTA capped quantum dots towards iron, we compared the iron response with other biologically relevant ionic species. The response of EDTA capped quantum dots to biologically relevant ions such as Na^{+}, K^{+}, Ca^{2+}, Mg^{2+}, Mn^{2+}, Cu^{2+} is shown in figure 5.8. The fluorescence intensity of quantum dots decreased by 20% to Na^{+}, K^{+}, Ca^{2+}, Mg^{2+}, and Mn^{2+}. Iron and copper ions quench the fluorescence emission of quantum dots by 60% and 90% respectively. The mechanism of cupper ions quenching the luminescence of EDTA coated quantum dots is not fully understood, probably due to the non-specific binding. However, the copper would not be a potential interference since these probes will be carried out in the iron rich cell culture.

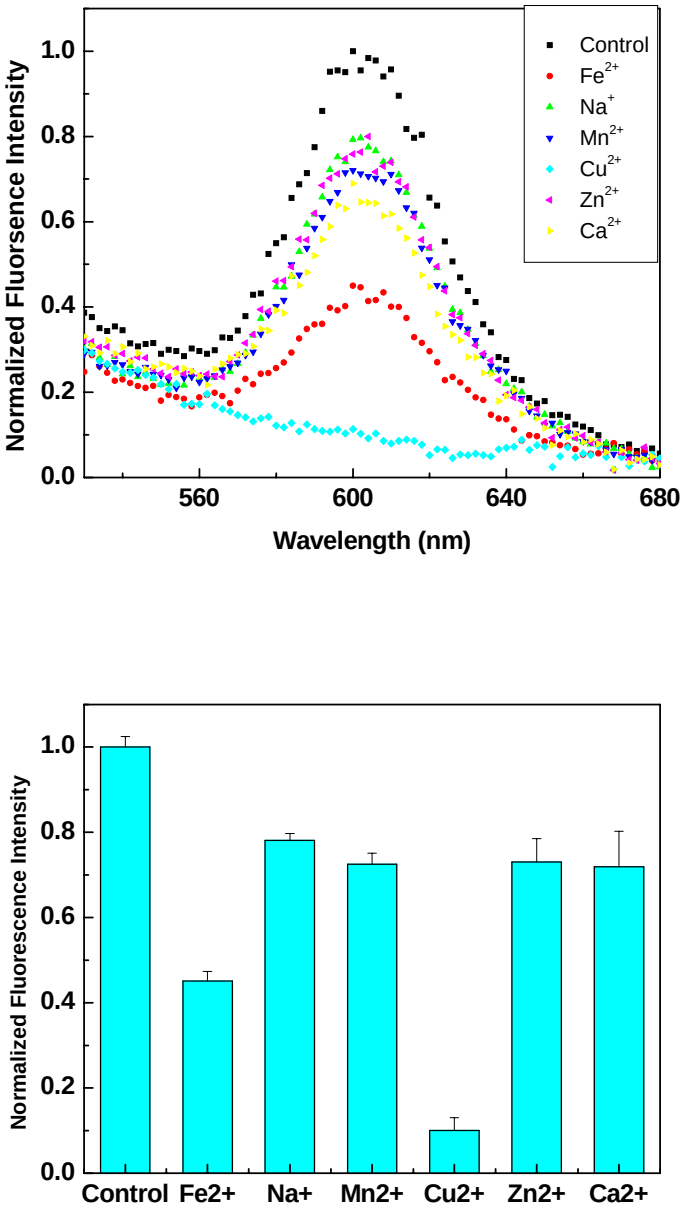

Figure 5.8 Effect of 200uM biologically relevant ions on the fluorescence emission of EDTA capped quantum dots.

5.3.4 Reversibility

The largest challenge of this project is the reversibility of quantum dots based iron sensor. Here two different iron chelators were used to carry out the reversibility of quantum dots iron sensor. 3-hydroxy-1,2-dimethyl-4(*1H*)-pyridone (HPO) comprised highly specific iron chelators. HPO is a bidentate chelator, which means three molecules can coordinate on Fe^{3+} in free solution (31). EDTA has relatively lower metal-binding affinity and specificity. The reversibility of quantum dots based iron sensors is depicted in figure 5.9. Temporal dependence measurement was carried out to provide the dynamic information. First, Fe^{2+} solutions were added into the EDTA coated quantum dots. As expected, a decrease in fluorescence intensity was observed. Then, the chelators were added to the above solution, the fluorescence intensity of quantum dots was increased over time. These results suggested that the chelator remove iron from the surface of quantum dots and de-quenched the fluorescence intensity of quantum dots. HPO shows higher recovery ability than EDTA due to the higher binding affinity. The recovery of quantum dots intensity by HPO and EDTA is 35% and 17% respectively in the level of 4.55 mM. This clearly demonstrated the reversibility of quantum dots based iron sensor. However, the quenching of EDTA coated quantum dots by iron can not be fully recovered with chelator EDTA or HPO. It is possible there is also some non-specific binding of iron on surface of quantum dots, which can't be removed by the EDTA or iron chelator.

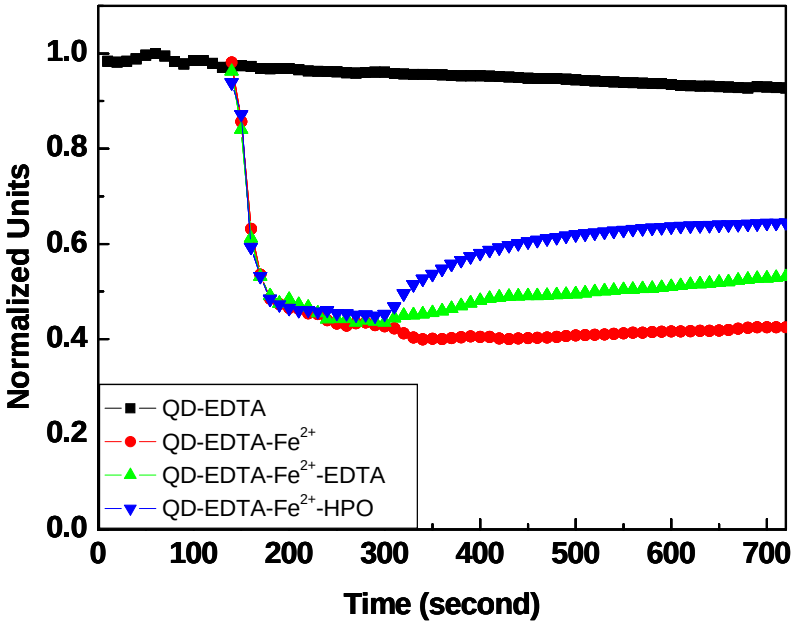

Figure 5.9 Reversibility of quantum dots based probes. Temporal dependence of EDTA coated quantum dots in the presence of the tested chelator. Fluorescence of EDTA coated quantum dots is quenched by Fe^{2+}, and reversed by adding the chelator EDTA and HPO

As we have observed, Cu^{2+} also quenched the fluorescence intensity of EDTA coated quantum dots. Actually Cu^{2+} showed a higher quenching activity compared with Fe^{2+}. Here, we also measured the reversibility of quantum dots based probes in the presence of Cu^{2+} (figure 5.10). The fluorescence intensity of quantum dots is quenched by 90% with 200uM Cu^{2+}. However, the fluorescence is not recovered by the chelator EDTA or HPO.

These results indicated that Cu^{2+} quench the fluorescence intensity of EDTA coated quantum dots is due to non-specific adsorption, and not due to the binding affinity between Cu^{2+} and EDTA on the surface of quantum dots.

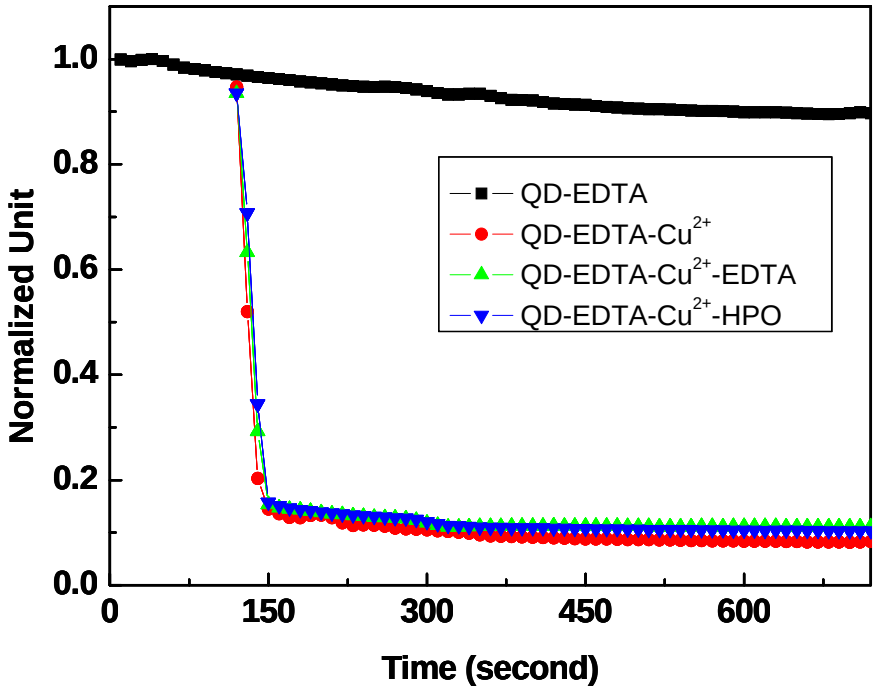

Figure 5.10 Temporal dependence of EDTA coated quantum dots in the presence of Cu^{2+} and tested chelator. Fluorescence of EDTA coated quantum dots is quenched by Cu^{2+}, and not reversed by adding the chelator EDTA and HPO.

5.4 Conclusions

Luminescent quantum dots have been a new approach to fluorescence sensing since they provide solutions to problems associated with use of organic fluorophores in cellular studies due their unique optical properties. Here, we describe for the first time the development of a reversible quantum dots based iron sensor. We have successfully synthesized and designed quantum dots based iron sensors. The effect of different capped ligand on the fluorescence intensity of quantum dots was investigated. MT as capped ligand of quantum dots could improve the stability of quantum dots through the multiple thiol bonds. MT capped quantum dots conjugated with aminobenzyl-EDTA to form the EDTA coated quantum dots, quantum dots based iron probes. However, the surface ligands have intense effects on fluorescence emission of quantum dots. It is very important to form the fully stable quantum dots, especially for quantum dots based sensors. The quantum dots probes show high sensitivity towards iron ions. A Stern-Volmer equation can best describe the iron concentration dependence of the quenching of fluorescence intensity of quantum dots. The insensitivity of MT coated quantum dots to iron ions indicates that the quenching mechanism is the binding affinity between iron and EDTA on the surface of quantum dots. Since Fe^{2+} rapidly oxidizes to Fe^{3+} when Fe^{2+} binds to EDTA, one should also be aware of inter filter effects of Fe^{3+} that may quench the fluorescence of quantum dots. By adding F^- ions to the quantum dots iron complex, the fluorescence intensity of quantum dots didn't recover, which indicates that the inner filter effect is not the reason for quenching. The selectivity of quantum dots based probes

is not perfect. Cu^{2+} show a higher quenching effect on the fluorescence of quantum dots than iron at 200 uM. Later, we found out that the quenching is due to non-specific adsorption, not specific binding affinity between Cu^{2+} and EDTA on the surface of quantum dots. Since these probes will be carried out in the iron rich cell culture, the Cu^{2+} will not be a potential interfering agent. The reversibility of quantum dots iron sensors also was investigated. Iron chelators remove iron from the surface of quantum dots, which results in the increase of the previously quenched fluorescence of quantum dots. 3-hydroxy-1,2-dimethyl-4(*1H*)-pyridone (HPO) showed a higher a recovery ability of fluorescence intensity of quantum dots than EDTA. However, neither of them shows a full florescence recovery. We are now using higher specificity iron chelator to monitor the reversibility of quantum dots probes. Furthermore, reducing the non-specific binding and improving the selectivity have to be done before carrying out these probe for intracellular assays of labile iron in iron enriched astrocytes.

5.5 References

1. Bierer, B. E.; Nathan, D.G. *Blood*, **1990**, 76 (10), 2052-2059
2. Esposito, B. P., Breuer, W., Cabantchik, Z.I., *Biomaetals* **2002**, 729-732
3. Bergeron, R.jL, Weigand, J. McManis, J.S., Bussenius, J., Smith, R.E., Weimar, W.R., *J. Med. Chem.,* **2003**, 46, 1470-1477
4. Barnham, K.J., Masters, C.L.l Bush, A.I., *Nat. Tev. Drug Discov.,* **2004**, 3, 205-214
5. Lieu, P.T., Heiskala, M., Peterson, P.A., Yang, Y., *Mol. Aspects Med.,* **2001** 22, 1-87
6. kalinowski, D. S.; Richardson, D. R. *Pharmacol Rev* **2005,** 57, 547-583,
7. *http://biolchem.huji.ac.il/cabantchik.htm*
8. Esposito, B. P.; Epsztejn, S.; Breuer, W.; Cabantchik, Z. I. *Anal. Biochem.* **2002**, 304, 1-18,
9. Cabantchik, Z.I., Kakhlon, O., Epsztejn, S., Zannielli, G., Breuer, W., *Adv. Exp. Med. Biol.,* **2002**, 509, 55-75
10. Glickstein, H., El, R.B., Link, G., Breure, W., Konijn, A.M., Kershko, C., Nick, H., Cabantchik, Z. I. *Blood.* **2006,** 108(9):3195-203.
11. Kakhlon, O., Cabantchik, Z.I., *Free Radic Biol Med*. **2002** 33(8):1037-1046.
12. Konijn, A. M., Glinkstein, H., Vaisman, B., Meyron-Holtz, E. G., Slotki, I. N., Cabantchik, Z.I., *Blood*. **1999, 94**(6), 2128-2134.
13. Epsztein, S., Kakhlon, O., Glickstein, H., Breuer, W., Cabantchik, Z.I., *Anal Biochem.* **1997**, 248(1):31-40
14. Cabantchik, Z.I., Glickstein, H., Milgram, P., Breuer, W., *Anal Biochem.* **1996**; 233(2):221-227.
15. Kakhlon, O, Gruenbaum, Y., Cabantchik, Z.I., *Biochem J.* **2002**; 363, 431-436.
16. Glickstein, H., EI, R.B., Shvartsman, M., Cabantchik, Z.I., *Blood*. **2005**; 106(9):3242-3250
17. Faucheux, B.A., Hirsch, E.C., Villares, J., Selimi, F., Mouatt-Prigent, A., Javoy-Agid, F., Hauw, J.J., Aqid, Y., *J. Neurochem.,* **1993,** 60 (6), 2338-2341
18. Chen, Y.; Rosenzweig, Z. *Anal. Chem.;* **2002**; *74*(19); 5132-5138
19. Gattas-Asfura, K.M.; Leblanc, R.M., *Chem. Commun*., **2003**, 2684-2685
20. Liang, J. G.; Ai, X. P.; He, Z. K.; Pang, D. W. *Analyst*, **2004**, 129, 619–622
21. Bo, C.; Ping, Z. *Anal. Bioanal. Chem.*, **2005**, 381, 986–992
22. Chen, J. L.; Gao, Y. C.; Xu, Z.B.; Wu, G.H.; Chen, C.C.; Zhou, C.Q. *Analytica Chimica Acta*., **2006**, 577, 77-84
23. Jin, W. J.; Costa-Fernandez, J. M.; Pereiro, R.; Sanz-Medel, A. *Anal. Chim. Acta*, **2004**, 522, 1–8
24. Jin, W. J. ; Fernandez-Arguelles, M. T.; Costa-Fernandez, J. M.; Pereiro, R.; Sanz-Medel, A. *Chem. Commun.*, **2005**, 883–885
25. Wu, C. L; Zhao, Y. B. *Anal Bioanal Chem.,* **2007**, 388(3):717-722.
26. Li, J.; Bao, D. S.; Hong, X.; Li, D.; Li, J.H.; Bai, Y. B.; Li, T. J. *Colloids and surfaces A: Physicochem. Eng. Aspects 257-258,* **2005,** 267-271
27. Chen, C.Y., Cheng, C.T.; Lai, C.W.; Wu, P. W.; Wu, K.C.; Chou, P. T.; Chou, Y. H.; Chiu, H.T., *Chem. Commun.,* **2006**, 263-265

28. Basabe-Desmonts, L.; Reinhoudt, D.N.; Crego-Calama, M. *Chem. Soc. Rev.*, **2007**, 36, 993-1017
29. Son, D.H., Hughes, S.M., Yin, Y., Alivisatos, A.P., *Science*, **2004,** 306, 1009-1012
30. Somers, R.C., Bawendi, M.G., Nocera, D.G. *Chem. Soc. Rev.*, **2007**, 36, 579-591
31. Abeysinghe, R.D., Roberts, P.J., Cooper, C.E., Maclean, K.H., Hider, R.C., Porter, J.B., *The Journal of Biolgoical chemistry*, **1996**, 271, 7965-7972

CHAPTER 6 SUMMARY AND CONCLUSIONS

Fluorescence, combined with digital microscopy and fluorescence resonance energy transfer (FRET), has been a very sensitive and powerful method for monitoring biological events. Molecule sensors able to monitor environmental changes, such as concentration of enzyme, pH, ionic species, etc, have been sought for probing biological phenomena in cells. CdSe/ZnS core/shell quantum dots have attracted great interest and emerged as a novel type of fluorescent probes in many biological and biomedical fields. They show unique photophysical properties, such as narrow and symmetrical emission spectra, broad absorption spectra, high quantum yield, high chemical stability, high photostability, and size dependent luminescence. In this Ph.D study, luminescent quantum dots based sensors have been developed for protease measurement, pH measurement and iron measurement.

In recent years, several studies have demonstrated the use of luminescent quantum dots as donors to detect biomolecules, such as DNA, RNA, protein, enzyme, etc. Chapter 3 describes, for the first time, the development of quantum dot FRET-based enzymatic activity probes and their use for the measurement of extracellular matrix metalloproteinases (MMPs) activity in normal and cancerous breast cell cultures. The methodology proposed in Chapter 3 is advantageous since it enables real-time monitoring of the proteolytic activity of MMPs and the measurement takes only 15 minutes to complete in both aqueous solution and cell culture. The use of molecular fluorophores as

acceptors enabled a ratiometric measurement technique to monitor FRET changes. This results in simultaneous changes in the quantum dots and fluorescent acceptors emission peaks. The high photostability of quantum dots enables long observation times that are required to monitor proteolytic activity. Chapter 3 discusses the fabrication, characterization, and applications of novel luminescent quantum dots FRET based protease activity probes. The luminescent probes are based on FRET between luminescent quantum dots that serve as donors and rhodamine acceptors that are immobilized to the surface of the quantum dots through peptide linkers that contain selective enzymatic cleavage sites. First the probes were used to test the enzymatic activity of trypsin in solution. The FRET signal changes were found to be dependent on trypsin concentration and time. The enzymatic assay was completed rapidly (less than 15 minutes). Meanwhile, the probes were capable of determining the different inhibition efficiency of three organic trypsin inhibitors, 4-(2-aminoethyl) benzene-sulfonyl fluoride hydrochloride, 4-amidinophenylmethane-sulfonyl fluoride hydrochloride and 1, 10 phenanthroline. In the experiments, we found out that it was difficult to determine the inhibition efficiency of larger protein trypsin inhibitors. It is possible that the bond between quantum dots and peptides is not very strong, and that protein molecules could displace the peptide-rhodamine from the surface of quantum dots and would result in FRET signal change even in the absence of trypsin. Using the probes we were able to discriminate between normal and cancerous cells in less than 15mins primarily due to the difference in the proteolytic activity of their extracellular matrices. To improve the stability of the quantum dots in biological media is very important to develop quantum dots based biosensor. For example, metallothionein will be used as an improved capping

ligand since it binds to the quantum dots through multiple cysteine residues. The novelty in this method is in the use of quantum dots as dynamic probes rather than imaging contrast agents. Another novel aspect of the study is the flexibility of the approach. While the current peptide linker enables discrimination between normal and cancer breast cells, modification of the peptide sequence will enable use of these probes to monitor other biological systems that are characterized by overexpression of proteolytic enzymes. Furthermore, the probes could also be used to screen for the efficiency of protease activators.

Change on pH is very important for the biological process. Taking advantage of unique properties of quantum dots and the high sensitivity of FRET, Chapter 4 demonstrates the development of quantum dots FRET based sensor for pH measurement. The FRET probes were synthesized by labeling MT coated quantum dots with rhodamine. The novelty of this probe is the FRET signal between quantum dots and rhodamine responded differently to pH in the wide range from 4.5 to 9.5. Another novel aspect is that the pH response could be monitored not only by the alteration on emission spectra, but also by the change on images. MT was used as the capping ligand to improve the stability of quantum dots. However, the digital fluorescence images show that the MT coated quantum dots are not stable and they aggregated at low pH. The MT coated quantum dots were very stable when pH >=6.5 and they can be stored over 1month in MOPS buffer. FRET efficiency was pH dependent and time dependent. The FRET efficiency achieves the maximum at pH 6.5 and decreases either in lower or higher pH. We expect that this quantum dots FRET based pH sensor could be used for investigating

biological process. This is an active research area to use quantum dots as fluorescence probes to monitor intracellular pH. Although some research groups, including us, have achieved some success on the process, there is still more research work necessary. The first thing is the surface modification of quantum dots to improve the stability and biocompatibility in cellular environment. The most important thing is to design the quantum dots based intracellular sensors which only specifically respond to protons (pH) in cellular environment, but are not affected by other factors, such as ionic species, temperature, and electric field.

In our laboratory, we have developed quantum dots based ion sensors by capping CdS quantum dots with thioglycerol, cysteine and polyphosphate. The luminescence of quantum dots responds differently to metal ions. However, the quench of luminescence of quantum dots by ions is permanent, so this sensor was not reversible. For the first time, chapter 5 demonstrates the development of a reversible quantum dots based iron sensor. The quantum dots were capped with EDTA and the fluorescence of quantum dots was quenched by iron. Iron chelators in solution removed iron from the surface of quantum dots, which resulted in the increase of the previously quenched fluorescence of quantum dots. In the experiments, we found out that the surface capping ligands could affect the fluorescence emission of quantum dots, which indicates that the surface chemistry would change the photophysical properties of quantum dots. The iron concentration dependence on the quench of quantum dots fluorescence intensity can be described by the Stern-Volmer equation. The control experiments showed that the fluorescence intensity of MT coated quantum dots was not affected by the same level of iron ions, which indicates that

the quench mechanism is probably the binding affinity between iron and EDTA on the surface of quantum dots. Moreover, the fluorescence intensity of quantum dots iron complex didn't change on the presence of F^- ions, which indicates that the inner filter effect is not the reason of quenching. However, the mechanism of the quench on luminescence of quantum dots by iron is not fully understood. More experiments are needed to be done to fully understand the quenching phenomenon. Copper ions also showed a quenching effect on the fluorescence of quantum dots 200 uM level. However, the quench on fluorescence intensity could not be recovered by EDTA, which suggested that the quenching by copper is possible not due to non-specific binding affinity between copper and EDTA on the surface of quantum dots. However, the copper would not be a potential interference since these probes will be carried out in the iron rich cell culture. The novelty of this quantum dots based iron sensor is the reversibility. The reversibility of quantum dots iron sensors also was investigated by adding the EDTA or iron chelator 3-hydroxy-1,2-dimethyl-4(*1H*)-pyridone(HPO). In the level of 4.45mM, the fluorescence intensity of quantum dots was recovered 35% by HPO, and only 17% by EDTA. However, either EDTA or HPO showed a full florescence recovery. It is possible there is also some non-specific binding of iron on surface of quantum dots, which can't be removed by the EDTA or iron chelator. Before applying these sensors for intracellular assays of labile iron in iron enriched astrocytes, the selectivity and specificity of the sensor need to be improved

Quantum dots have the advantages as fluorescence probes over organic dyes. However, quantum dot have their limitations in biological application. Surface

modification on quantum dots to impart the aqueous solubility and functional groups for bioconjugation usually would decrease the quantum yield of quantum dots. Also quantum dots have limited pH stability and tend to aggregate in biological media. Meanwhile quantum dots have large surface-to-volume ratio, which allow a large number of biomolecules able to be conjugated to the surface of a quantum dot. However, it is hard to quantify the number of biomolecules conjugated on the surface of quantum dot. Nonspecific binding or adsorption of small molecules on the surface of quantum dots also was observed. Another concern is about cytotoxicity of quantum dots in experiments on living cell or animal since cadmium and selenium are known to be toxic. All these problems still need to be solved. Therefore, in the future, it is very important to modify quantum dots to make them less toxic, more stable, biocompatible, and more efficiently delivered/targeted into cells while remaining their optical properties intact.

VITA

The author was born in Fujian, China. She obtained her Bachelor's degree and M.S. degree in chemistry from Xiamen University in 1999 and 2002. To pursue higher education, in 2003 she came to the chemistry department at the University of New Orleans and became a member of Professor Zeev Rosenzweig's research group.